Influence of the seabed on surface noise intensity vector in shallow water

Abu-Sitta, F. H.

Award date:
1995

Awarding institution:
University of Bath

Dedicated to:

the memory of my father who gave
me love as well as a love of knowledge,

my mother for her constant support and love.

Influence of the Seabed on Surface Noise Intensity Vector in Shallow Water

Ph. D. **1995** **F. H. Abu-Sitta**

UNIVERSITY OF BATH.

ProQuest LLC
789 East Eisenhower Parkway
P.O. Box 1346
Ann Arbor, MI 48106-1346

Influence of the Seabed on Surface Noise Intensity Vector in Shallow Water

Submitted by F. H. Abu-Sitta

for the degree of

Doctor of Philosophy

of the University of Bath.

1995

Abstract

It is known that the directionality of sea surface noise (pressure squared) in shallow water is related to seabed structure (see for example M. J. Buckingham and S. A. Jones, J. Acoust. Soc. Am. **81** pp. 938-945, 1987). The present project uses a new approach, the main principle being that the sea surface noise acoustic intensity has been considered as a vector quantity. This approach involves resolving the sea surface noise acoustic intensity into its (x,y,z) orthogonal planes. The horizontal plane has shown to be very sensitive to the seabed structure.

The theoretical part of this thesis has introduced three models which represent three different seabed structures. In the first model the seabed was taken to be divided into four equal regions within a circle. In the other two models the seabed was assumed to be uniform over a circle apart from a small area. The second model takes the small area to be a small circle, whereas the third model takes the small area to be a section of an annulus. For these models, the acoustic intensity in the horizontal plane has been shown to be dependent on the structure of the seabed. The second and third models show the capability of this approach in detecting the location and size of the small patch, and the difference in the two seabed types.

The experimental part of the thesis starts with measurements taken in the laboratory. The measurements were taken to examine the ability of the acoustic intensity vector approach for detecting the direction of a harmonic point source and a noise point source. The success in detecting the direction of these sources led to experiments being carried out at sea. These experiments were inconclusive and indicated the difficulties to be encountered in using the seabed related information in the vector intensity in a real survey application.

Acknowledgements

I am sincerely grateful to my supervisor Nick Pace for giving me the opportunity to work in this new area of underwater acoustics. The work described in this thesis is a result of his valuable guidance and encouragement over the period of this research.

I am especially grateful to Mair Jones and Paul Chinnery for many useful discussions and suggestions during the theoretical studies, and for assisting with the preparation and proof-reading of this document.

I would also like to thank all members of the Acoustics Group, past and present, for their support and friendly discussions.

Finally, I wish to express my deepest gratitude to Faiz Obaid, Jehad Abu-Sitta and Abd-Alrazig Abu-Sitta who have encouraged and supported me throughout my time in England.

Table of Contents

Chapter One

1. Introduction and Background

1.1 Introduction

Noise is the unwanted signal. Ambient noise is the noise that exists in the medium because of uncontrolled sources. The underwater ambient noise can be identified with three main sources; natural noise, man made noise and biological activity. Natural noise is mainly caused by the disturbance of the sea surface (caused by wind and rain), earthquake and volcano. Man-made noise arises from traffic noise, industrial activity near the coast and explosives. Biological noise is generated by marine life in the sea, for example whales, fish etc.

The surface noise was found to be the most significant noise source in the ocean[1,2]. In general the presence of this noise is a nuisance. The use of an array of sensors may provide some cancellation of this noise, the degree of cancellation can be expressed by

the array gain. This technique was used in many papers, some of them referred to deep ocean[3-7], while others were employed in shallow water[8-10].

Based upon the above studies, the most important conclusion that has been noticed is that the distribution of the surface noise in shallow water is strongly dependent on the seabed type, the sea surface and the medium of propagation[11]. This leads to the fact that surface noise can be used in order to obtain useful information about the sea environment. These advantages have been addressed in a number of papers, some of them have used the surface noise signal to investigate the weather conditions above the sea[12,13], while others have used the surface noise to classify the seabed[11,14,15].

The interest in this project is to find an alternative method for mapping the seabed with the advantage of using the surface noise. Former methods[11,14,15] were based on measuring the distribution of the noise intensity around the horizontal relative to the hydrophones by measuring the pressure squared which is a scalar quantity. This research is using an entirely different approach. The main concept of the new approach is the development of the use of the surface noise intensity vector. This allows us to measure the magnitude and the direction of the noise intensity. The acoustic surface noise intensity in the horizontal plane (x,y), has been shown to have a greater sensitivity to the structure of the seabed. In order to measure the intensity vector in the three planes, six hydrophones have been used. The pressure midway between the two hydrophones is related to the mean acoustic pressure, whereas the difference between the pressures correspond to the pressure gradient which in turn is proportional to the particle velocity.

1.2 Background and Literature Survey

As this project covers two areas: the advantage of the surface noise in relation to seabed sensing, and the nature of the acoustic intensity vector itself, the following literature survey will split into two main parts. The first discusses the ambient noise in the sea which includes the following topics:-

1.2.1.1 Ambient noise spectrum.

1.2.1.2 Mechanisms of surface noise

1.2.1.3 Surface noise as nuisances

1.2.1.4 Advantage of surface noise

The second part, briefly discusses the acoustic intensity vector which includes the following topics

1.2.2.1 Nature of acoustic intensity vector.

1.2.2.2 Acoustic intensity vector measurement.

1.2.2.3 Mathematical summary of acoustic intensity vector.

1.2.1 Ambient Noise in the Sea

In order to obtain a complete picture of the significant effect of the sea surface noise in the sea, this section begins with an overview of the various main sources of ambient noise in the sea. This review shows that the surface noise dominates over a wide frequency range, which implies that this noise is caused by different processes. A list of the processes which generate surface noise is presented. The final task of this section is to introduce the disadvantage and the advantage of the surface noise.

1.2.1.1 Ambient Noise Spectrum

Under certain conditions various sources of ambient noise were found to dominate in different regions of the ambient noise spectra. A summary of these sources was reviewed in Figure 1.1 [1]. The following review will begin with those sources which are significant at low frequencies, and later will consider the dominant sources at high frequencies, which may be classified as follows:-

- Seismic noise
- Non-acoustic sources
- Biological activity
- Distant traffic
- Surface Noise
- Thermal noise

1.2.1.1.1 Seismic Noise

Seismic noise can be classified into two types: man-made and natural. Man-made seismic noise is caused by explosives (*e.g.* explosives were used in offshore seismic exploration for oil). Natural noise originates by natural phenomena such as earthquakes and volcanoes. Man-made seismic noise in areas such as the North Pacific [16] and the Gulf of Mexico [17] were reported to predominate over ambient noise. In the case of Mexico, impulsive seismic exploration noises were almost at all times audible over a 12-hour period. The larger proportion of the energy from this noise has been observed at frequencies below 100 Hz [1]. As for noise of volcanic origin, observable acoustic pressure has been reported at frequencies up to 500 Hz [1]. Earthquake noise is predominant over ambient noise under 100 Hz [1].

1.2.1.1.2 Non-acoustic Noise

The origins and causes of non-acoustic noise sources in the infrasonic band 1-10 Hz are listed below [2,18]:

1. Tidal currents causes temperature changes, thereby causing piezoelectric transducers to produce a change in voltage. In order to avoid the effect of this noise, hydrophones are recommended to be protected by thermal shields.

2. In placing a hydrophone in the sea at any depth, noise is observed originating from:

A. Turbulent water flowing past the hydrophones thus causing pressure changes on the hydrophone surface

B. Initially steady currents flowing past hydrophones generating pressure fluctuations

C. Self-noise which is created by currents which causes the hydrophone and its mounting to vibrate.

1.2.1.1.3 Biological Noise

Sources of biological noise can be classified into three main types [2]:

A. Crustacean (or shellfish)

B. Marine mammals (such as whales)

C. Certain types of fish (such as croakers)

In certain areas, noise from biological sources is received at frequencies between 10 Hz and 100 Hz. The reasons that marine animals make noises have been classified by biologists, and are listed:

1. Communication; whales are said to communicate between members of a school.

2. Defence, attempting to scare away attackers.

3. Sexual attraction, noise normally made by the male sex only.

4. Pleasurable for a marine animal to make noise, just as in the humming of a tune by a human being.

5. Location, as in the echo-ranging of porpoises.

1.2.1.1.4 Distant Traffic

Distant traffic noise is generated by ships located at distances of around 1000 miles from the measuring hydrophone. The examples summarised below suggests that a major component of ambient noise in the band between 20 and 200 Hz is caused by such noises:

1. Ambient noise, unaffected by wind or weather conditions, arrives at nearly horizontal angles.

2. The shape of the observed ambient noise spectra at this frequency band exactly coincides with the radiated noise spectra of ships.

3. Ambient noise is reported to be higher and less affected by wind where ship traffic is dense, than in areas where traffic is light.

However, the component of distant traffic in ambient noise is a function of transmission loss, number of ships, and the relative position of ships.

1.2.1.1.5 Surface Noise

Knudsen's [19] early studies on the effect of the sea surface on ambient noise were summarised in the widely used Knudsen Curves, which are, straight lines on a logarithmic frequency scale which relate the sea state and wind force to the spectral level of ambient noise within the 100 Hz to 25 kHz frequency range. Wenzs [1] study reached similar findings except at low frequency. In his review, five different areas in shallow and deep ocean with different wind speeds were examined. In some of these areas the wind speed dependence decreases as the frequency decreased to below 500Hz. At 100Hz or lower, little or no dependence was seen. While in other areas, wind speed dependence extended to frequencies as low as 50 Hz. Subsequent studies have indicated the significant dependence of the ambient noise on the wind speed at very low frequencies [20-24]. Generally, the contribution of surface noise has been found to be significant at frequencies above 100 Hz and between 10 and 15 Hz.

In shallow water, in the absence of local shipping and biological noise, the distant noise becomes less significant as the effect of wind noise dominates over its entire frequency spectrum. The weakness in the distant noise arises due to the absence of the favourable propagation paths.

1.2.1.1.6 Thermal Noise

Hydrophone sensitivity is affected at high frequencies by the thermal noise generated by the molecules of the sea. This has been shown by Mellen [25], who computed theoretically the equivalent plane-wave pressure for thermal noise in water. The equivalent noise spectrum level for a nondirectional hydrophone which is perfectly efficient in converting acoustic to electric energy is

$$NL = -15 + 20 \log f \quad \textit{dB re } 1\mu\text{Pa}$$

at ordinary temperatures, where f is the frequency in *kHz*. Given this acoustic background, the spectrum level of the hydrophone rises with frequency at the rate of 6dB per octave (see Figure 1.1), and imposes a limit on the minimum observable pressure level in the sea.

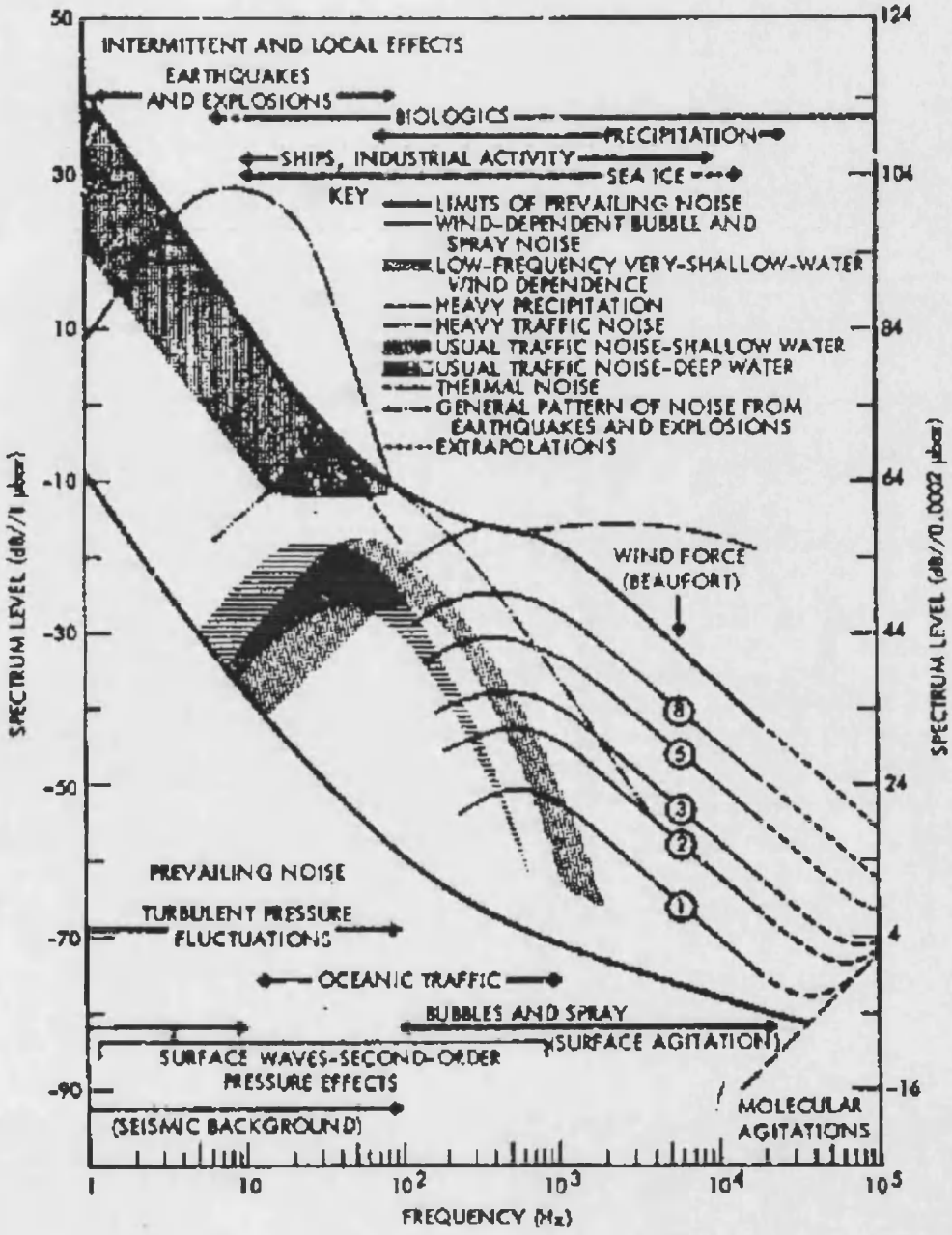

Figure 1.1 Average ambient noise spectrum level in the band 1 Hz to 100 kHz adapted from Wenz [1]

1.2.1.2 The Mechanisms Of Surface Noise

Based upon the previous discussion, under certain conditions, the surface noise is shown to be the significant noise source in the sea over a wide frequency range of the ambient noise spectrum. This suggests that surface generated noise might be caused by different mechanisms. These mechanisms can be classified into four parts, each part dominated in a different portion of the overall frequency range. In the following section a brief review of these mechanisms will be given. The review will start with those mechanisms which dominate in the low frequency region, and end with those mechanisms which become significant at high frequencies.

1.2.1.2.1 Surface Wave Interaction

In an early study, Longuet-Higgins [26] showed that the interaction of two surface waves of the same wavelength travelling in opposite directions would form a standing wave whose acoustic pressure does not decrease with depth. Based upon this formula, Marsh [27] presented a theory attributing the ambient noise spectra of Knudsen, Alford and Emling [19] to the motion of surface waves. Good agreement was found between theory and experiment. This mechanism was also found to be in good agreement with measured data below 10 Hz [22].

1.2.1.2.2 Wind Turbulence

In 1969 Isakovich and Kur'yanov [28] were the first to achieve a theoretical approach to describe the energy transferred from the wind field into the underwater acoustic field as a result of turbulent pressure fluctuations in the atmosphere near the ocean surface. The comparison of their theoretical model with the experimental results which were available at the time, shows that the direct action of the wind on the water surface is possibly the principal cause of the generation of low-frequency noise. This model was modified ten years later by Wilson [23]. He showed that the wind speed and the frequency dependence of the calculated source spectrum level agrees well with data measured in the Northeast pacific ocean (this data was not available to Isakovich and Kur'yanov at the time of their study) for low shipping noise conditions in the infrasonic band 5 to 50 Hz.

1.2.1.2.3 The Interaction of Surface Waves and Oceanic Turbulence

This mechanism, has been studied by Goncharov [29]. Under certain assumptions concerning the properties of the turbulence, he shows that the estimated source spectrum levels are in reasonable agreement with experimental data at 10 to 100 Hz.

1.2.1.2.4 Bubbles and spray

Air bubbles at or near the sea surface is due to trapped air in the water. This trapped air is caused by a number of different processes such as breaking waves, surface turbulence, and water drop impact. Such air bubbles were found to be dominant in the frequency band 50 Hz to 10 kHz of the ambient noise spectrum. Oscillation and collapsing of air bubbles was suggested to be behind the emission of this noise. The oscillating bubbles were caused by surface agitation, resulting from the action of wind, while the collapsing process occurs when the total external pressure surrounding the air-vapour cavity of sufficient radius is reduced by an amount referred to as the threshold cavitation pressure, with the result that the bubble explodes. The above conclusion was first mentioned by Wenz in 1962 [1]. In a different study[30], bubbles were considered as a significant contribution to sea noise for frequencies in the region 1-60 kHz at the instant of their formation.

1.2.1.3 Surface Noise As Nuisance

Lots of attention has been focused on surface generated noise. The reason for this is due to the major contribution of the surface noise on the range of sonar systems. Numerous studies have been made in order to reduce the effect of this noise on the desired signals [3-10]. The use of an array of sensors may provide some cancellation of the noise. An early theoretical model for deep water noise was proposed by Cron

and Sherman [3], they developed both a volume and surface noise model. In the surface noise model they assumed that the surface noise consists of noise sources uniformly distributed on a large circular area of a plane, and noise sources are assumed to be directional. They were the first to be able to present an analytical expression for the cross correlation function between the output of a pair of sensors for directional noise. This model in effect assumes that there is no energy reflected from the seabed.

In order to be more realistic, especially in shallow water, the effect of the sea bottom should be considered. Adding this parameter has resulted in a significant effect on the distribution of the noise field in the ocean. Kuperman and Ingenito [9] were able to show the great influence of the seabed. Their results indicates that the noise field depends on whether the bottom is a low-loss or high-loss boundary. In the high-loss case the contribution of energy at the receiver is due to the far-field noise (multi reflection via long paths) being minimal, which is a result of the severe attenuation in the seabed. Therefore, the main contribution to the detected noise is due to continuous radiation from the near sources, *i.e.* direct waves from the surface which do not interact with the bottom. In the low-loss case the contribution from the multiple reflections can not be neglected, due to the low attenuation in the seabed. The result of this is that the distant sources, extending over a very large area, make the main contribution to the noise field via discrete model propagation over long distances.

1.2.1.4 The Advantage Of Surface Noise

The above discussion gives a brief review of the work done in trying to understand the characteristics of the ambient noise in the sea in order to reduce its effect on the sonar systems. One of the conclusions from these studies is that the surface noise can be used to obtain useful information about the seabed, the sea surface and the medium of propagation.

Buckingham and Jones [11] were the first to show that surface generated noise in shallow water can be used to obtain useful information about the seabed. They used the fact that grazing angles less than the critical angle θ_c are totally internally reflected, whereas rays with grazing angles greater than θ_c are heavily attenuated on encountering the seabed. In the absence of interference from local shipping, the noise field shows a peak symmetrical distribution on the horizontal. This distribution enabled them to measure the critical angle θ_c, and hence are able to compute the compressional sound speed in the seabed. In their experiment a vertical-line-array sonobuoys was used in order to measure the vertical directionality and the vertical coherence at six sites around the U. K. coast. Their model showed very good agreement with independent seismic surveys available in the Celtic sea. The critical angle estimated by Buckingham and Jones's measurements is θ_c=26 whereas the critical angle obtained from more conventional seismic measurements is θ_c=28.

In a different approach B.M.F. Chapman [14] has used the surface generated noise in order to obtain useful information about the seabed. In his simple model the following assumptions were made:-

i- The sources of the surface noise were uniformly distributed at the sea surface and each of them has a dipole directivity.

ii- The ocean was assumed to be non-absorbing, isospeed layers of constant depth, so that acoustic rays are straight lines and the acoustic intensity spreads spherically from point sources.

iii- The reflectivity of the seabed was based on the plane-wave reflection coefficient at a plane boundary between a homogeneous fluid and a homogeneous, lossy, elastic solid.

iv- Ray theory was used, the noise intensity received from any direction after L reflections with the sea surface and the seabed along a multi-linear path, is equivalent to intensity along a linear path, arriving in the same direction from a source located on the L^{th} image plane.

Six different seabed types were studied, silt, fine sand, coarse sand, gravel, glacial till, and soft sedimentary rock. The acoustic noise intensity was observed above and below the horizontal relative to the hydrophone. The noise intensity arriving from a particular patch is actually a combination of direct rays and multi reflected rays from

particular patch is actually a combination of direct rays and multi reflected rays from the sea surface and the seabed. This model of noise directionality exhibits a strong sensitivity to the seabed type. For low loss seabed (fine sand and coarse sand) the model shows good agreement with the results of Buckingham and Jones.

The above simple model was modified by H. Dupuis and A Weill [15] to be more realistic. In addition to the previous assumptions, the model takes into account the water absorption and the seabed attenuation. The model also considered the shallow water as a three layer homogeneous structure: water/sediment/sub-bottom. Two typical seabed configurations have been studied. One with high contrast between velocity and density, the other with low contrast. Their results showed that the amount of acoustic intensity arriving at the hydrophone increases more or less rapidly as a function of the frequency and the depth, which is a result of the effect of the water attenuation and the seabed reflectivity. The critical angle of the seabed was observed to have a significant effect on the acoustic intensity arriving at the hydrophones. However, the contribution of the seabed decreases with increasing depth. For depths larger than 300 m and for the higher part of the frequency range, the effect of the seabed is negligible.

1.2.2 Acoustic Intensity Vector

The acoustic intensity vector has been known for a long time to be the most powerful tool for identifying the distribution and the direction of a noise source. However, it is only lately that the acoustic intensity vector has been employed in practical applications. The delay in the implementation of the acoustic intensity is due to the difficulty in measuring it. The difficulty in measuring this quantity lies in the difficulty in measuring the particle velocity, since acoustic intensity vector is the product of the pressure and the particle velocity.

The following literature review is split into three sections, the first summarising the studies concerning the nature of the complex vector intensity, the second assessing experimental work which measures the acoustic intensity as a vector quantity, and the third summarises the mathematical relationships of the acoustic intensity vector.

1.2.2.1 The Nature Of The Complex Intensity

The concept of a "complex acoustic intensity" was proposed to give a qualitative description of the acoustic field by use of the ***reactive*** intensity (imaginary part) to complement descriptions of the net power flow from the ***active*** intensity (real part). Moreover, the ***vectorial*** studies of these intensities leads to a better understanding of the sound field properties. The vectorial nature of the active and the reactive

intensities, can be understood by applying both the curl and the divergence of the complex intensity. The curl of the active intensity is non-zero (rotational), meaning that the active intensity can flow in closed paths, while the curl of the reactive intensity is zero (irrotational). Similarly, taking the divergence of the active and the reactive intensities shows that the active part is zero and the reactive part is solenoidal. These results have been discussed by Tichy[31], who expressed the complex intensity in terms of the propagating velocity and the non-propagating velocity. Some other interesting results have been achieved in this work, being that using the active intensity alone in the near field will make the source identification difficult. Such radiation from these sources is noted from taking the far-field as a point source. The reactive intensity, originating from the sources, is especially useful since the vectors point out areas of maximum medium flow, showing very clearly the source distribution.

J. Pascal [32] did an interesting analysis of the complex intensity vector by splitting the active intensity field into two other fields (scalar and vector quantity). Taking the example of interfering waves, conclude that the term corresponding to the irrotational field is the energy which propagates to the far-field, and the vector term represents the near-field intensity responsible for circulating flow.

1.2.2.2 Acoustic Measurement

Schultz [33] was one of the first to consider the measurement of the acoustic intensity vector due to a point source. His proposal was based on the definition of the intensity

as the time averaged product of the pressure and the particle velocity. The instrument employed for measuring the pressure and pressure gradient, was an acoustic wattmeter. This device was able to give a direct reading of the acoustic intensity over 50 dB in the frequency range up to 10 kHz. The technique used two pressure microphones for detection. The sum of the signal from the two microphones gave a value for the pressure at the midway point between the microphones, and the difference between the two pressures gave the pressure gradient. This method is an approximation to the actual pressure and pressure gradient at the field point of interest. This approximation can cause significant error, as will be discussed later. Electrical modifications were used in order to measure the particle velocity. By multiplying the pressure with the particle velocity and averaging them in a moving-coil dynamometer the acoustic intensity vector is obtained.

The above method has formed the original basis for acoustic intensity vector measurement. However a more general approach has been adopted to measure the intensity. This new approach relies on the relationship between the cross spectrum of the pressure signal from the two closely spaced microphones and the resulting intensity spectrum. The imaginary part of the cross spectral density of the two microphone measurements yields a value proportional to the acoustic intensity vector. It should be noted that, because a two microphone pressure method is used, this approach still relies on the finite difference approximation. Fahy [34] was the first to employ this approach which is now the standard method for the measurement of the acoustic intensity vector.

The accuracy of the method described above is strongly dependent upon the validity of the approximations employed. Three sources of error are listed below and is followed by a brief discussion of each.

i) error due to the finite difference approximation,

ii) error due to the near-field effect,

iii) error due to the instrumentation phase mismatch.

1.2.2.2.1 The Finite Difference Approximation

As shown in Figure 1.2, the approximation for measuring the pressure and the pressure gradient (the pressure gradient is proportional to the particle velocity) at the midway between the two microphones is given by,

$$P \approx \frac{P_1 + P_2}{2} \quad \text{and} \quad \frac{\partial P}{\partial r} \approx \frac{P_2 - P_1}{\Delta r}$$

These expressions for the pressure and pressure gradient depends strongly on choosing the microphone spacing and the wavelength. Consequently, the approximation is reasonable at low frequencies, where the wavelength is large compared to the microphone spacing Δr. In contrast, the approximation is poor when the frequency becomes high. If the wavelength is of the order of the spacing of the microphones, or even smaller, the measured pressure and the pressure gradient will be wrong.

Thompson and Tree [35] studied the effects of the finite difference approximation for several ideal sources (monopole, dipole and quadrapole sources). The results of their study will be briefly summarised in the following points:-

i) An accurate measurement of the acoustic intensity vector can be achieved from the near-field with the two microphone technique. The accuracy of this measurement depends on definite optimum ranges of the measurement parameters $k\Delta r$ and $\frac{\Delta r}{r}$, (where k, r and Δr are the wave number, the distance from the source to the microphone and the microphones separation, respectively).

ii) It was observed that, the optimum values of these parameters decreases with increasing number of sources.

iii) The magnitude of the possible errors suggests that selection of measurement parameters must be given careful consideration.

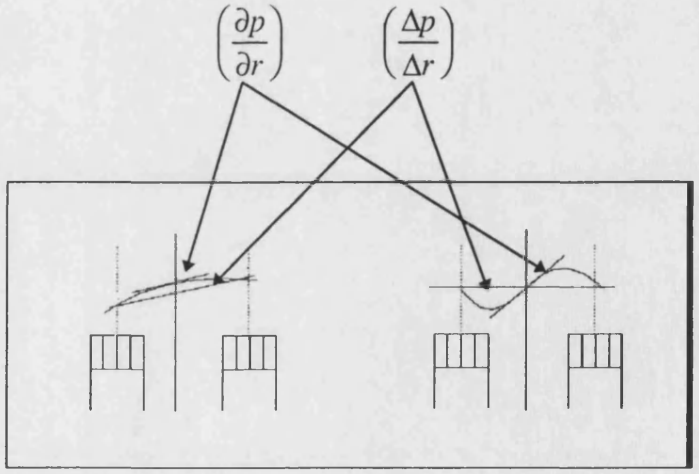

Figure 1.2 Illustration of the error due to the finite difference approximation.

1.2.2.2.2 Error Due To The Near-Field

This error occurs if the intensity changes within the microphone spacing. However, as indicated from the above study, the error is not only a function of the separation distance between the two microphones, but also depends on the distance between the sources and the probe. To overcome this problem, it was suggested by Thompson and Tree [35] that the microphone separation must be much smaller than the distance between the sources and the pressure microphones $\Delta r << r$. In this project, because the measurement is done in the far field, this error will be irrelevant.

1.2.2.2.3 Instrumentation Phase Mismatch

As shown in Figure 1.2, we note that for $\lambda << \Delta r$ the approximation of measuring the pressure and the pressure gradient is incorrect. As the wavelength increases the measurement accuracy will increase. Consequently, the finite difference error theoretically tends to zero as the frequency goes to zero.

However, at low frequencies, the actual phase difference between the two pressure signals becomes very small and is eventually beyond the accuracy of the instrument. The most convenient way of avoiding this error at low frequency is to increase the value of the physical phase difference, which corresponds to increasing the microphone

spacing. S Gade [36] illustrates the error caused by a negative instrumentation phase mismatch of 0.3^o for several microphone spacings.

It has been shown by the previous discussion that for a given microphone spacing and measurement tolerance there exists an upper and lower frequency limit. For the practical applications, a compromise must be found and a suitable microphone spacing chosen that covers the frequency band of interest.

1.2.2.3 Summary Of The Complex Acoustic Relations

The purpose of this section is to introduce the basic relationships between the instantaneous acoustic intensity and the complex acoustic intensity.

1.2.2.3.1 Active Intensity

The product of the in-phase components of pressure p and particle velocity $\vec{u}$ at a distance r from the source yields the instantaneous active acoustic intensity,

$$\vec{I}_i(r,t) = [Re\{p(r,t)\}][Re\{\vec{u}(r,t)\}] \qquad (1.1)$$

or

$$\vec{I}_i(r,t) = [Im\{p(r,t)\}][Im\{\vec{u}(r,t)\}] \qquad (1.2)$$

The active intensity is found by taking the time average,

$$\langle \vec{I}_a \rangle = \frac{1}{T}\int_0^T \{Re[p(r,t)]\, Re[\vec{u}(r,t)]\}dt = Re\left(\frac{1}{2}p\vec{u}^*\right) \quad (1.3)$$

or

$$\langle \vec{I}_a \rangle = \frac{1}{T}\int_0^T \{Im[p(r,t)]\, Im[\vec{u}(r,t)]\}dt = Re\left(\frac{1}{2}p\vec{u}^*\right) \quad (1.4)$$

This is the definition of the active intensity which represents the transmitted energy.

1.2.2.3.2 Reactive Intensity

The product of the pressure p out of phase with the particle velocity $\vec{u}$ yields the instantaneous reactive intensity, and is given by

$$\vec{I}_i(r,t) = [Re\{p(r,t)\}][Im\{\vec{u}(r,t)\}] \quad (1.5)$$

or

$$\vec{I}_i(r,t) = [Im\{p(r,t)\}][Re\{\vec{u}(r,t)\}] \quad (1.6)$$

The time average of this equation corresponds to the stored energy or standing wave in the near-field, which is called the reactive intensity. However, the mathematical expression for this quantity can be represented as follows,

$$\langle \vec{I}_{rea} \rangle = \frac{1}{T}\int_0^T \{Re[\,p(r,t)]\, Im[\vec{u}(r,t)]\}dt = Im\left(\frac{1}{2}p\vec{u}^{*}\right) \qquad (1.7)$$

or

$$\langle \vec{I}_{rea} \rangle = \frac{1}{T}\int_0^T \{Im[\,p(r,t)]\, Re[\vec{u}(r,t)]\}dt = Im\left(\frac{1}{2}p\vec{u}^{*}\right) \qquad (1.8)$$

Chapter Two

2. A Study of a Point Source Near a Surface

2.1 Introduction

Generally, surface generated noise is assumed to consist of uniformaly distributed point sources lying immediately beneath the sea surface. This distribution will allow the sources to have a dipole radiation. In order to represent a model of the surface noise intensity vector, it was suggested to begin with a study of a single harmonic point source located near the surface. In this study the definition of the acoustic intensity vector will be used. This definition will enable us to present the magnitued and the direction of the propagating energy. The propagating energy will be represented by arrow notation. The size of the arrow corresponds to the magnitued of the propagated energy, while its angle represents the direction. In this chapter, the characteristic of the acoustic intensity vector for a point source located near the sea surface and near the seabed will be considered. Placing a point source near the sea surface shows that the total acoustic intensity vector can be divided into four regions, the near field, the interference field, the far field, and the dipole

radiation. These regions occur at certain positions dependent on the position of the source, the receiver, the sea surface and the frequency. Placing a point source close to the seabed (different arbitrary values of the reflection coefficient has been chosen) may give us an insight into the significance of the acoustic intensity vector, which describes the magnitude and the direction of propagating energy.

2.2 Point Source Located Near a Surface

The total acoustic pressure at a point Q (see Figure 2.1), due to a harmonic point source located near a surface is the sum of the direct and reflected rays, which is represented as follows

$$P(r_1, r_2, t) = P(r_1, t) + P(r_2, t) \qquad (2.1)$$

$P(r_1, t)$ corresponds to the direct acoustic pressure, which is expressed mathematically as follows

$$P(r_1, t) = \frac{A}{r_1} exp\left[j(\omega t - kr_1)\right] \qquad (2.2)$$

where:

- A is the amplitude of the signal,
- ω and k are the angular frequency and the wave number respectively,
- r_1 represents the path length from the source to the receiver, which from the gometery in Figure 2.1 can be expressed in terms of the horizontal distance x and the depth z of the reciever and the source depth h as follows

$$r_1 = \sqrt{x^2 + (z-h)^2}$$

$P(r_2,t)$ corresponds to the acoustic pressure arrived at the receiver via the surface which is given as follows

$$P(r_2,t) = \frac{RA}{r_2} exp\left[j(\omega t - kr_2)\right] \qquad (2.3)$$

where ;

- R is the reflection coefficient of the surface,
- r_2 represents the distance from the image of the source to the receiver, similarly this can be written in terms of the horizontal distance x and the depth z of the reciever and the source depth h as follows

$$r_2 = \sqrt{x^2 + (z+h)^2}$$

$$r_2 = \sqrt{x^2 + (z+h)^2}$$

In order to calculate the total particle velocity at the point Q Euler's equation is now used;

$$\vec{U}(r_1, r_2, t) = -\frac{1}{j\omega\rho}\nabla P(r_1, r_2, t)$$

$$= -\frac{1}{j\omega\rho}\nabla\left(P(r_1)exp\left[j(\omega t - \phi(r_1))\right] + P(r_2)exp\left[j(\omega t - \phi(r_2))\right]\right) \qquad (2.4)$$

Here for simplicity the following terms have been used

$$P(r_1) = \frac{A}{r_1}, \qquad P(r_2) = \frac{AR}{r_2}, \qquad \phi(r_1) = kr_1, \qquad \phi(r_2) = kr_2$$

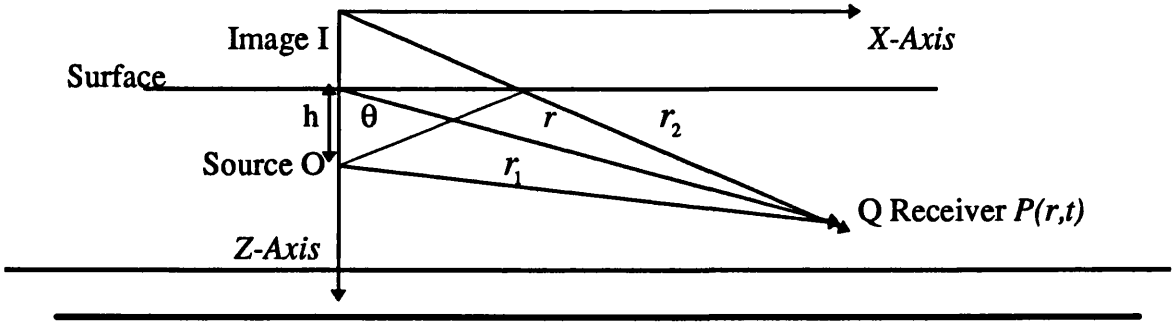

Figure 2.1 Illustrates the direct and the surface reflected paths between the source at O and the receiver at Q. I is the image of O.

The total instantaneous acoustic intensity vector is obtaind by multiplying the in-phase component of the acoustic pressure and the particle velocity at the point Q

$$\vec{I}_i(r_1,r_2,t) = Re\left(P(r_1,r_2,t)\right) Re\left(\vec{U}(r_1,r_2,t)\right) \quad (2.5)$$

where from equations (2.1), (2.2) and (2.3) the real part of the acoustic pressure is

$$Re\left(P(r_1,r_2,t)\right) = \left(P(r_1)C_1 + P(r_2)C_2\right) \quad (2.6)$$

and from equation (2.4) the real part of the particle velocity is

$$\mathrm{Re}\left(\vec{U}(r_1,r_2,t)\right) = -\frac{1}{\omega\rho}\left(\nabla P(r_1)S_1 - P(r_1)\nabla\phi(r_1)C_1 + \nabla P(r_2)S_2 - P(r_2)\nabla\phi(r_2)C_2\right). \quad (2.7)$$

In order to reduce the complexity of equations (2.6) and (2.7), the following variables have been used

$$S_1 = sin\left(\omega t - \phi(r_1)\right), \qquad C_1 = cos\left(\omega t - \phi(r_1)\right),$$

$$S_2 = sin\left(\omega t - \phi(r_2)\right), \qquad C_2 = cos\left(\omega t - \phi(r_2)\right).$$

By substituting equations (2.6) and (2.7) into equation (2.5) we obtain

$$\vec{I}_i = -\frac{1}{\omega\rho}\left(\left[P(r_1)C_1 + P(r_2)C_2\right]\left[\nabla P(r_1)S_1 - P(r_1)\nabla\phi(r_1)C_1 + \nabla P(r_2)S_2 - P(r_2)\nabla\phi(r_2)C_2\right]\right)$$

After multiplication of the terms in the square brackets this becomes

$$\vec{I}_i = -\frac{1}{\omega\rho}\left(L_1L_2 - P^2(r_2)\nabla\phi(r_2)C_2^2 - P^2(r_1)\nabla\phi(r_1)C_1^2 - P(r_1)P(r_2)L_3C_1C_2\right) \qquad (2.8)$$

Where,

$$L_1 = \left[P(r_1)C_1 + P(r_2)C_2\right],$$

$$L_2 = \left[\nabla P(r_1)S_1 + \nabla P(r_2)S_2\right],$$

$$L_3 = \left[\nabla\phi(r_2) + \nabla\phi(r_1)\right].$$

Equation (2.8) represents the total instantaneous intensity due to a point source located near the surface. The time average of the acoustic intensity vector can be obtained either by taking the time average of equation (2.8), or by using the real part of the complex acoustic intensity (see section (1.2.2.3.1) equation (1.3)). However both reach the same result, which is

$$\langle \vec{I}_a \rangle = \frac{1}{2\omega\rho}\left(P^2(r_1)\nabla\phi(r_1) + P^2(r_2)\nabla\phi(r_2) + P(r_2)P(r_1)L_3\cos(\omega\tau) + L_4\sin(\omega\tau)\right) \quad (2.9)$$

where τ is the difference in time between the direct ray and the reflected ray, and

$$L_4 = \left[P(r_1)\nabla P(r_2) - P(r_2)\nabla P(r_1)\right]$$

equation (2.9) represents the time average of the acoustic intensity vector (active intensity) at the point Q due to a point source located at the surface.

2.3 A Point Source Located Near the Sea Surface

The nature of the active intensity vector (the time average of the propagating energy) due to a point source located near the sea surface is easily obtained by substituting the reflection coeffeicient R=-1 in equation (2.9). The equation is then rewritten in terms of the horizontal distance x and the depth z of the hydrophone and the source depth h as follows,

$$\langle \vec{I}_a \rangle_x = \frac{A^2}{2\omega\rho}[B_1 \sin(\omega\tau) - B_2 \cos(\omega\tau) + B_3]\hat{xi} \qquad (2.10a)$$

$$\langle \vec{I}_a \rangle_z = \frac{A^2}{2\omega\rho}\left([B_1 \sin(\omega\tau) - B_2 \cos(\omega\tau) + B_3]z\hat{k} + [B_4 \sin(\omega\tau) - B_2 \cos(\omega\tau) + B_3]h\hat{k}\right) \qquad (2.10b)$$

Where

$$B_1 = \left(\frac{1}{r_2^3 r_1} - \frac{1}{r_1^3 r_2}\right), \qquad B_2 = \frac{k}{r_1 r_2}\left(\frac{1}{r_1} + \frac{1}{r_2}\right),$$

$$B_3 = k\left(\frac{1}{r_1^3} + \frac{1}{r_2^3}\right), \qquad B_4 = \left(\frac{1}{r_2^3 r_1} + \frac{1}{r_1^3 r_2}\right).$$

Equations (2.10a) and (2.10b) represents the acoustic active intensity (time average of the acoustic intensity) in the x and z directions respectively due to a point source located near the sea surface. Figure 2.2 represents the magnitude of this intensity in $\left(\frac{watt}{m^2}\right)$ versus the horizontal distance between the source and the hydrophone in metres.

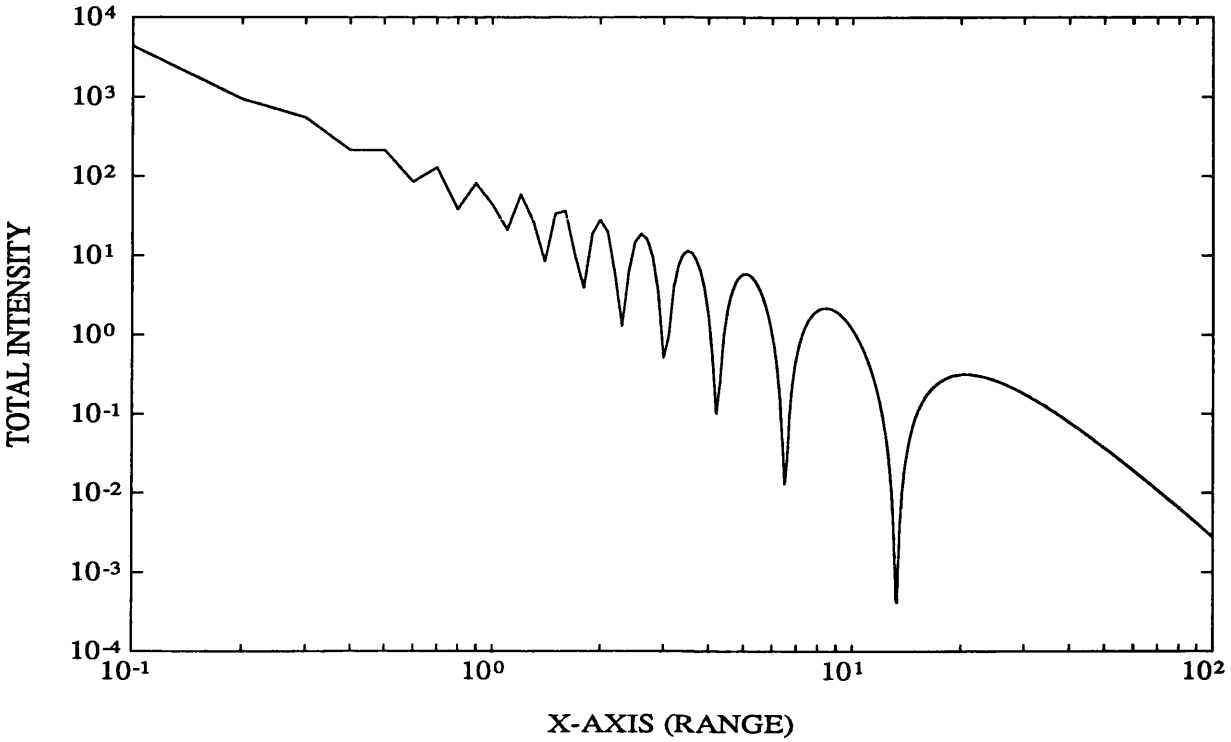

Figure 2.2 represents the total acoustic active intensity against the horizontal distance x in metres, where f=10 kHz, h=1m and R=-1

From equations (2.10a) and (2.10b) and from Figure 2.2, the acoustic active intensity field divides into four regions as follows

2.3.1 Near-Field

At a range close to the source, where $r_2 >> r_1$, the second term in equation (2.1) is insignificant and the intensity falls off inversely as the square of the direct distance r_1.

With increasing range, the second or the interference term becomes increasingly important.

2.3.2 Interference field

In this region strong peaks and nulls are observed in the received signal, as range increases. In this region the two paths may be taken to be of equal length, so that we can write $r_1 = r_2 = r$. From equations (2.10a) and (2.10b) the acoustic active intensity now becomes,

$$\langle \vec{I}_a \rangle = \langle \vec{I}_a \rangle_x + \langle \vec{I}_a \rangle_z = \frac{A^2 k}{\omega \rho r^2}\left((1 - cos(\omega\tau))\hat{r} + \frac{h}{r^2} sin(\omega\tau)\hat{k} \right)$$

Where

$$\hat{r} = \frac{\left(x\hat{i} + z\hat{k}\right)}{\sqrt{x^2 + z^2}}$$

For a source located near the surface $r >> h$, we get

$$\langle \vec{I}_a \rangle = \frac{A^2}{\rho c r^2}(1 - cos(\omega\tau))\hat{r}$$

To evaluate the time difference between the two paths, we note that

$$r_1^2 = x^2 + (z-h)^2 = x^2 + z^2 - 2hz + h^2$$

$$r_2^2 = x^2 + (z+h)^2 = x^2 + z^2 + 2hz + h^2$$

$$r_2^2 - r_1^2 = (r_2 + r_1)(r_2 - r_1) = 4hz \Rightarrow \Delta r = \frac{4zh}{2r}$$

where $\Delta r = r_2 - r_1$ and $2r = r_2 + r_1$ or $\tau = \frac{\Delta r}{c} = \frac{2zh}{cr}$

So

$$\langle \vec{I}_a \rangle = \frac{A^2}{\rho c r^2}\left(1 - \cos\left(\frac{4\pi zh}{\lambda r}\right)\right)\hat{r} \qquad (2.11)$$

where $\frac{\omega}{c}$ has been replaced by $\frac{2\pi}{\lambda}$. If we define a reference distance to be $r_0 = \frac{4zh}{\lambda}$, the above equation can be rewritten as

$$\langle \vec{I}_a \rangle = \frac{A^2}{\rho c r^2}\left(1 - \cos\left(\frac{\pi r_0}{r}\right)\right)\hat{r} \qquad (2.12)$$

We find that $\left|\langle \vec{I}_a \rangle\right|$ has zeros at $r/r_0 = 1/2, 1/4, 1/6, \ldots\ldots$, and has a maximum when $r/r_0 = 1, 1/3, 1/5, 1/7, \ldots\ldots$ Thus the interference field consists of a series of maxima and minima.

2.3.3 Far Field

In equation (2.12), the argument of the cosine term becomes small when r becomes large. If this term is expanded in terms of the powers of its argument,

$$\cos\left(\frac{\pi r_0}{r}\right) = 1 - \left(\frac{\pi r_0}{r}\right)^2 + \ldots\ldots\ldots$$

and terms of order higher than r_0^3 ignored, we obtain

$$\langle \vec{I}_a \rangle = \frac{A^2}{\rho c r^2}\left(\frac{\pi r_0}{r}\right)^2 \hat{r}$$

and we note that the active intensity falls off inversely as the fourth power of the range.

2.3.4 Dipole Radiation

In Figure 2.1, if we define an angle θ such that $cos\theta = \frac{z}{r} = \frac{z}{r_1} = \frac{z}{r_2}$ then equation (2.11) becomes,

$$\langle \vec{I}_a \rangle = \frac{A^2}{\rho c r^2}\left(1 - cos\left(\frac{4\pi h cos\theta}{\lambda}\right)\right)\hat{r}$$

For small arguments of the cosine, for example, for a low frequency source near the surface, the preceding equation becomes

$$\langle \vec{I}_a \rangle = \frac{A^2}{\rho c r^2}\left(\frac{4\pi h}{\lambda} cos\theta\right)^2 \hat{r}.$$

This equation demonstrates the dipole radiation for a point source located near the sea surface. However this approximation is valid only when the depth of the source is small compared to the distance of the measurement. These results are illustrated in Figure 2.3.

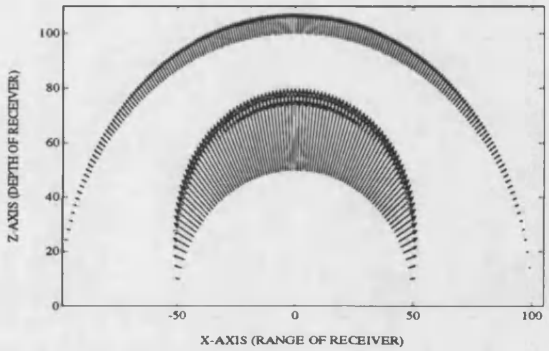

Figure 2.3a h=0.045m shows the dipole radation of a point source located immediately beneath the sea surface

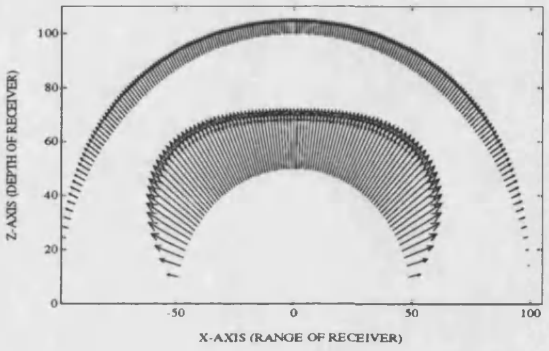

Figure 2.3b h=0.1m, behaves less like a dipole as the source depth increases.

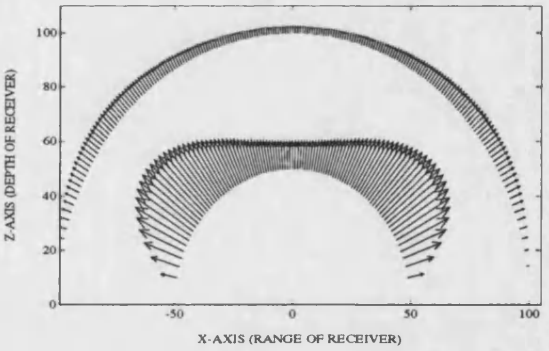

Figure 2.3c h=0.12m for greater source depth there is no dipole effect.

Figure 2.3 Shows the acoustic intensity $\left(\frac{watt}{m^2}\right)$ in terms of its magnitude and direction due to a point source located near the sea surface, f=5kHz, R=-1.

2.4 A Point Source Located Near Different Types of Seabed

An interesting result can be obtained from equation (2.9) by taking different values of the reflection coefficient. Figure 2.4a shows that for a reflection coefficient of zero (one source) the total acoustic intensity falls off as the inverse square of the range *r*. When the reflection coefficient equals 0.2 as in Figure 2.4b we note that the magnitude of the total intensity again falls off, however this time the change is not smooth, but contains peaks and nulls. The peaks and nulls are due to interference between the direct and reflected waves. Consequently, in Figure 2.4c where the reflection coefficient has been further increased to 0.4, the peaks and nulls also increase.

The information in Figure 2.4 can be expressed, by the use of an arrow notation. The size of the arrow represents the magnitude and its inclination represents the angle. Figure 2.5 illustrate the results plotted by this representation.

The main purpose of the above discussion is to show how a vector field map of the acoustic active intensity enables the investigator to quickly visualize how the sound energy propagates. However, it may be easy from the geometry to predict the direction of the acoustic intensity vector due to a point source located near a surface, but it is hard to imagine how noise control could ever be accomplished without this vector field information.

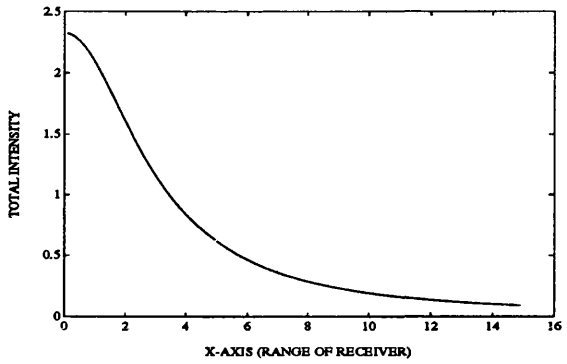

Figure 2.4a R=0, the total acoustic intensity falls off as $\frac{1}{r^2}$.

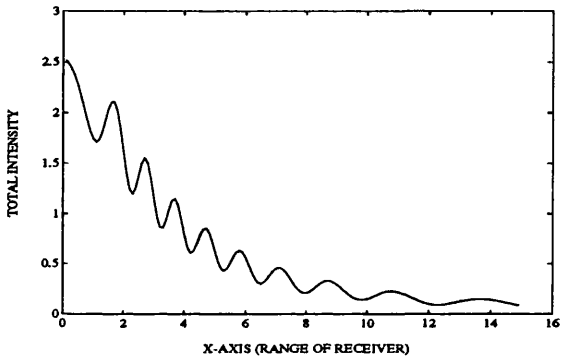

Figure 2.4b R=0.2, the total acoustic intensity falls off with peaks and troughs superimposed.

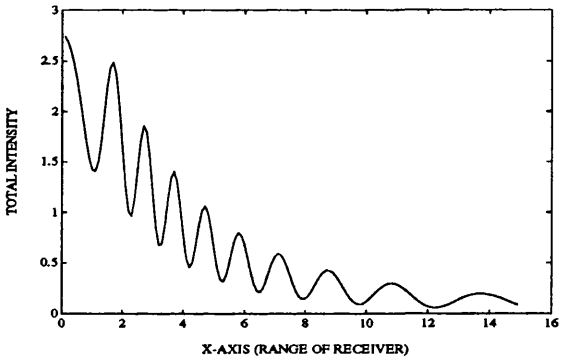

Figure 2.4c R=0.4, the magnitude of the peaks and troughs are greater.

Figure 2.4 Shows the magnitude of the total acoustic intensity $\left(\frac{watt}{m^2}\right)$ versus the horizontal distance between the source and the receiver for different values of reflection coefficient, f=5kHz, h=2m, z=5m.

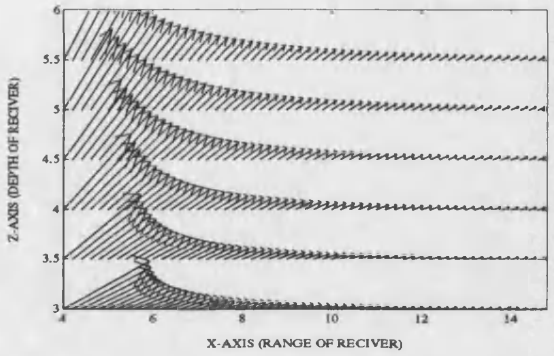

Figure 2.5a R=0, shows the distributed acoustic intensity due to a point source in free space.

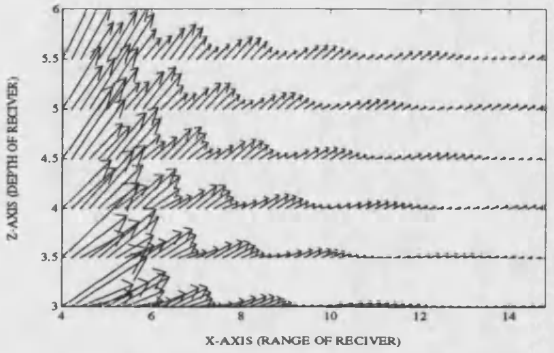

Figure 2.5b R=0.2, the direction of the acoustic intensity becomes smaller as the horizontal distance of the receiver increases. The peaks and troughs are caused by the interference between the direct and reflected rays

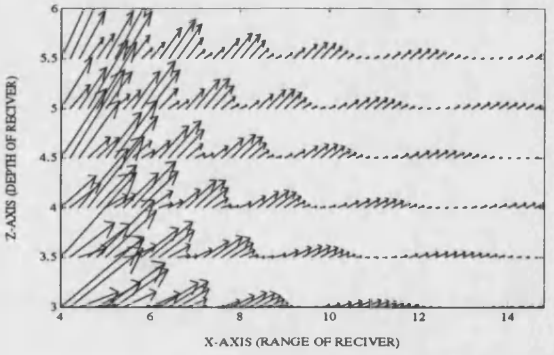

Figure 2.5c R=0.4, greater interference between the direct and the reflected rays caused by an increase in the reflection coefficient.

Figure 2.5 Shows the acoustic intensity $\left(\frac{watt}{m^2}\right)$ in terms of its magnitude and direction for a point source located near different seabed, where f=5kHz, h=2m.

Chapter Three

3. Model of the Surface Noise Intensity Vector

3.1 Introduction

In the previous chapter, the nature of the acoustic intensity vector due to a harmonic point source located near a surface was discussed. The presence of a point source lying immediately beneath the sea surface was shown to produce a dipole radiation. In this chapter, an infinite number of random, independent point sources will be considered. These sources are assumed to be distributed uniformly over a large circular plane lying immediately below the sea surface.

This chapter will begin with a study of the surface noise intensity vector in deep ocean where the effect of the seabed is insignificant. Following this, a model of the surface noise intensity vector in shallow water will be presented. This model shows that the acoustic intensity in the plane (x,y) is strongly dependent on the structure of the seabed. In order to clarify the nature of this dependence, a simple model in terms of

the seabed structure is given. In this simple model, the seabed has been divided into four equal regions. Despite the fact that this model will not be practically achievable, it will help to give a better understanding of the nature of the acoustic intensity vector in shallow water.

3.2 Deep Ocean Model

Surface noise can be considered to consist of an infinite number of independent random point sources distributed uniformly immediately under the sea surface. This distribution will allow each source to act as a dipole with directivity given by $S(\theta) = cos^2(\theta)$, where θ is the angle from the normal (see Figure 3.1). Before presenting the model the following assumptions have been made:-

1. The sea was assumed to be non absorbing. In addition there is no variation in the sound speed with depth.

2. Accordingly, this allows the acoustic rays to be represented by straight lines with the intensity of the sound diminishing as $\frac{1}{r^2}$, where r is the distance between the source and the receiver.

3. The seabed is assumed to be homogeneous, loosely fluid, extending to infinity.

Based upon the above assumptions and Figure 3.1, the form of the acoustic intensity in the *r*-direction at a receiver at depth *z* due to a single point source can be expressed as follows :-

$$\vec{I}_r = \frac{S(\theta)}{r^2}\hat{r} = \frac{cos^2\theta}{r^2}\hat{r} \qquad (3.1)$$

where the term $\frac{1}{r^2}$ represents the spherical spreading, while the term $\hat{r}$ corresponds to the unit vector. Resolving the above equation into its components gives the following:-

$$\vec{I}_z = \frac{cos^2\theta}{r^2}cos(\theta)\hat{z} \qquad (3.2)$$

$$\vec{I}_x = \frac{cos^2\theta}{r^2}sin(\theta)cos(\varphi)\hat{x} \qquad (3.3)$$

$$\vec{I}_y = \frac{cos^2\theta}{r^2}sin(\theta)sin(\varphi)\hat{y} \qquad (3.4)$$

where the terms $cos\theta$ and $sin\theta$ resolves the form of the acoustic intensity in the z-direction and the horizontal plane (x,y) respectively, while the terms $cos\varphi$ and $sin\varphi$ further resolves the form of the the acoustic intensity in the x-direction and y-direction respectively.

The form of the total acoustic intensity given by the sea surface generated noise can be estimated by taking the integration of the above equation over the effective radius (beyond this radius there is no significant change in the received acoustic intensity) as follows:-

$$\vec{I}_z = \int_0^{2\pi}\int_0^{r_0}\left(\frac{cos^2\theta}{r^2}cos(\theta)\right)adad\varphi\hat{z} = \frac{2\pi}{3}\left(1-cos^3\theta_0\right)\hat{z} \qquad (3.5)$$

$$\vec{I}_x = \int_0^{2\pi}\int_0^{r_0}\left(\frac{cos^2\theta}{r^2}sin(\theta)cos(\varphi)\right)adad\varphi\hat{x} = 0 \qquad (3.6)$$

$$\vec{I}_y = \int_0^{2\pi}\int_0^{r_0}\left(\frac{cos^2\theta}{r^2}sin(\theta)sin(\varphi)\right)adad\varphi\hat{y} = 0 \qquad (3.7)$$

Where r_0 is the effective surface noise radius and $cos\,\theta_0 = \frac{z}{\sqrt{r_0^2+z^2}}$.

These equations show that the form of the total acoustic intensity is due to the form of the acoustic intensity in the z-direction, as the acoustic intensity in the horizontal plane (x,y) is zero due to the symmetry of the surface noise. Equation (3.5) indicates that the acoustic intensity is at a maximum when $r_0 \to \infty$ (very large radius) or $\theta_0 \to 90^o$. However, the effective surface noise radius for a particular receiver depth need not be extended to infinity to be significant. Figure 3.2 represents the acoustic intensity versus increases in the radius of the surface noise. This graph shows that the effective radius can be easily estimated.

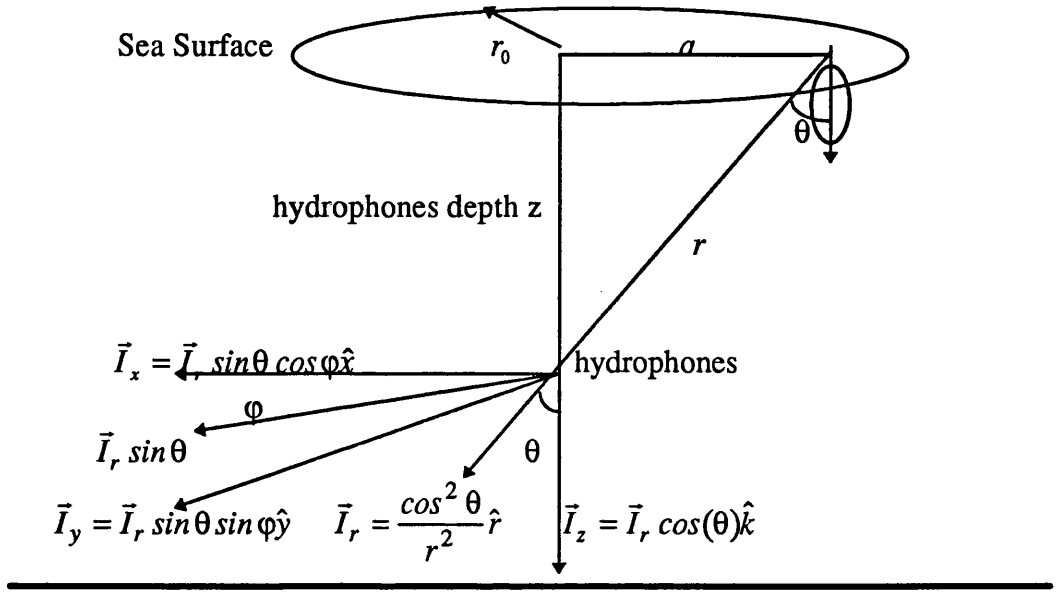

Figure 3.1 An illustration of the form of the acoustic intensity vector model in deep ocean.

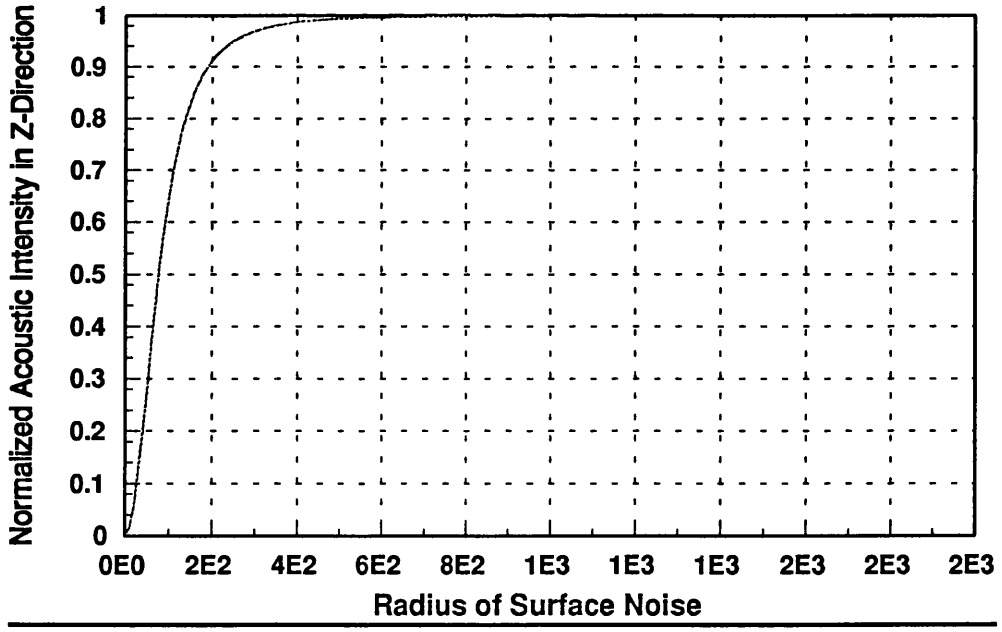

Figure 3.2 Shows the effect of surface generated noise in deep ocean. The normalized acoustic intensity increases rapidly when the radius of the surface generated noise is less than 400m, receiver depth z is 100m.

3.3 The Model In Shallow Water

In addition to the previous assumptions regarding the deep ocean model, the effect of the seabed will now be considered. Adding this parameter allows the acoustic intensity to arrive at the receiver from above and below the horizontal via multi-reflections with the seabed and the sea surface. In order to simplify the derivation of this model, the formula representing the form of the received acoustic intensity will be sub-divided into three parts. The first part corresponds to the direct rays, while the second and the third parts represent the form of the received acoustic intensity from the seabed and the sea surface respectively, (after several reflections with the seabed and the sea surface), see Figure 3.3.

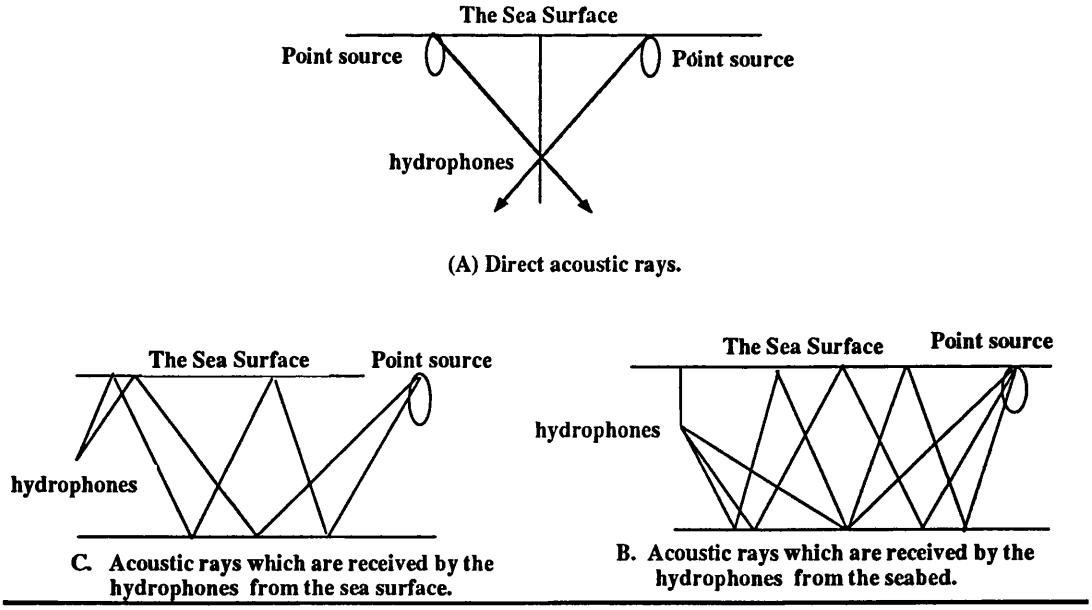

Figure 3.3 Represents direct acoustic intensity and received acoustic intensity from above and below the horizontal.

As the last two parts of the formula depends on the reflection coefficient of the seabed, this section will therefore start with an introduction to the definition of the reflection coefficient used in this model. Following this, the model of surface generated noise in shallow water will be presented.

3.3.1 The Definition of the Reflection Coefficient

The reflectivity of the seabed (based upon the plane wave reflection coefficient of the fluid seabed) can be expressed as follows :-

$$R_s(\theta_{qL}) = \left(\frac{m_s \cos\theta_{qL} - \sqrt{n_s^2 + \sin^2\theta_{qL}}}{m_s \cos\theta_{qL} + \sqrt{n_s^2 + \sin^2\theta_{qL}}} \right) \qquad (3.8)$$

Where:-

L is the number of reflections with the seabed.

$q=1$ corresponds to received rays from above the horizontal and $q=2$ corresponds to received rays from below the horizontal.

R_s is the reflection coefficient of the region s.

$n_s = \frac{k_s}{k} = \frac{c}{c_s}$ is the refractive index, c and c_s is the sound speed in the water and the seabed region s, respectively.

$m_s = \frac{\rho_s}{\rho}$ is the ratio between the densities of the medium s and the sea water.

The image method can be explained thus: the received acoustic intensity from the direction θ after L reflections along a multi-linear path, is equivalent to the intensity along a linear path, arriving in the same direction from a source located on the L^{th} image plane, see Figure 3.4.

According to this method the path length between the source and the receiver can be expressed in terms of the receiver depth *z*, the depth of the shallow water H, the horizontal distance between the source and the receiver *a* and the number of reflections with the seabed L=1,2,3,.....

$$z_{1L} = 2HL - z,$$

$$z_{2L} = 2HL + z$$

where z_{1L} represents the image depth for received rays from the seabed, while z_{2L} corresponds to the image depth for received rays from the sea surface. Using the image method the following relationships can be easily visualised:

$$\cos\theta_{1L} = \frac{z_{1L}}{r_{1L}},$$

$$\sin\theta_{1L} = \frac{a}{r_{1L}}$$

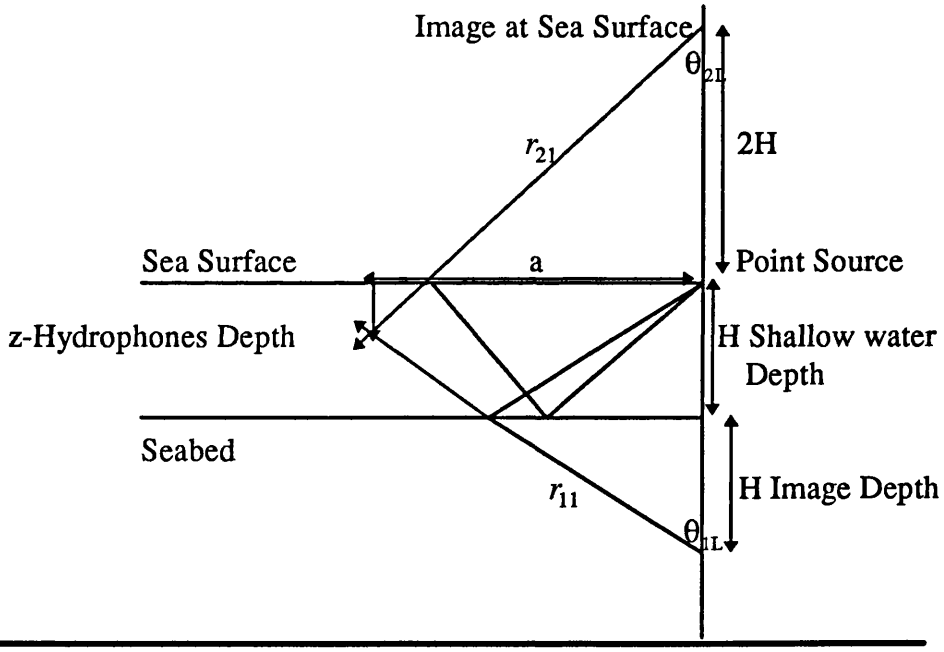

Figure 3.4 Illustration of reflected waves from the seabed and the sea surface.

3.3.2 The Model

The model which describes surface generated noise in shallow water is more complicated than that which describes such noise in deep ocean (as the effect of the seabed is included). In addition to the direct rays arriving at the receiver, further large numbers of acoustic rays (from above and below the horizontal) will arrive at the receiver due to the effect of the seabed in shallow water.

As stated previously, this model will be subdivided into three parts as follows:-

3.3.2.1 Direct Rays

These rays represent the received acoustic intensity which have no likelihood of hitting the seabed. As a result of symmetry, the acoustic intensity in the (x,y) direction is zero. The form of the received acoustic intensity in the z-direction is non-zero and is represented by the same equation which described the model in deep ocean, equation (3.5).

3.3.2.2 Received Rays from the Seabed

These rays represent the received intensity from the seabed (below the horizontal of the hydrophones) after several reflections with the seabed and the sea surface.

To simplify the mathematical aspect of the model, one point source located in the x-direction resulting in one reflection with the seabed will be considered as follows, see Figure 3.5:

$$\vec{I}_{r11} = \frac{R_s^2(\theta_{11})\cos^2\theta_{11}}{r_{11}^2}\hat{r} \qquad (3.9)$$

where:

R_s is the reflection coefficient of the region s,

$r_{11} = \sqrt{(2H-z)^2 + a^2}$ represents the distance between the source image and the hydrophones

$\cos\theta_{11} = \frac{2H-z}{\sqrt{(2H-z)^2 + a^2}}$ is obtained from the geometry of Figure 3.4

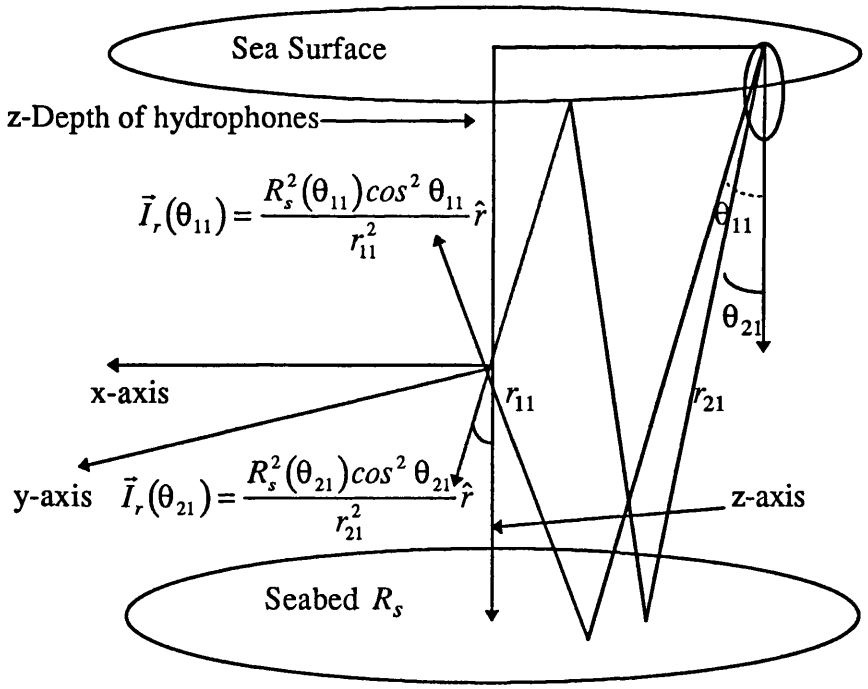

Figure 3.5 An illustration of the acoustic intensity vector model in shallow water.

Consequently, the form of the received acoustic intensity due to one point source after several reflections with the seabed and the sea surface is expressed as follows:-

$$\vec{I}_{r_{1L}} = \sum_{L=1}^{L=L_0} \left(\frac{R_s^{2L}(\theta_{1L}) \cos^2 \theta_{1L}}{r_{1L}^2} \right) \hat{r} \qquad (3.10)$$

where:

L represents the number of reflections with the seabed, L_0 is the effective reflection number.

$r_{1L} = \sqrt{(2LH - z)^2 + a^2}$ represents the path length for each acoustic ray via L reflections with the seabed.

The form of the acoustic intensity in the r-direction due to surface generated noise is obtained by taking the integration of equation (3.10) over the effective radius as follows:-

$$\vec{I}_{r_{1L}} = \sum_{L=1}^{L=L_0} \int_0^{2\pi r_0} \int_0^{} \left(\frac{R_s^{2L}(\theta_{1L}) \cos^2 \theta_{1L}}{r_{1L}^2} \right) a \, da \, d\varphi \hat{r} \qquad (3.11)$$

The form of the acoustic intensity is resolved into its components, and is given by

$$\vec{I}_{z_{1L}} = -\sum_{L=1}^{L=L_0} \int_0^{2\pi} \int_0^{r_0} \left(\frac{R_s^{2L}(\theta_{1L}) \cos^3 \theta_{1L}}{r_{1L}^2} \right) a \, da \, d\varphi \hat{z} \qquad (3.12a)$$

$$\vec{I}_{x_{1L}} = \sum_{L=1}^{L=L_0} \int_0^{2\pi} \int_0^{r_0} \left(\frac{R_s^{2L}(\theta_{1L}) \cos^2 \theta_{1L}}{r_{1L}^2} \sin \theta_{1L} \cos \varphi \right) a \, da \, d\varphi \hat{x} \qquad (3.12b)$$

$$\vec{I}_{y_{1L}} = \sum_{L=1}^{L=L_0} \int_0^{2\pi} \int_0^{r_0} \left(\frac{R_s^{2L}(\theta_{1L}) \cos^2 \theta_{1L}}{r_{1L}^2} \sin \theta_{1L} \sin \varphi \right) a \, da \, d\varphi \hat{y} \qquad (3.12c)$$

Equation (3.12) represents the form of the received acoustic intensity from the seabed (below the horizontal) due to surface generated noise in the three directions (x,y,z) after L reflections with the seabed.

3.3.2.3 Received Rays from the Sea Surface

These rays correspond to the rays arriving at the receiver from the sea surface after several reflections with the sea surface and the seabed. The equation representing these rays is the same as the one derived above (see section **3.3.2.2**) except that the path length of each ray will have an extra reflection with the sea surface, where:

$$r_{2L} = \sqrt{(2LH + z)^2 + a^2} \, .$$

Applying the same integration method as above, the form of the acoustic intensity received from the sea surface (above the horizontal) in the three directions can be expressed as follows:-

$$\vec{I}_{z_{2L}} = \sum_{L=1}^{L=L_0} \int_0^{2\pi} \int_0^{r_0} \left(\frac{R_s^{2L}(\theta_{2L}) cos^3 \theta_{2L}}{r_{2L}^2} \right) a da d\varphi \hat{z} \qquad (3.13a)$$

$$\vec{I}_{x_{2L}} = \sum_{L=1}^{L=L_0} \int_0^{2\pi} \int_0^{r_0} \left(\frac{R_s^{2L}(\theta_{2L}) cos^2 \theta_{2L}}{r_{2L}^2} sin\theta_{2L} \, cos\varphi \right) a da d\varphi \hat{x} \qquad (3.13b)$$

$$\vec{I}_{y_{2L}} = \sum_{L=1}^{L=L_0} \int_0^{2\pi} \int_0^{r_0} \left(\frac{R_s^{2L}(\theta_{2L}) cos^2 \theta_{2L}}{r_{2L}^2} sin\theta_{2L} \, sin\varphi \right) a da d\varphi \hat{y} \qquad (3.13c)$$

3.3.2.4 The Total Acoustic Intensity

The main conclusion to be drawn from the above model is that the acoustic intensity in the (x,y) directions is very sensitive to the structure of the seabed. In the case of uniformity in the seabed structure over the effective radius of the sea surface and the effective number of reflections with the seabed, the acoustic intensity in the plane (x,y) has been cancelled. In the case of any asymmetry in the seabed, the acoustic intensity in the plane (x,y) will depend on the structure of the seabed. However, before proceeding further with the capability of this model for classifying the seabed, the nature of the acoustic intensity vector as a function of the surface noise radius will first be introduced.

3.3.3 The acoustic intensity as a function of the surface noise radius

In order to explain how acoustic intensity responds to the variation in the radius of the surface noise, a simple model (in terms of the seabed structure) is presented. Despite the fact that it is not possible to achieve this in practice, it will help to provide a deeper understanding of the relationship between the surface noise and its received acoustic intensity at the hydrophones. In this model, the seabed has been divided into four equal regions (see Figure 3.6). The seabed reflectivity of each region is based on the reflection coefficient, defined in equation (3.8).

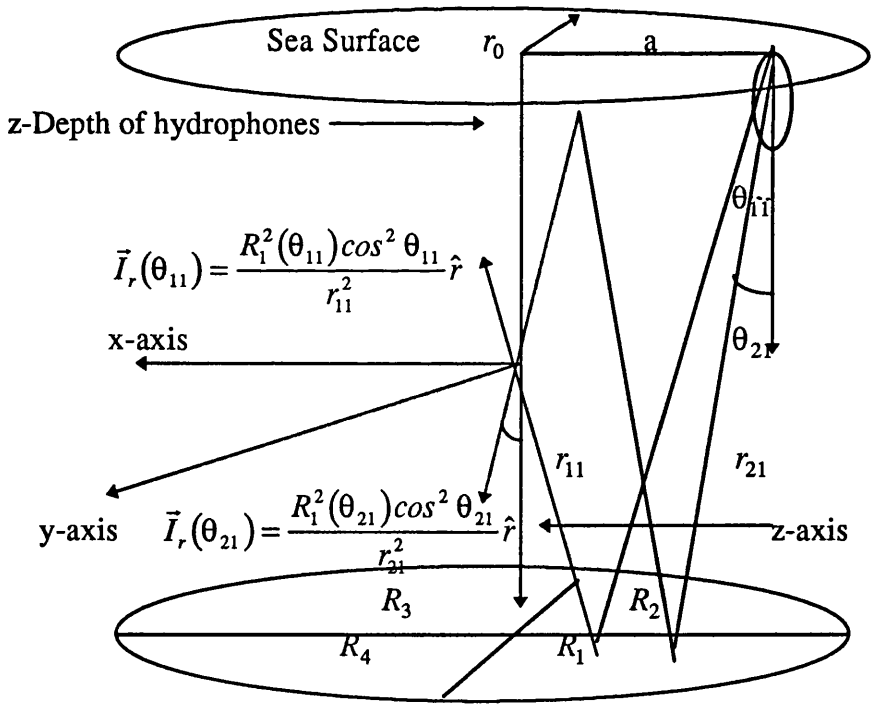

Figure 3.6 An illustration of the acoustic intensity vector model in shallow water for four different types of seabed..

Based upon the derivation given in the previous sections, the form of the total acoustic intensity in the z-direction can be represented as follows:

$$\vec{I}_z = \vec{I}_d + \vec{I}_{z1L} + \vec{I}_{z2L}$$

where: $\vec{I}_d$ is the form of the direct intensity which corresponds to equation (3.5), $\vec{I}_{z1L}$ is the form of the received intensity from the seabed which can be expressed as follows:-

$$\vec{I}_{z1L} = -\frac{\pi}{2}\sum_{L=1}^{L=L_0}\int_0^{r_0}\left(R_1^{2L}(\theta_{1L}) + R_2^{2L}(\theta_{1L}) + R_3^{2L}(\theta_{1L}) + R_4^{2L}(\theta_{1L})\right)\frac{\cos^3\theta_{1L}}{r_{1L}^2}ada\hat{z}$$

(3.14a)

where R_1^{2L}, R_2^{2L}, R_3^{2L} and R_4^{2L} represent the reflection coefficient for each of the four regions. The form of the acoustic intensity arriving from the sea surface is:-

$$\vec{I}_{z2L} = \frac{\pi}{2}\sum_{L=1}^{L=L_0}\int_0^{r_0}\left(R_1^{2L}(\theta_{2L}) + R_2^{2L}(\theta_{2L}) + R_3^{2L}(\theta_{2L}) + R_4^{2L}(\theta_{2L})\right)\frac{\cos^3\theta_{2L}}{r_{2L}^2}ada\hat{z}$$

(3.14b)

The form of the acoustic intensity in the x-direction can be represented as follows:

$$\vec{I}_x = \vec{I}_{x1L} + \vec{I}_{x2L}$$

in which $\vec{I}_{x1L}$ corresponds to the form of the acoustic intensity arriving from the seabed which is expressed more fully as follows:

$$\vec{I}_{x1L} = \sum_{L=1}^{L=L_0} \int_0^{r_0} \left(R_1^{2L}(\theta_{1L}) - R_2^{2L}(\theta_{1L}) + R_3^{2L}(\theta_{1L}) - R_4^{2L}(\theta_{1L})\right) \frac{\cos^2\theta_{1L} \sin\theta_{1L}}{r_{1L}^2} ada\hat{x}$$

(3.15a)

The form of the acoustic intensity for the rays coming from above the horizontal $\vec{I}_{x1L}$ can be presented as follows:

$$\vec{I}_{x2L} = \sum_{L=1}^{L=L_0} \int_0^{r_0} \left(R_1^{2L}(\theta_{2L}) - R_2^{2L}(\theta_{2L}) + R_3^{2L}(\theta_{2L}) - R_4^{2L}(\theta_{2L})\right) \frac{\cos^2\theta_{2L} \sin\theta_{2L}}{r_{2L}^2} ada\hat{x}$$

(3.15b)

Similarly, the form of the acoustic intensity in the y-direction can be obtained from the sum of the received intensities from the seabed and the sea surface. The form of the received acoustic intensity from the seabed is expressed as follows

$$\vec{I}_{y1L} = \sum_{L=1}^{L=L_0} \int_0^{r_0} \left(R_1^{2L}(\theta_{1L}) + R_2^{2L}(\theta_{1L}) - R_3^{2L}(\theta_{1L}) - R_4^{2L}(\theta_{1L})\right) \frac{\cos^2\theta_{1L} \sin\theta_{1L}}{r_{1L}^2} ada\hat{y}$$

(3.16a)

While the form of the acoustic intensity received from the sea surface is given as follows

$$\vec{I}_{y2L} = \sum_{L=1}^{L=L_0} \int_0^{r_0} \left(R_1^{2L}(\theta_{2L}) + R_2^{2L}(\theta_{2L}) - R_3^{2L}(\theta_{2L}) - R_4^{2L}(\theta_{2L})\right) \frac{\cos^2\theta_{2L} \sin\theta_{2L}}{r_{2L}^2} ada\hat{y}$$

(3.16b)

The physical significance of this model is as follows. The model shows that the form of the acoustic intensity in the *z*-direction is probably dominated by the direct rays, while the reflected rays are relatively insignificant. The form of the acoustic intensity in the *x*-*y* direction represented by equations (3.15) and (3.16) are strongly dependent on the symmetry of the seabed structure, *i.e.* no effect by direct rays. This conclusion may be presented more clearly by applying the model to a simple example (in terms of the seabed structure). In this example assume the following (these values are chosen arbitrarily):

1. The first three types of the seabed will be made of Coarse Sand.

2. The fourth seabed is considered to be Very Fine Sand.

3. The distinction between the two types of seabed is given via their reflection coefficient shown in equation (3.8) which is dependent upon the refractive index and the ratio between the density of the sea and the density of the seabed [37]. Figure (3.7) to Figure (3.10) shows the reflection coefficient of the two types of seabed versus the increase in the radius of the surface for received rays from above and below the horizontal.

4. The depth of the shallow water and the hydrophones are H=200m and z=100m, respectively.

5. The maximum radius of the surface noise is chosen to be 2 km.

Although this example is very simple, it may occur in real life. In order to estimate the three components of the acoustic intensity, a FORTRAN program has been developed (see Appendix 3A section 3.4). The numerical integration using the NAG libraries[38] has been employed in order to carry out the integration of the equations describing this example. Figure 3.11 to Figure 3.15 illustrate the results of this example for different numbers of reflections 'L' with the seabed. Figure 3.11 considers the normalised acoustic intensity in the *z*-direction in a situation where L=1 (the acoustic rays have only one chance to interact with the seabed). The conclusions made from this figure is explained as follows:-

1. For a small radius, the received normalised acoustic intensity increases rapidly with an increase in the radius of the surface noise. This rise in intensity is mainly caused by the direct rays.

2. As the radius of the surface noise increases, there is a specific point at which the normalised received intensity decreases. This effect can be related to the critical angle of the intensity coming from the seabed.

3. However, this decreasing of the normalised acoustic intensity will at some point thereafter begin to increase. It is evident that the received intensity from above the hydrophone has reached the critical angle.

4. Consequently, because there is no transmitted energy from the seabed after the critical angle, the direct intensity will again dominate.

The normalised acoustic intensity in the x and y directions behave similarly in this example. For this reason, it is sufficient to discuss the normalised acoustic intensity in the x-direction only. Figure 3.12 represents the acoustic intensity in this direction for L=1. The main feature of this figure is summarised as follows:

1. The normalised acoustic intensity increases rapidly with increases in the radius of the surface noise. This is due to the increase in the asymmetry of the seabed, which is related to the increase in the number of sources and the magnitude of the reflection coefficient of the seabed.

2. As the seabed in this example is divided into two regions and only two rays are represented, this graph shows the effect of the critical angle at two different points.

3. Due to the symmetry of the seabed after the critical angle, the normalised acoustic intensity will be constant even if the radius of the surface noise increases. The effective radius in this case can be identified. Here, it is approximately 900m

Other examples (in terms of the reflection number with the seabed) have been illustrated in Figure 3.13 to Figure 3.15. Here, the only difference with the previous example is the number of reflected rays from above and below the horizontal. Figure 3.13, where 'L=2', shows that in addition to the resluts observed in the previous example, there is another decrease followed by an increase in the normalised acoustic intensity in the z-direction. This time the drop in the normalised acoustic intensity will be smaller. However, this perturbation is due to the critical angle for both rays above and below the horizontal interacting with the seabed twice. These peaks and troughs in the intensity will increase in occurrence as the number of the rays interacting with the seabed is increased, see Figure 3.14.

The size of the effective radius in the x-direction will not remain stable for as long as the case of one reflection. The effect of this radius will increase as the number of reflections with the seabed increases. This can be concluded from Figure 3.15 where L=2. However, this effect will be limited after a certain number of reflections. This will be examined in detail in the next chapter.

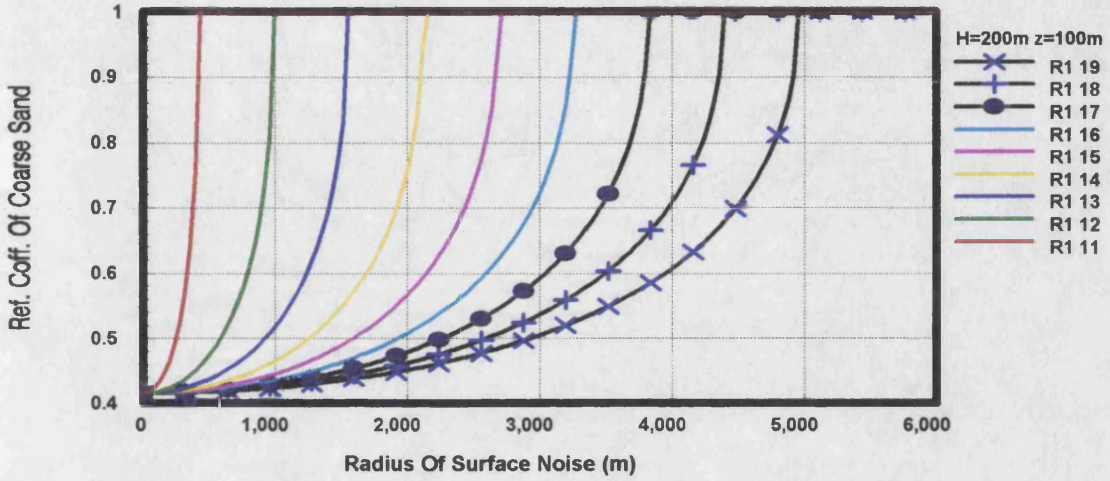

Figure 3.7 Shows the reflection coefficient for the Coarse Sand seabed for up to nine reflections with the seabed. This represents the received rays from the seabed.

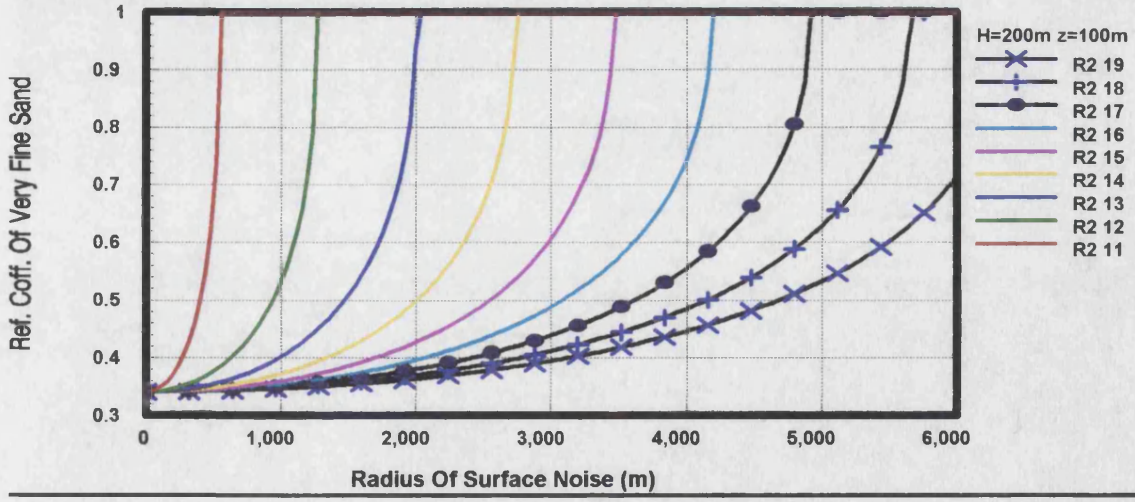

Figure 3.8 Shows the reflection coefficient for the Very Fine Sand seabed for up to nine reflections with the seabed. This represents the received rays from the seabed.

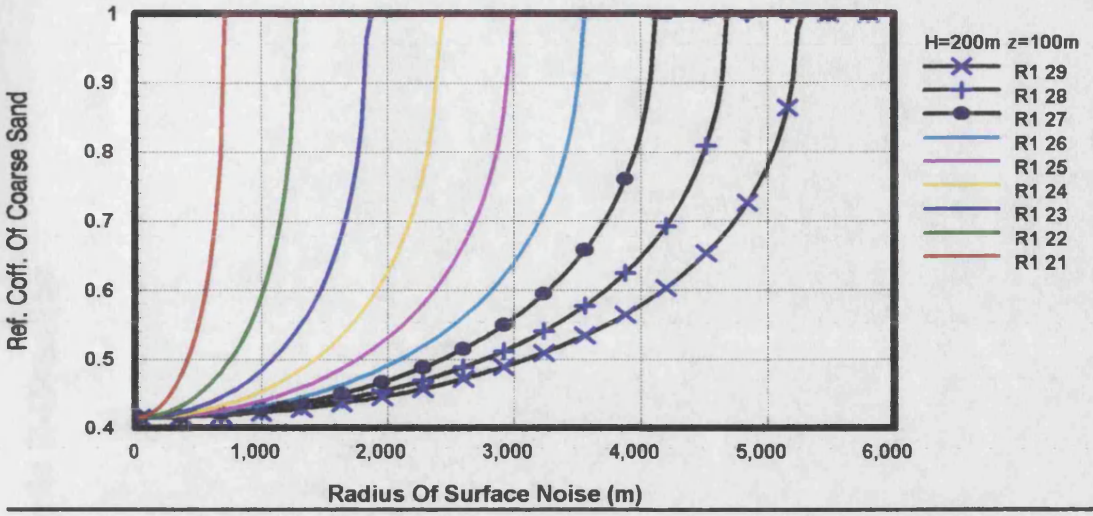

Figure 3.9 Shows the reflection coefficient for the Coarse Sand seabed for up to nine reflections with the seabed. This represents the received rays from the sea surface.

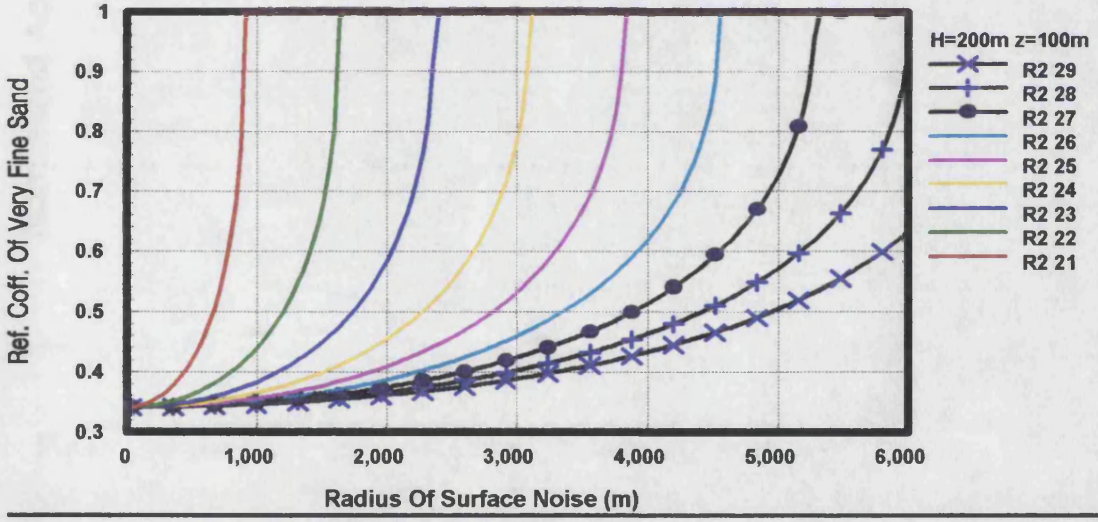

Figure 3.10 Shows the reflection coefficient for the Very Fine Sand seabed for up to nine reflections with the seabed. This represents the received rays from the sea surface.

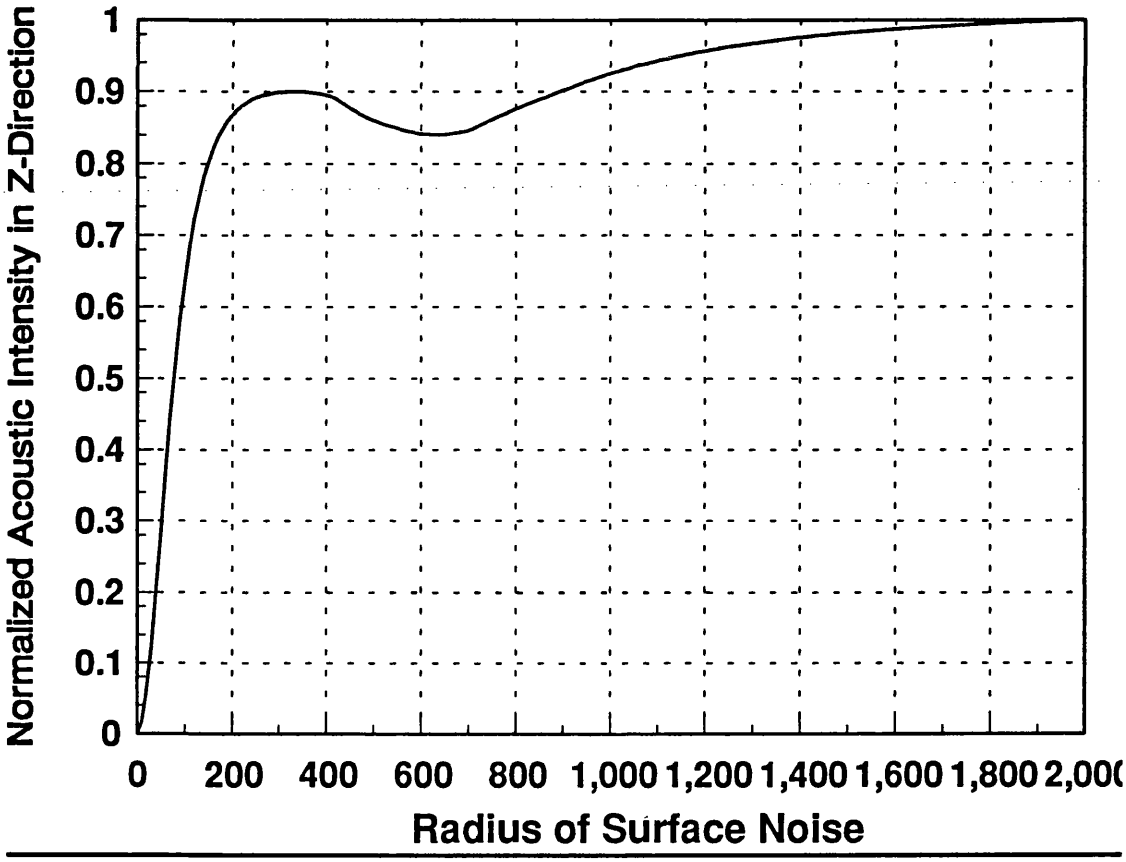

Figure 3.11 is composed of the direct and the reflected rays from the seabed and the sea surface due to surface generated noise for L=1. The decrease in the normalised acoustic intensity between 400m and 800m is due to the critical angle. H=200m, z=100m.

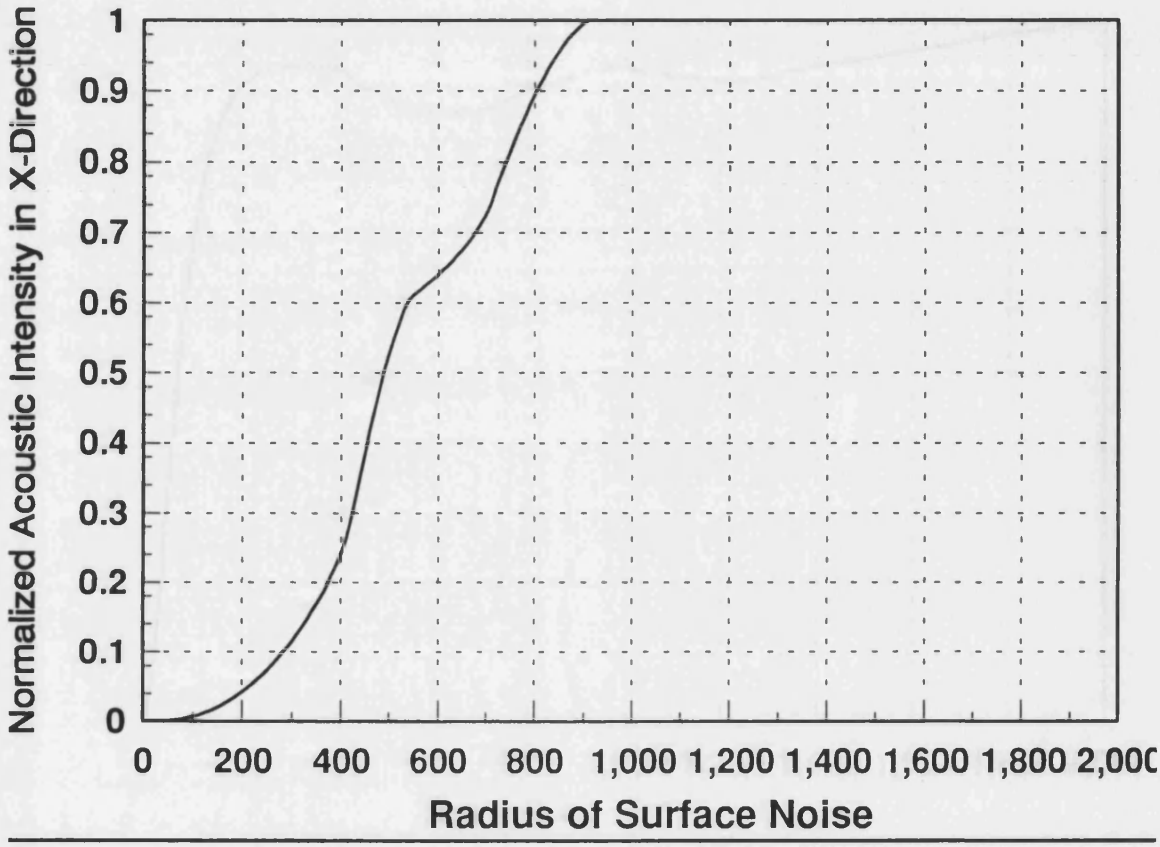

Figure 3.12 Shows the reflected rays from the seabed and the sea surface in the x-direction for L=1. The effect of the critical angle, for rays coming from the seabed can be seen at 470m, for rays that come from the sea surface, the effect of the critical angle can be seen at 850m. H=200m, z=100m.

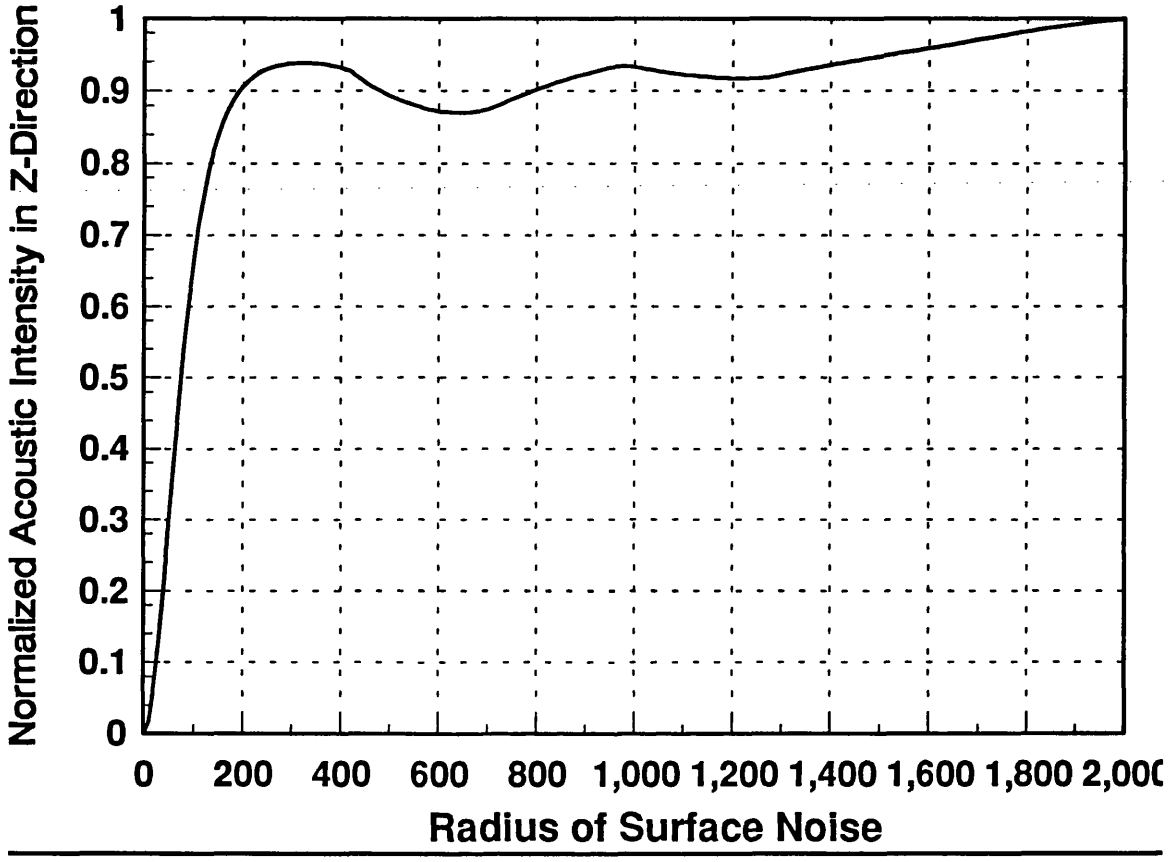

Figure 3.13 shows the normalised acoustic intensity in the z-direction due to surface noise for L=2. Here the drop in the acoustic intensity occurs twice, at 400m and 1000m. These drops are due to the critical angle. H=200m, z=100m.

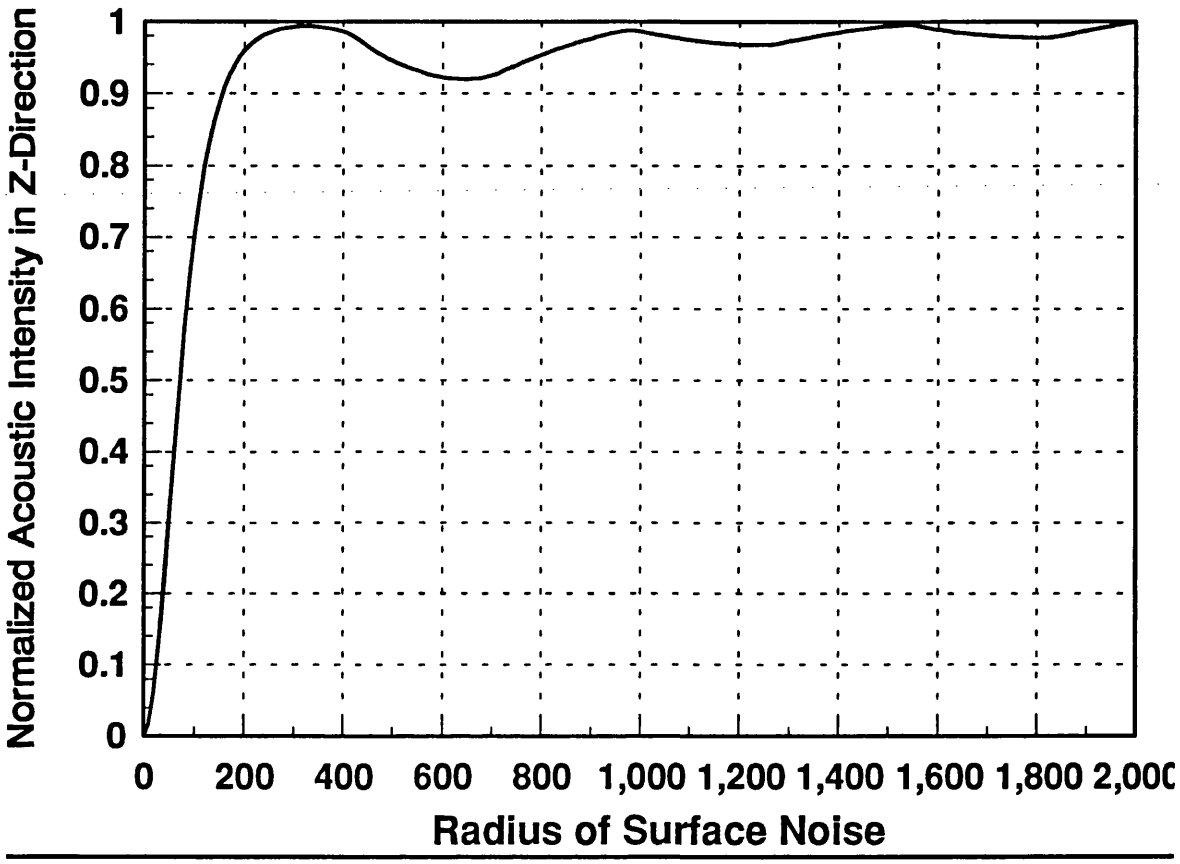

Figure 3.14 supports the results in Figure 3.13. As L increases, so does the number of troughs. The depth of these troughs decreases as L increases

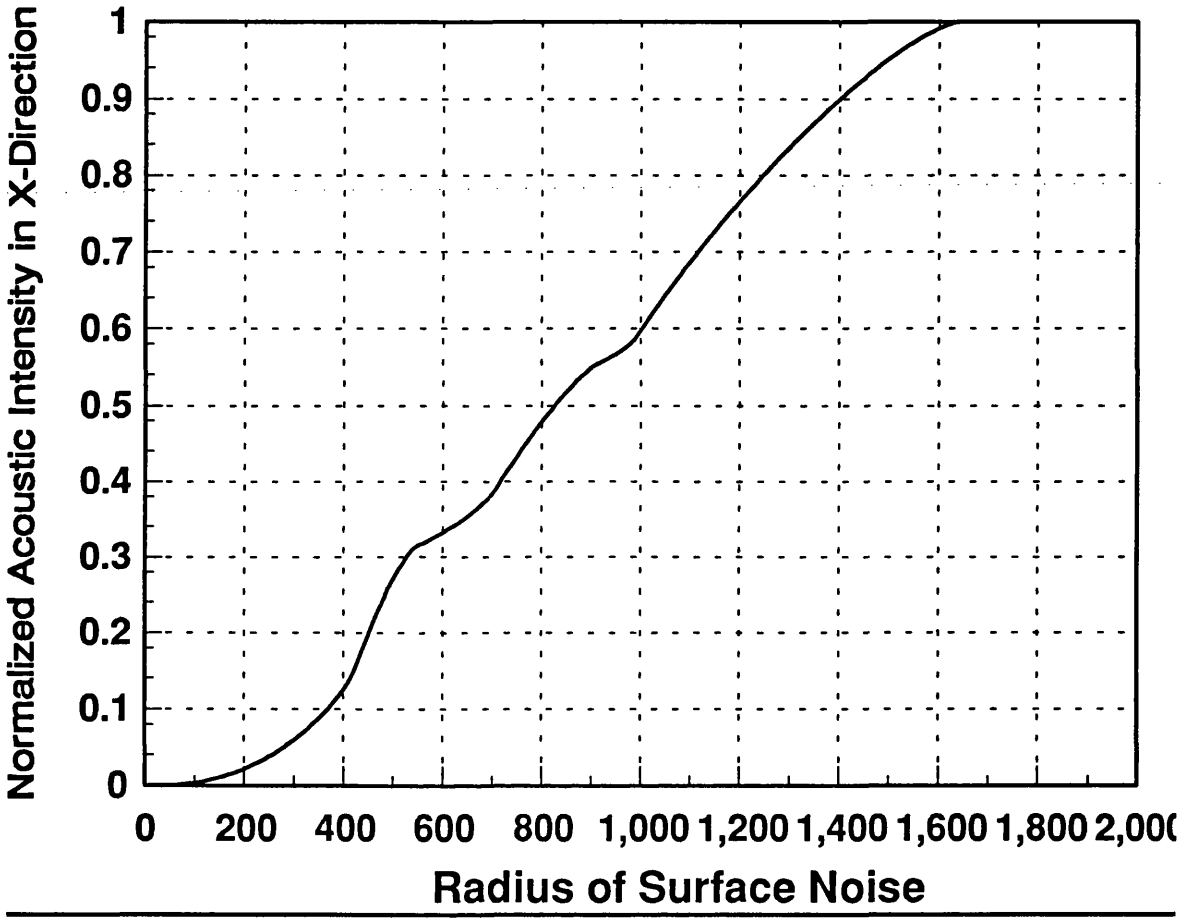

Figure 3.15 shows the normalised acoustic intensity in the x-direction for L=2. The limit of the effective radius is now at 800m. This shows that as L increase the effective radius increases. H=200m, z=100m

3.4 APPENDIX 3A

The aim this FORTRAN program is to calculate the acoustic intensity vector due to surface generated noise. The numerical integration of the acoustic intensity in the x,y and z directions will be obtained using the NAG-LIBRARY.

```
      DOUBLE PRECISION IX1(5),IX2(5),IX3(5),IX4(5),IX5(5),IXT
      DOUBLE PRECISION IZ1(5),IZ2(5),IZ3(5),IZ4(5),IZ5(5),IZT,IZ0,IZT1
      DOUBLE PRECISION Z1N,M1,M2,M3,M4,N1,N2,N3,N4,H,Z
      DOUBLE PRECISION RHO,RHO1,RHO2,RHO3,RHO4,C,C1,C2,C3,C4
      DOUBLE PRECISION RFC1,RFC2,RFC3,RFC4
      DOUBLE PRECISION ANS1,ANS2,ANS3,ANS4,FUN1,FUN2,FUN3,FUN4
      DOUBLE PRECISION ANS10,ANS11,ANS12,ANS13
      DOUBLE PRECISION RELERR,EPSR,D1,D2,TH30
      DOUBLE PRECISION IY1(5),IY2(5),IY3(5),IY4(5),IY5(5),IYT,X01AAF
      INTEGER IFAIL1,IFAIL2,IFAIL3,IFAIL4,NLIMIT,NI,L

C                       EXTERNAL FUNCTIONS
C                       ******************

      EXTERNAL X01AAF,FUN1,FUN2,FUN3,FUN4
      EXTERNAL D01AJF,STOR

C                         COMMON BLOCKS
C                       ******************

      COMMON/COMM2/Z1N,M1,M2,M3,M4
      COMMON/COMM3/N1,N2,N3,N4
      COMMON/COMM4/NI
      COMMON/COMM5/RFC1,RFC2,RFC3,RFC4

C                      PARAMETERS
C                    *************

      INTEGER LW,LIW
```

```
      PARAMETER (LW=800, LIW=LW/4)
      DOUBLE PRECISION W(LW)
      INTEGER IW(LIW)

C                OUTPUT FILES
C               **************

      OPEN(25,FILE='IZT1.dat')
      OPEN(26,FILE='IXT1.dat')

C                INPUT DATA
C               ************

      PRINT*,'INPUT THE VALUE OF SHALLOW WATER DEPTH H'
      READ(*,*)H
      PRINT*,'INPUT THE VALUE OF RECEIVERS DEPTH Z'
      READ(*,*)Z
      PRINT*,'INPUT THE VALUES OF DENSITIES OF THE
     *  SEA SURFACE RHO AND SEABED RHO1, RHO2, RHO3, RHO4'
      READ(*,*)RHO,RHO1,RHO2,RHO3,RHO4

      M1=RHO1/RHO
      M2=RHO2/RHO
      M3=RHO3/RHO
      M4=RHO4/RHO

      PRINT*,'INPUT THE VALUES OF THE SOUND SPEED IN SEA WATER C
     *     AND THE SOUND SPEED IN SEABED C1,C2,C3,C4'
      READ (*,*)C,C1,C2,C3,C4

      N1=C/C1
      N2=C/C2
      N3=C/C3
      N4=C/C4

C       INCREMENT OF THE SURFACE NOISE RADIUS D2
C      ****************************************

      DO 55 D2=0,2000,10
```

```
C     L REPRESENTS THE INTENSITY WHICH IS RECEIVED FROM ABOVE
C       THE HORIZONTAL, L=2, AND BELOW THE HORIZONTAL, L=1
C   ******************************************************

  DO 15 L=1,2
     IZ1(L)=0.0
     IZ2(L)=0.0
     IZ3(L)=0.0
     IZ4(L)=0.0
     IY1(L)=0.0
     IY2(L)=0.0
     IY3(L)=0.0
     IY4(L)=0.0
     IX1(L)=0.0
     IX2(L)=0.0
     IX3(L)=0.0
     IX4(L)=0.0

C  NI+1 IS THE NUMBER OF REFLECTIONS WITH THE SEABED
C  ************************************************

  29 NI=0,3

C  Z1N IS THE DEPTH OF THE IMAGE OF THE SOURCE
C  *******************************************

  IF(L.EQ.1)THEN
    Z1N=2*H*(1+NI)-Z
    ELSE
      Z1N=2*H*(1+NI)+Z
      END IF

C  THE FOLLOWING PART OF THE PROGRAM CALCULATES THE NUMERICAL
C  INTEGRATION OF THE FORM OF THE ACOUSTIC INTENSITY IN THE (X,Y,Z)
C  DIRECTIONS BY USING THE NAG-LIBRARY (SEE REF. 38)
C  ************************************************************

        D1=0.0E0
        EPSR=0.0001
        NLIMIT=0
```

```
C ESTIMATES THE FORM OF THE ACOUSTIC INTENSITY IN THE (X,Y) PLANE DUE
C TO THE REFLECTED RAYS FROM THE FIRST REGION.
C ***************************************************************

  IFAIL1=-1
  CALL D01AJF(FUN1,D1,D2,NLIMIT,EPSR,ANS1,RELERR,W,LW,IW,LIW
 *            ,IFAIL1)
  IF(IFAIL1.NE.0)THEN
     PRINT*,'IFAIL1=',IFAIL1
     END IF
     IF(IFAIL1.LE.5)THEN
        WRITE(*,24)'IX1=',ANS1,'ERROR=',RELERR,'W(1)=',IW(1)
        END IF

C ESTIMATES THE FORM OF THE ACOUSTIC INTENSITY IN THE (X,Y) PLANE DUE
C TO THE REFLECTED RAYS FROM THE SECOND REGION.
C ***************************************************************

  IFAIL2=-1
  CALL D01AJF(FUN2,D1,D2,NLIMIT,EPSR
 *       ,ANS2,RELERR,W,LW,IW,LIW,IFAIL2)
  IF(IFAIL2.NE.0)THEN
     PRINT*,'IFAIL2=',IFAIL2
     END IF
     IF(IFAIL2.LE.5)THEN
        WRITE(*,24)'IX2=',-ANS2,'ERROR=',RELERR
        END IF

C ESTIMATES THE FORM OF THE ACOUSTIC INTENSITY IN THE (X,Y) PLANE DUE
C TO THE REFLECTED RAYS FROM THE THIRD REGION.
C ***************************************************************

  IFAIL3=-1
  CALL D01AJF(FUN3,D1,D2,NLIMIT,EPSR
 *          ,ANS3,RELERR,W,LW,IW,LIW,IFAIL3)
  IF(IFAIL3.NE.0)THEN
    PRINT*,'IFAIL3=',IFAIL3
    END IF
      IF (IFAIL3.LE.5)THEN
         WRITE(*,24)'IX3=',ANS3,'ERROR=',RELERR
```

```
        END IF

C ESTIMATES THE FORM OF THE ACOUSTIC INTENSITY IN THE (X,Y) PLANE DUE
C TO THE REFLECTED RAYS FROM THE FOURTH REGION.
C ***************************************************************

  IFAIL4=-1
  CALL D01AJF(FUN4,D1,D2,NLIMIT,EPSR
 *      ,ANS4,RELERR,W,LW,IW,LIW,IFAIL4)
  IF(IFAIL4.NE.0)THEN
    PRINT*,'IFAIL4=',IFAIL4
    END IF
    IF(IFAIL4.LE.5)THEN
    WRITE(*,24)'IX4=',-ANS4,'ERROR=',RELERR
    END IF
 24  FORMAT(3(A,E10.4,2X))
     IX1(L)=IX1(L)+ANS1
     IY1(L)=IY1(L)+ANS1
     IX2(L)=IX2(L)+(-ANS2)
     IY2(L)=IY2(L)+ANS2
     IX3(L)=IX3(L)+ANS3
     IY3(L)=IY3(L)+(-ANS3)
     IX4(L)=IX4(L)+(-ANS4)
     IY4(L)=IY4(L)+(-ANS4)
     IX5(L)=IX1(L)+IX2(L)+IX3(L)+IX4(L)
     IY5(L)=IY1(L)+IY2(L)+IY3(L)+IY4(L)

C   THE FOLLOWING SUBROUTINE CALCULATES THE FORM OF THE
C   ACOUSTIC INTENSITY IN THE Z-DIRECTION.
C   ***************************************************************

    CALL STOR(H,Z,M1,M2,M3,M4,N1,N2,N3,N4,NI,L,ANS10,ANS11,
   *       ANS12,ANS13,D2)
    IZ1(L)=IZ1(L)+ANS10
    IZ2(L)=IZ2(L)+ANS11
    IZ3(L)=IZ3(L)+ANS12
     IZ4(L)=IZ4(L)+ANS13
     IZ5(L)=IZ1(L)+IZ2(L)+IZ3(L)+IZ4(L)

 29  CONTINUE
```

```
 15   CONTINUE

      TH30=ACOS(Z/SQRT(D2**2+Z**2))
      IZ0=(1-(COS(TH30))**3)
      IXT=IX5(1)+IX5(2)
      IYT=IY5(1)+IY5(2)
      IZT1=IZ0+IZ5(1)
      IZT=IZ0+IZ5(1)+IZ5(2)
      WRITE(25,25)D2,IZT,IZ0,IZ5(1),IZ5(2)
      WRITE(26,25)D2,IXT,IX5(1),IX5(2)
 25   FORMAT(5(E10.4,2X))
 55   CONTINUE
END

      DOUBLE PRECISION FUNCTION FUN1(A)
      DOUBLE PRECISION TH,TH1,Z1N,R1N,A,M1,M2,M3,M4
      DOUBLE PRECISION N1,RFC1,N2,N3,N4,RFC2,RFC3,RFC4
      COMPLEX RF1
      COMMON/COMM2/Z1N,M1,M2,M3,M4
      COMMON/COMM3/N1,N2,N3,N4
      COMMON/COMM4/NI
      COMMON/COMM5/RFC1,RFC2,RFC3,RFC4
      R1N=SQRT(A**2+Z1N**2)
      TH=(Z1N/R1N)
      TH1=(A/R1N)
      RF1=(M1*TH-SQRT(CMPLX(N1**2-(TH1)**2)))
     *    /(M1*TH+SQRT(CMPLX(N1**2-(TH1)**2)))
      RFC1=(SQRT((REAL(RF1))**2+(AIMAG(RF1))**2))**(2*NI+2)
      FUN1=(RFC1*A*(TH)**2*(TH1))/R1N**2
      RETURN
      END

      DOUBLE PRECISION FUNCTION FUN2(A)
      DOUBLE PRECISION TH,TH1,Z1N,R1N,A,M1,M2,M3,M4
      DOUBLE PRECISION N1,RFC2,N2,N3,N4,RFC1,RFC3,RFC4
      COMPLEX RF2
      COMMON/COMM2/Z1N,M1,M2,M3,M4
      COMMON/COMM3/N1,N2,N3,N4
      COMMON/COMM4/NI
      COMMON/COMM5/RFC1,RFC2,RFC3,RFC4
```

```
      R1N=SQRT(A**2+Z1N**2)
      TH=(Z1N/R1N)
      TH1=(A/R1N)
      RF2=(M2*TH-SQRT(CMPLX(N2**2-(TH1)**2)))
     *     /(M2*TH+SQRT(CMPLX(N2**2-(TH1)**2)))
      RFC2=(SQRT((REAL(RF2))**2+(AIMAG(RF2))**2))**(2*NI+2)
      FUN2=(RFC2*A*(TH)**2*(TH1))/R1N**2
      RETURN
      END

         DOUBLE PRECISION FUNCTION FUN3(A)
         DOUBLE PRECISION TH,TH1,Z1N,R1N,A,M3,M1,M2,M4
         DOUBLE PRECISION N3,RFC3,N1,N2,N4,RFC1,RFC2,RFC4
         COMPLEX RF3
         COMMON/COMM2/Z1N,M1,M2,M3,M4
         COMMON/COMM3/N1,N2,N3,N4
         COMMON/COMM4/NI
         COMMON/COMM5/RFC1,RFC2,RFC3,RFC4
         R1N=SQRT(A**2+Z1N**2)
         TH=(Z1N/R1N)
         TH1=(A/R1N)
         RF3=(M3*TH-SQRT(CMPLX(N3**2-(TH1)**2)))
     *     /(M3*TH+SQRT(CMPLX(N3**2-(TH1)**2)))
         RFC3=(SQRT((REAL(RF3))**2+(AIMAG(RF3))**2))**(2*NI+2)
         FUN3=(RFC3*A*(TH)**2*(TH1))/R1N**2
         RETURN
         END

         DOUBLE PRECISION FUNCTION FUN4(A)
         DOUBLE PRECISION TH,TH1,Z1N,R1N,A,M4,M1,M2,M3
         DOUBLE PRECISION N4,RFC4,N1,N2,N3,RFC1,RFC2,RFC3
         COMPLEX RF4
         COMMON/COMM2/Z1N,M1,M2,M3,M4
         COMMON/COMM3/N1,N2,N3,N4
         COMMON/COMM4/NI
         COMMON/COMM5/RFC1,RFC2,RFC3,RFC4
         R1N=SQRT(A**2+Z1N**2)
         TH=(Z1N/R1N)
         TH1=(A/R1N)
         RF4=(M4*TH-SQRT(CMPLX(N4**2-(TH1)**2)))
```

```
*      /(M4*TH+SQRT(CMPLX(N4**2-(TH1)**2)))
       RFC4=(SQRT((REAL(RF4))**2+(AIMAG(RF4))**2))**(2*NI+2)
       FUN4=(RFC4*A*(TH)**2*(TH1))/R1N**2
       RETURN
       END


 SUBROUTINE STOR (H,Z,M1,M2,M3,M4,N1,N2,N3,N4,NI,L,ANS10,ANS11,
*               ANS12,ANS13,D2)

DOUBLE PRECISION Z1N,M11,M12,M13,M14,N11,N12,N13,N14,H,Z
DOUBLE PRECISION ANS10,ANS11,ANS12,ANS13,FUNZ1,FUNZ2,FUNZ3,FUNZ4
DOUBLE PRECISION X01AAF,RELERRZ1,EPSREL,D1,D2,RELERRZ2,RELERRZ3
DOUBLE PRECISION RELERRZ4
DOUBLE PRECISION M1,M2,M3,M4,N1,N2,N3,N4
INTEGER IFAILZ1,IFAILZ2,IFAILZ3,IFAILZ4,NLIMIT,NI,L,NII
INTEGER LW,LIW
PARAMETER (LW=800,LIW=LW/4)
DOUBLE PRECISION W(LW)
INTEGER IW(LIW)
EXTERNAL X01AAF,FUNZ1,FUNZ2,FUNZ3,FUNZ4
EXTERNAL D01AJF

COMMON/COMM2/Z1N,M11,M12,M13,M14
COMMON/COMM3/N11,N12,N13,N14
COMMON/COMM4/NII
M11=M1
M12=M2
M13=M3
M14=M4
N11=N1
N12=N2
N13=N3
N14=N4

    IF(L.EQ.1)THEN

PRINT*,'THE REFLECTED INTENSITY IN THE Z-DIRECTION FROM THE SEABED'
       WRITE(*,58)'BELOW HORIZONTAL AFTER SEVERAL RFLECTIONS='
```

```
          Z1N=2*H*(1+NI)-Z
           ELSE

  PRINT*,'THE REFLECTED INTENSITY IN THE Z-DIRECTION FROM SEASURFACE'
           WRITE(*,58)'ABOVE HORIZONTAL AFTER SEVERAL RFLECTIONS='

           Z1N=2*H*(1+NI)+Z
        END IF
        PRINT*,NI+1
 58      FORMAT(A,1X,E10.4,1X)

        D1=0
        EPSREL=0.0001
        NLIMIT=0
        IFAILZ1=-1
        CALL D01AJF(FUNZ1,D1,D2,NLIMIT,EPSREL,ANS10,RELERRZ1
     *                                  ,W,LW,IW,LIW,IFAILZ1)
        IF(IFAILZ1.NE.0)THEN
           PRINT*,'IFAILZ1=',IFAILZ1
           END IF
        IF(IFAILZ1.LE.5)THEN
           WRITE(*,24)'IZ1=',ANS10,'ERROR=',RELERRZ1
           END IF

        IFAILZ2=-1
        CALL D01AJF(FUNZ2,D1,D2,NLIMIT,EPSREL,ANS11,RELERRZ2
     *                                 ,W,LW,IW,LIW,IFAILZ2)
        IF(IFAILZ2.NE.0)THEN
          PRINT*,'IFAILZ2=',IFAILZ2
          END IF
            IF(IFAILZ2.LE.5)THEN
              WRITE(*,24)'IZ2=',ANS11,'ERROR=',RELERRZ2
              END IF

        IFAILZ3=-1
        CALL D01AJF(FUNZ3,D1,D2,NLIMIT,EPSREL,ANS12,RELERRZ3
     *                                 ,W,LW,IW,LIW,IFAILZ3)
        IF(IFAILZ3.NE.0)THEN
          PRINT*,'IFAILZ3=',IFAILZ3
          END IF
```

```
          IF (IFAILZ3.LE.5)THEN
            WRITE(*,24)'IZ3=',ANS12,'ERROR=',RELERRZ3
            END IF

       IFAILZ4=-1
       CALL D01AJF(FUNZ4,D1,D2,NLIMIT,EPSREL,ANS13,RELERRZ4
     * ,W,LW,IW,LIW,IFAILZ4)
       IF(IFAILZ4.NE.0)THEN
          PRINT*,'IFAILZ4=',IFAILZ4
           END IF
           IF(IFAILZ4.LE.5)THEN
           WRITE(*,24)'IZ4=',ANS13,'ERROR=',RELERRZ4
           END IF
 24    FORMAT(2(A,E10.4,2X))
       IF(L.EQ.1)THEN
          ANS10=-ANS10
          ANS11=-ANS11
          ANS12=-ANS12
          ANS13=-ANS13
        END IF
       END

        DOUBLE PRECISION FUNCTION FUNZ1(A)
        DOUBLE PRECISION TH,TH1,Z1N,R1N,A,M11,M12,M13,M14
        DOUBLE PRECISION N11,RFC1,N12,N13,N14
        COMPLEX RF1
        COMMON/COMM2/Z1N,M11,M12,M13,M14
        COMMON/COMM3/N11,N12,N13,N14
        COMMON/COMM4/NII
        R1N=SQRT(A**2+Z1N**2)
        TH=(Z1N/R1N)
        TH1=(A/R1N)
        RF1=(M11*TH-SQRT(CMPLX(N11**2-(TH1)**2)))
     *    /(M11*TH+SQRT(CMPLX(N11**2-(TH1)**2)))
        RFC1=(SQRT((REAL(RF1))**2+(AIMAG(RF1))**2))**(2*NII+2)
        FUNZ1=(RFC1*A*(TH)**3)/R1N**2
        RETURN
        END
```

```
      DOUBLE PRECISION FUNCTION FUNZ2(A)
      DOUBLE PRECISION TH,TH1,Z1N,R1N,A,M11,M12,M13,M14
      DOUBLE PRECISION N11,RFC2,N12,N13,N14
      COMPLEX RF2
      COMMON/COMM2/Z1N,M11,M12,M13,M14
      COMMON/COMM3/N11,N12,N13,N14
      COMMON/COMM4/NII
      R1N=SQRT(A**2+Z1N**2)
      TH=(Z1N/R1N)
      TH1=(A/R1N)
      RF2=(M12*TH-SQRT(CMPLX(N12**2-(TH1)**2)))
     *   /(M12*TH+SQRT(CMPLX(N12**2-(TH1)**2)))
      RFC2=(SQRT((REAL(RF2))**2+(AIMAG(RF2))**2))**(2*NII+2)
      FUNZ2=(RFC2*A*(TH)**3)/R1N**2
      RETURN
      END

      DOUBLE PRECISION FUNCTION FUNZ3(A)
      DOUBLE PRECISION TH,TH1,Z1N,R1N,A,M11,M12,M13,M14
      DOUBLE PRECISION N11,RFC3,N12,N13,N14
      COMPLEX RF3
      COMMON/COMM2/Z1N,M11,M12,M13,M14
      COMMON/COMM3/N11,N12,N13,N14
      COMMON/COMM4/NII
      R1N=SQRT(A**2+Z1N**2)
      TH=(Z1N/R1N)
      TH1=(A/R1N)
      RF3=(M13*TH-SQRT(CMPLX(N13**2-(TH1)**2)))
     *     /(M13*TH+SQRT(CMPLX(N13**2-(TH1)**2)))
      RFC3=(SQRT((REAL(RF3))**2+(AIMAG(RF3))**2))**(2*NII+2)
      FUNZ3=(RFC3*A*(TH)**3)/R1N**2
      RETURN
      END

      DOUBLE PRECISION FUNCTION FUNZ4(A)
      DOUBLE PRECISION TH,TH1,Z1N,R1N,A,M11,M12,M13,M14
      DOUBLE PRECISION N11,RFC4,N12,N13,N14
      COMPLEX RF4
      COMMON/COMM2/Z1N,M11,M12,M13,M14
      COMMON/COMM3/N11,N12,N13,N14
```

```
      COMMON/COMM4/NII
      R1N=SQRT(A**2+Z1N**2)
      TH=(Z1N/R1N)
      TH1=(A/R1N)
      RF4=(M14*TH-SQRT(CMPLX(N14**2-(TH1)**2)))
     *    /(M14*TH+SQRT(CMPLX(N14**2-(TH1)**2)))
      RFC4=(SQRT((REAL(RF4))**2+(AIMAG(RF4))**2))**(2*NII+2)
      FUNZ4=(RFC4*A*(TH)**3)/R1N**2
      RETURN
      END
```

Chapter Four

4. Studies of the Surface Noise Intensity Vector in Shallow Water

4.1 Introduction

A model of the surface noise intensity vector in deep ocean was presented in the last chapter. The model indicates that the total acoustic intensity in deep ocean (where the effect of the seabed is insignificant) is due to the acoustic intensity in the z-direction. Further, the model shows that the effective radius of the surface noise is easily predictable. This model was also modified in order to present the form of the surface noise acoustic intensity vector in shallow water. The modified model shows that the form of the acoustic intensity in the (x,y) directions is strongly dependent on the structure of the seabed. This conclusion was supported by a model using a certain structure of the seabed. In this structure, the seabed was divided into four equal regions, each extending to infinity.

The variation of the normalised acoustic intensity in the (x,z) directions due to the increase of the surface noise radius was studied. It was observed from this study that the normalised acoustic intensity in the z-direction may be dominated by the direct rays (which have no likelihood of hitting the seabed), while the normalised acoustic intensity in the x-direction is free from these rays and depends only on the symmetry of the seabed. This last observation warrants more careful examination of the normalised acoustic intensity in the x-direction, such as is presented in this chapter. Consequently, in this study the seabed is assumed to be symmetrical everywhere except in a small patch. The small patch was first considered to have a circular shape. Computation using this shape took a very long time. Thus, to simplify the problem and to cut down on computation time, as a second example a section of an annulus shape was considered. Hence, in this chapter both shapes will be discussed. The normalised acoustic intensity in the x-direction was examined by moving the hydrophones towards the asymmetry in the seabed, firstly when the small patch is considered to be circular in shape, and secondly, when it is a section of an annulus. Only the model describing the second shape incorporates the scattering effect of the sea surface. In both studies, however, the arrived intensity in the x-direction from above and below the horizontal are considered separately.

The last two examples studied in this chapter takes the shape to be a section of an annulus. In the first example, the normalised acoustic intensity due to different sizes of surface noise and small patches are discussed. In the second, the normlised acoustic intensity in the x-direction is considered for different types of seabed for the small patch.

4.2 Normalised Acoustic Intensity in the x-Direction Over a Circular Patch

This section investigates the nature of the normalised acoustic intensity in the x-direction by moving the hydrophones parallel to the seabed towards the small patch. This aspect of the normalised acoustic intensity was observed simultaneously with increases in the radius of the surface noise. The following arbitrary assumptions have been made for this example:

1. The small patch considered is a circle with a radius A=400m, see Figure 4.1.
2. The circular patch lies in the x-direction which leads to a symmetry in the y-direction (no intensity will be observed in this direction)
3. The depth of the hydrophones and the shallow water are 100m and 200m respectively.
4. The circular patch is made of Very Fine Sand, while the rest of the seabed is made of Coarse Sand.
5. The hydrophones move in steps of 200m towards the small patch.

The mathematical expression of the form of the acoustic intensity in the x-direction can be expressed as follows:-

$$\vec{I}_x = \vec{I}_{x_1} + \vec{I}_{x_2}$$

Where $\vec{I}_{x_1}$ represents the form of the acoustic intensity which arrives from the small patch direction and is given as follows:-

$$\vec{I}_{x_1}(\theta,\varphi) = \sum_{q=1}^{q=2}\left(\sum_{L=1}^{L=L_0}\int_{\varphi}\int_{0}^{-\varphi r_0}\left(\frac{\left(R_1^{NR_1}(\theta_{qL})R_2^{NR_2}(\theta_{qL})\right)^2\cos^2\theta_{qL}\sin\theta_{qL}\cos\varphi}{r_{qL}^2}\right)adad\varphi\,\hat{x}\right)$$

Where:

For $q=1$ the acoustic intensity is considered to arrive at the hydrophones from below the horizontal, while $q=2$ represents the acoustic intensity received from above the horizontal. NR_1 and NR_2 are the number of reflections which hit the large and the small areas respectively. Due to the circular shape of the small patch, this form of the acoustic intensity shows a dependence in the horizontal direction. The form of the acoustic intensity arriving at the hydrophones from other directions can be expressed as:

$$\vec{I}_{x_2}(\theta) = \sum_{q=1}^{q=2}\left(\sum_{L=0}^{L=L_0}\int_{\varphi}\int_{0}^{\varphi_1 r_0}\left(\frac{R_1^{2L}(\theta_{qL})\cos^2\theta_{qL}\sin\theta_{qL}\cos\varphi}{r_{qL}^2}\right)adad\varphi\,\hat{x}\right)$$

where $\varphi_1 = 360 - \varphi$, and R_1 is the reflection coefficient of the large patch of the seabed.

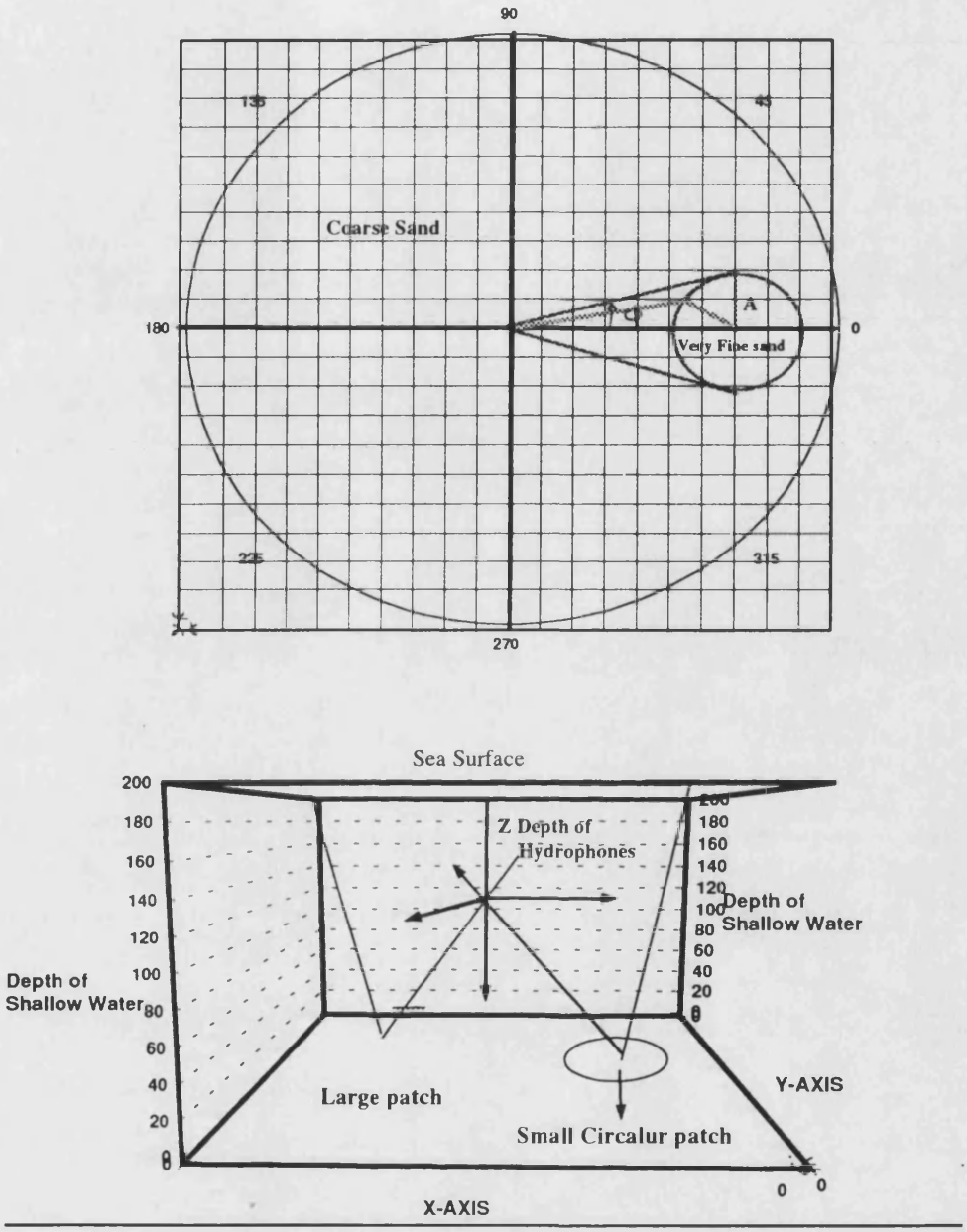

Figure 4.1 Illustrates the 2-dimensional and 3-dimensional representation of the reflected acoustic intensity from a seabed separated into two types. The small patch represents a circular shape, and the large patch corresponds to the seabed as a whole.

In order to facilitate the above study, a computer program written in FORTRAN was developed (for more details, see Appendix 4A, section 4.4). The program used the Extended Simpson Rule in order to carry out the integration over the effective radius of the surface noise. Acoustic intensities from above and below the horizontal were studied separately.

To gain a better understanding, the normalised acoustic intensities in the x-direction will first of all be studied with a small number of reflections between the seabed and the sea surface. Figure 4.4 and Figure 4.5 represents the received normalised acoustic intensity (the normalisation is with respect to the received intensity from the first reflection with the seabed and the first location of the hydrophones) from the seabed and the sea surface, respectively, after one reflection with the seabed (L=1), for different locations of the hydrophones with respect to the small circular patch (Very Fine Sand). To be able to get a clearer view of the behaviour of the normalised acoustic intensity, the x-axis has been divided into two axes. The first axis (black) represents the radius of the surface noise while the second (blue) shows the location of the received rays from the seabed (for example a ray from a point source located at 6000m hits the seabed at 2000m). This can be visualised clearly from Figure 4.2, however, the number of these axes depends on the reflection number L.

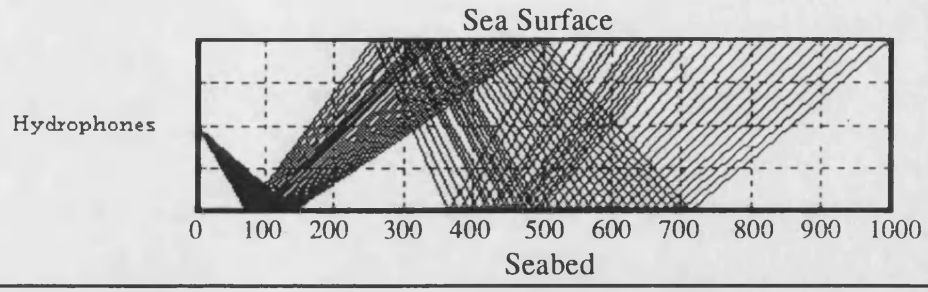

Figure 4.2 illustrates the reflected acoustic intensity from the seabed after two reflections. A point source located at 1000m will hit the seabed twice, first at approximately 700m and the last reflection at about 150m

The conclusion drawn from Figure 4.4 and Figure 4.5 can be summarised as follows:-

1. The magnitude of the normalised acoustic intensity will increase rapidly as the radius of the surface noise increases when the hydrophones are located near the small patch (i.e. A1=400m, where A1 is the distance between the hydrophones and the centre of the small patch). This rise in the intensity occurs due to the decrease in the symmetry of the seabed (bearing in mind that the normalised acoustic intensity is the resultant from the two different seabed types). However, this rise in the normalised acoustic intensity will be constant after a certain point. The location of this point depends on the reflection coefficient of the seabed. For the rays arriving from the seabed this point is about 200m, while for the received rays from the sea surface this point is close to 300m (refer to the blue axis in both graphs). The minus sign indicates the direction of the propagating acoustic intensity.

2. Figure 4.4 shows that there is no received acoustic intensity for hydrophones located at distances greater than A1=400m. This may be taken to indicate that all the received acoustic intensity rays reach the critical angle before they hit the small patch. Since the received acoustic intensity from above the horizontal has a longer range before the critical angle is reached, shown in Figures 3.7 to 3.10 (see chapter three), there exists some received acoustic intensities for hydrophones located at distances greater than A1=400m, see Figure 4.5. However, these intensities have a smaller magnitude as they reach the critical angle before they pass the small patch.

The above example becomes more complicated as the reflection number increases. The following table shows the possibilities of hitting the small patch as the reflection number increases, see Figure 4.3

$$\text{L=1} \qquad R_1 \text{ or } R_2$$

$$\text{L=2} \qquad R_1^2 \text{ or } R_1R_2 \text{ or } R_2^2$$

$$\text{L=3} \qquad R_1^3 \text{ or } R_1R_2^2 \text{ or } R_1^2R_2 \text{ or } R_1^3$$

$$\text{L=4} \qquad R_1^4 \text{ or } R_1R_2^3 \text{ or } R_1^3R_2 \text{ or } R_1^2R_2^2 \text{ or } R_2^4$$

where R_1 and R_2 represents the reflection coefficient of the large and small patches, respectively.

Consequently, for two reflections with the seabed, there are three different combinations of hitting the two types of seabed. Either the ray hits one type twice, or hits both types once. However, these possibilities depend on the size of the small patch, the location of

the point source, the depth of the shallow water and the depth of the hydrophones. The computer model has been developed in order to take into account all the above possibilities (see Appendix 4A section 4.4, subroutine SUBW111).

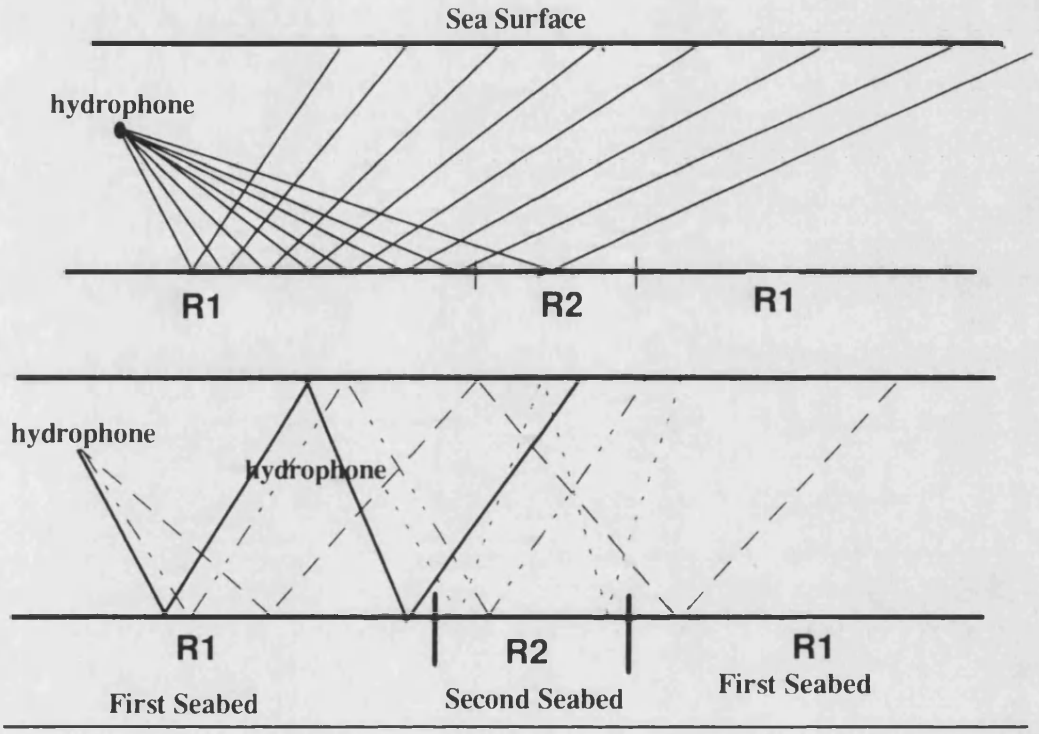

Figure 4.3 This diagram shows the different possibilities for the rays to hit the seabed after one and two reflections

Figure 4.6 and Figure 4.7 shows the normalised received acoustic intensity (similarly, the normalisation is with respect to the received intensity from the first reflection with the seabed and the first location of the hydrophones) from above and below the horizontal

after two reflections with the seabed. The behaviour of these normalised acoustic intensities can be explained as follows:

1. The received normalised acoustic intensity will be small at smaller radii since the magnitude of the reflection coefficient is small.

2. The normalised intensity increases rapidly as its reflection coefficient increases until it reaches the critical angle where all the rays from all directions are the same and will cancel each other out.

3. As for the previous example (L=1), the magnitude of the received normalised acoustic intensity will get smaller and smaller until it reaches zero as the hydrophone moves further away from the small patch.

However, for higher number of reflections with the seabed, see Figure 4.8 to Figure 4.11, the normalised acoustic intensity will behave in almost the same way as the previous example, the only differences being as follows:

1. The received normalised acoustic intensity will be smaller in magnitude since it has a longer path length (a consequence of spherical spreading).

2. Since the location of the critical angle depends on the number of reflections with the seabed, the acoustic intensity will increase at larger distances (since most of the energy is absorbed in the seabed at small angles).

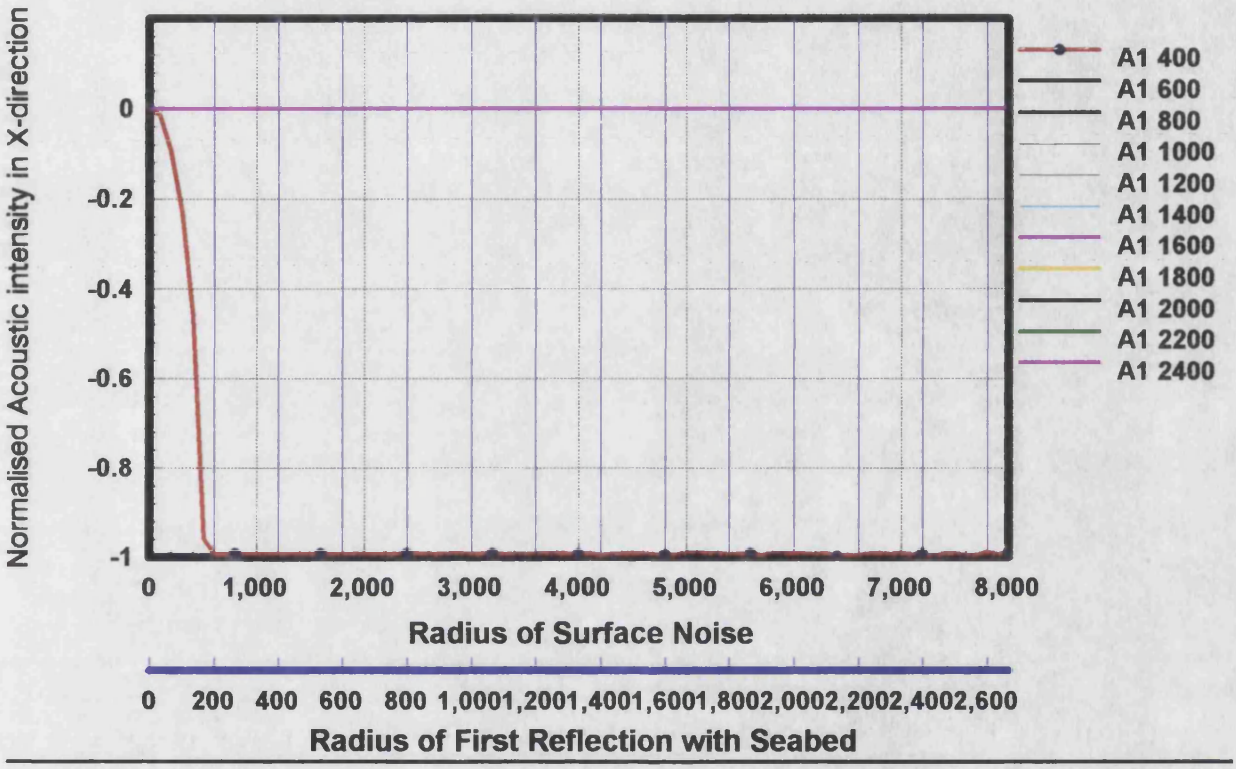

Figure 4.4 represents the normalised acoustic intensity received from the seabed after one reflection with the seabed in the x-direction. This acoustic intensity is plotted against the increases in the radius of the surface noise in meters. A1 corresponds to the locations of the hydrophones relative to the centre of the circular patch. The depth of the shallow water and the hydrophones are H=200m and z=100m respectively, the radius of the small area is 400m. The graph shows that for A1 bigger than 400m the normalised acoustic intensity is zero.

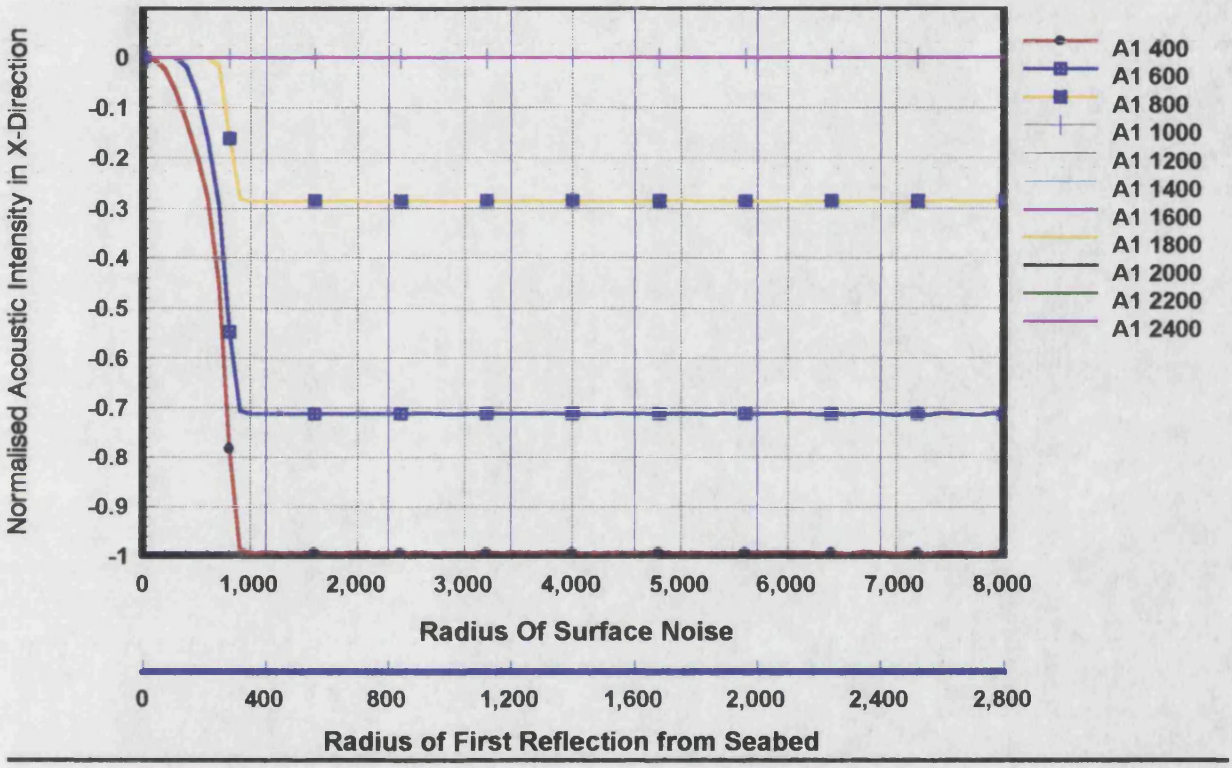

Figure 4.5 represents the normalised acoustic intensity arriving from the sea surface after one reflection with the seabed. The same variables as Figure 4.4 is taken in this figure.

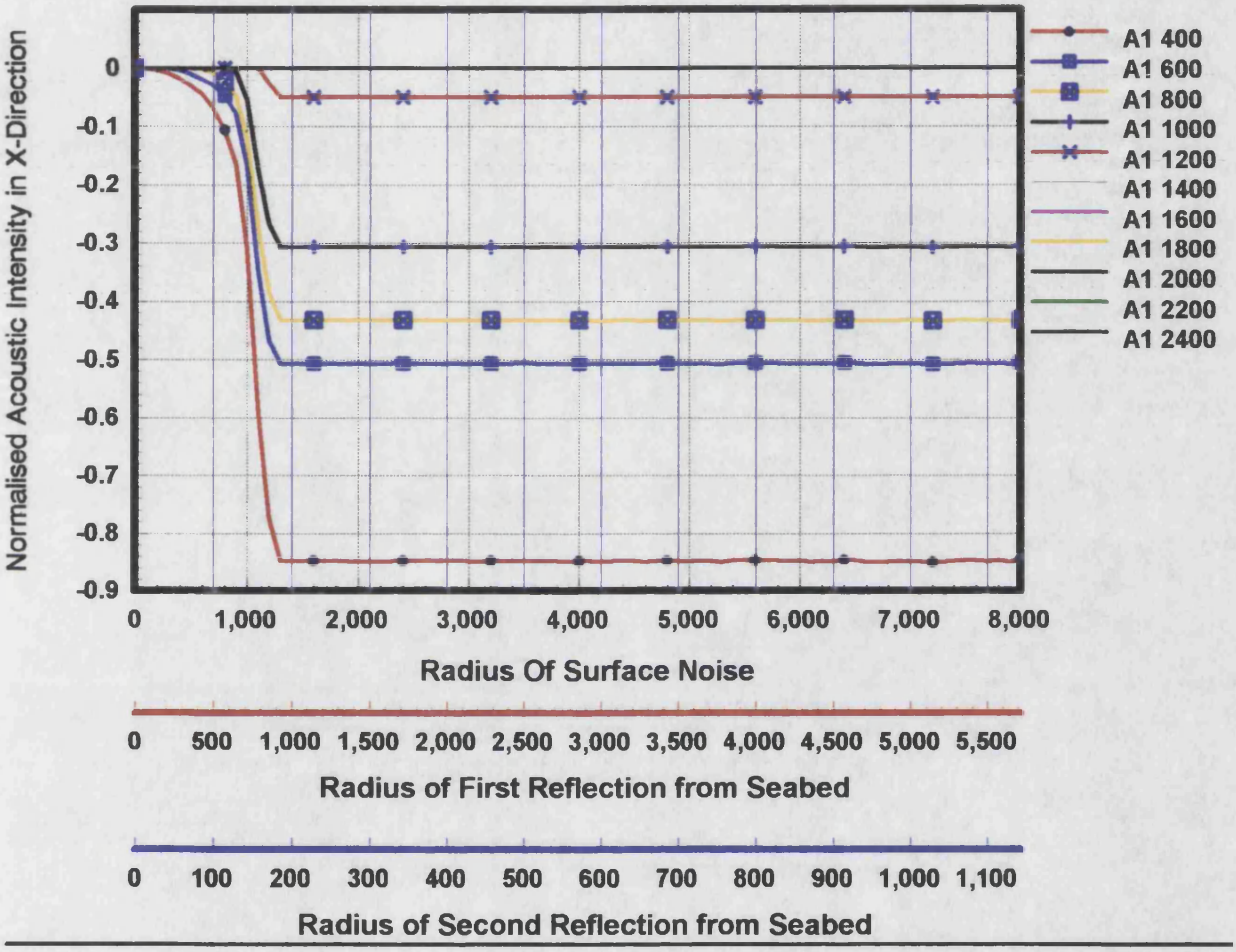

Figure 4.6 represents the normalised acoustic intensity in the x-direction arriving from the seabed after two reflections with the seabed. The same variables as Figure 4.4 is taken in this figure.

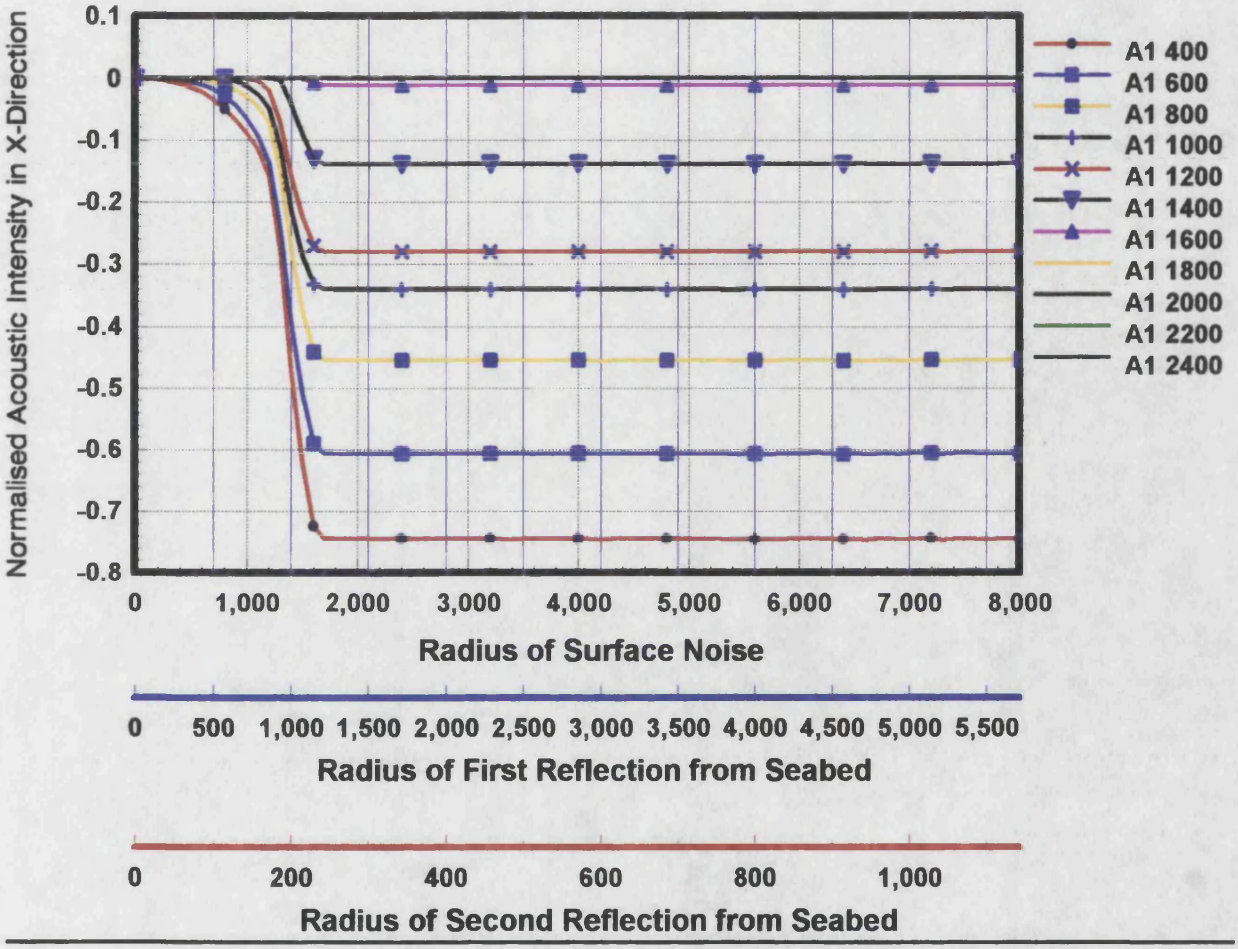

Figure 4.7 corresponds to the normlized acoustic intensity in the x-direction arriving from the sea surface after two reflections with the seabed. The same variables as Figure 4.4 is taken in this figure.

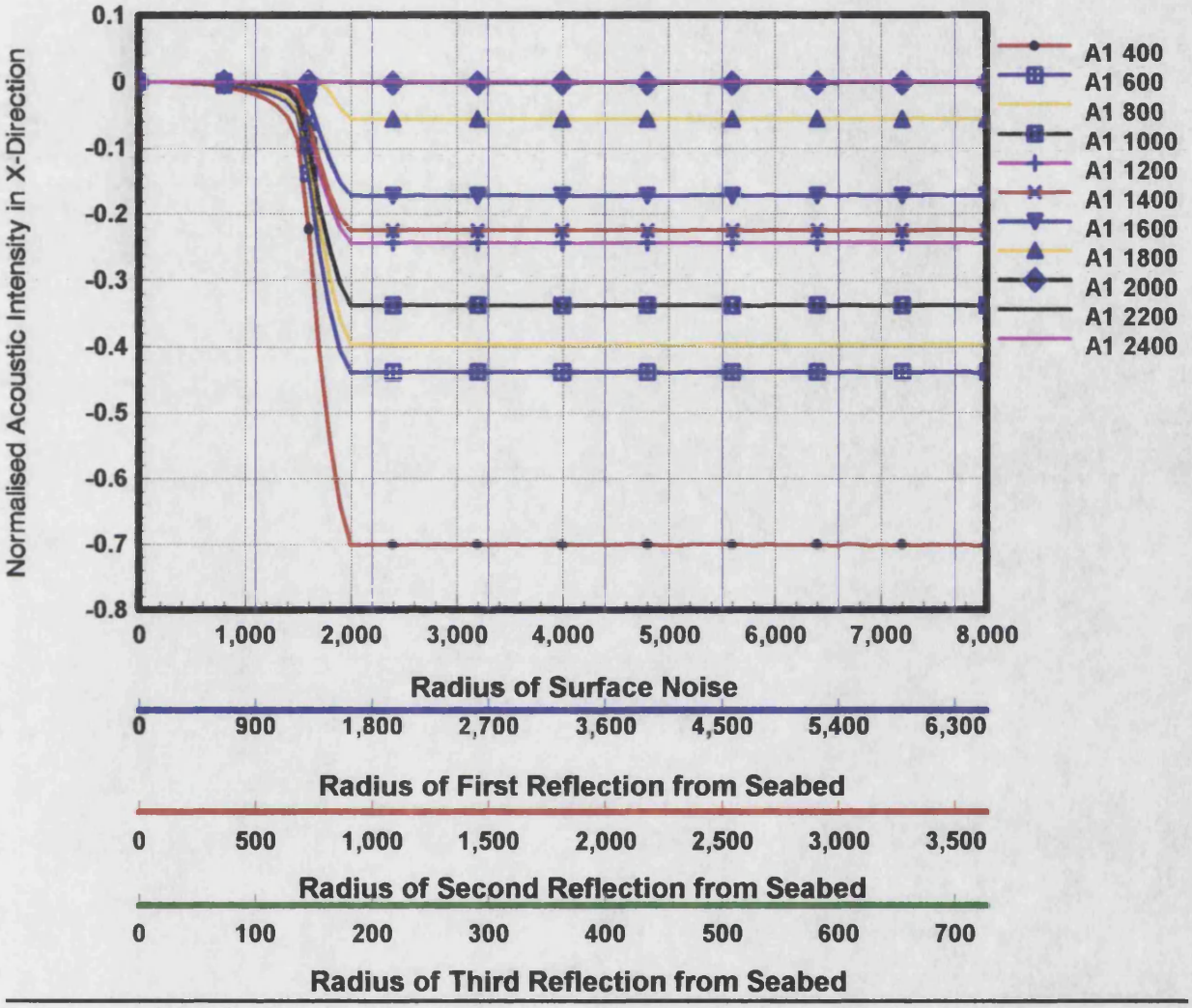

Figure 4.8 shows the normalised acoustic intensity in the x-direction arriving from the seabed after three reflections with the seabed. The same variables as Figure 4.4 is taken in this figure.

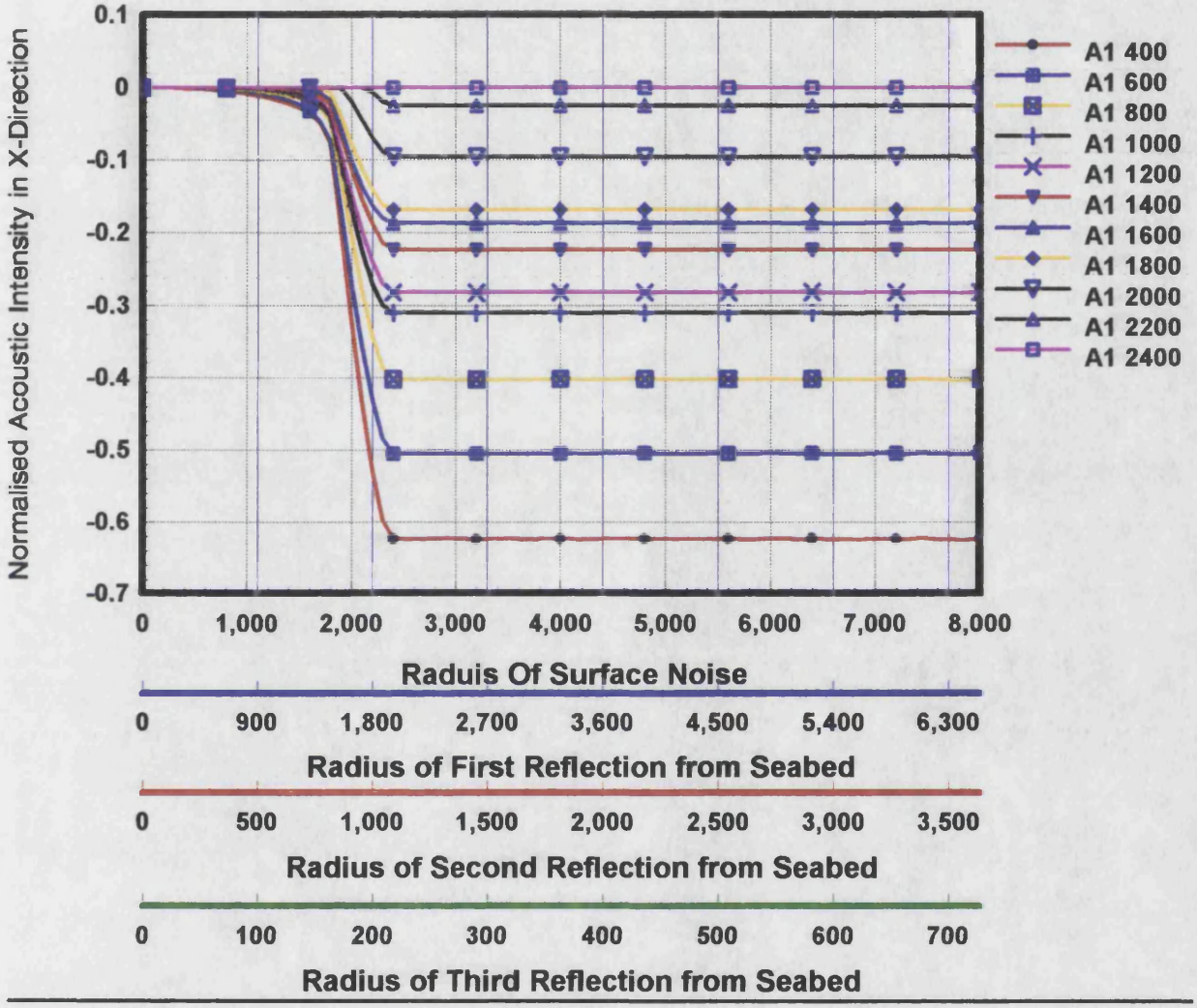

Figure 4.9 shows the normalised acoustic intensity in the x-direction arriving from the sea surface after three reflections with the seabed. The same variables as Figure 4.4 is taken in this figure.

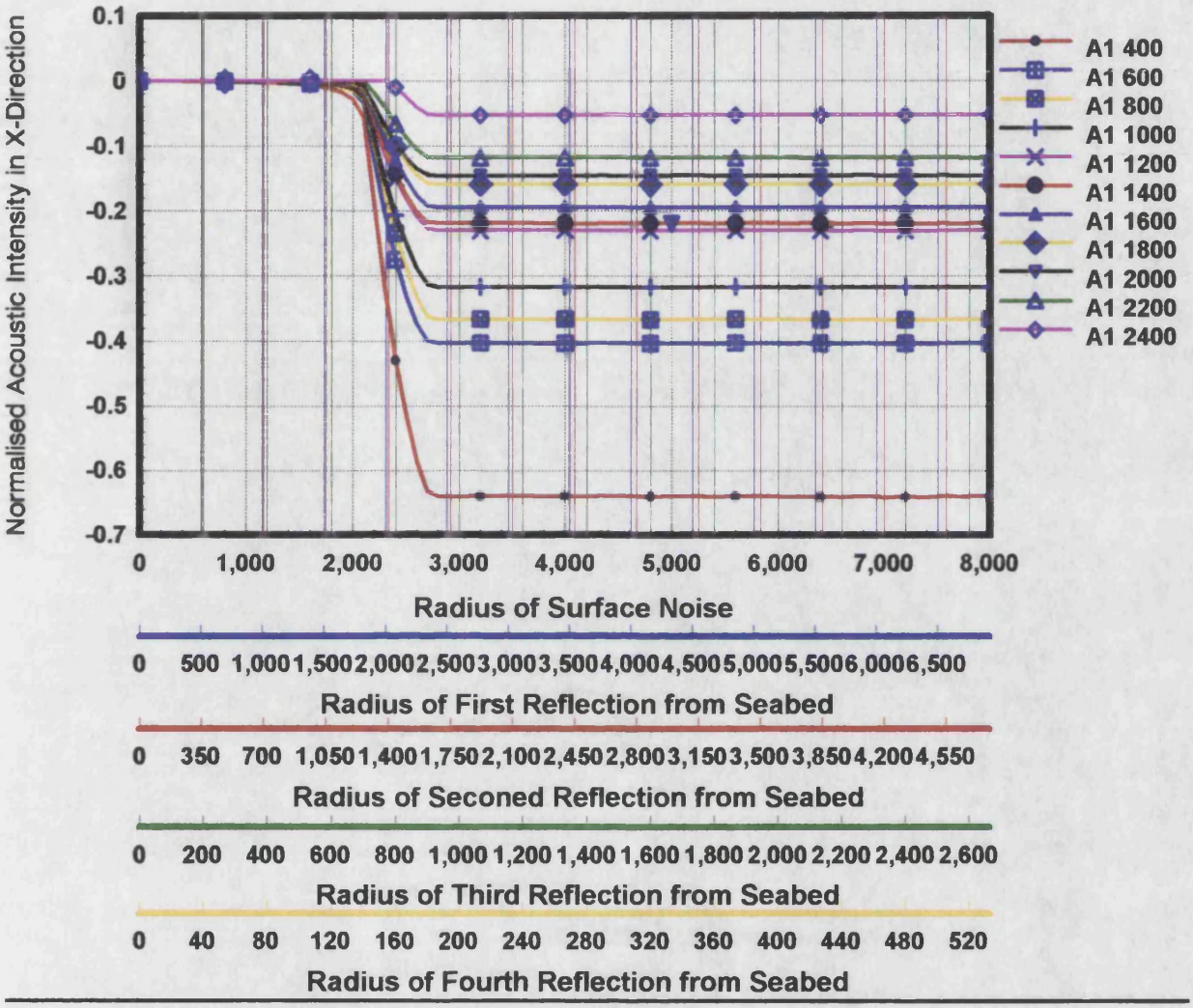

Figure 4.10 shows the normalised acoustic intensity in the x-direction arriving from the seabed after four reflections with the seabed. The same variables as Figure 4.4 is taken in this figure.

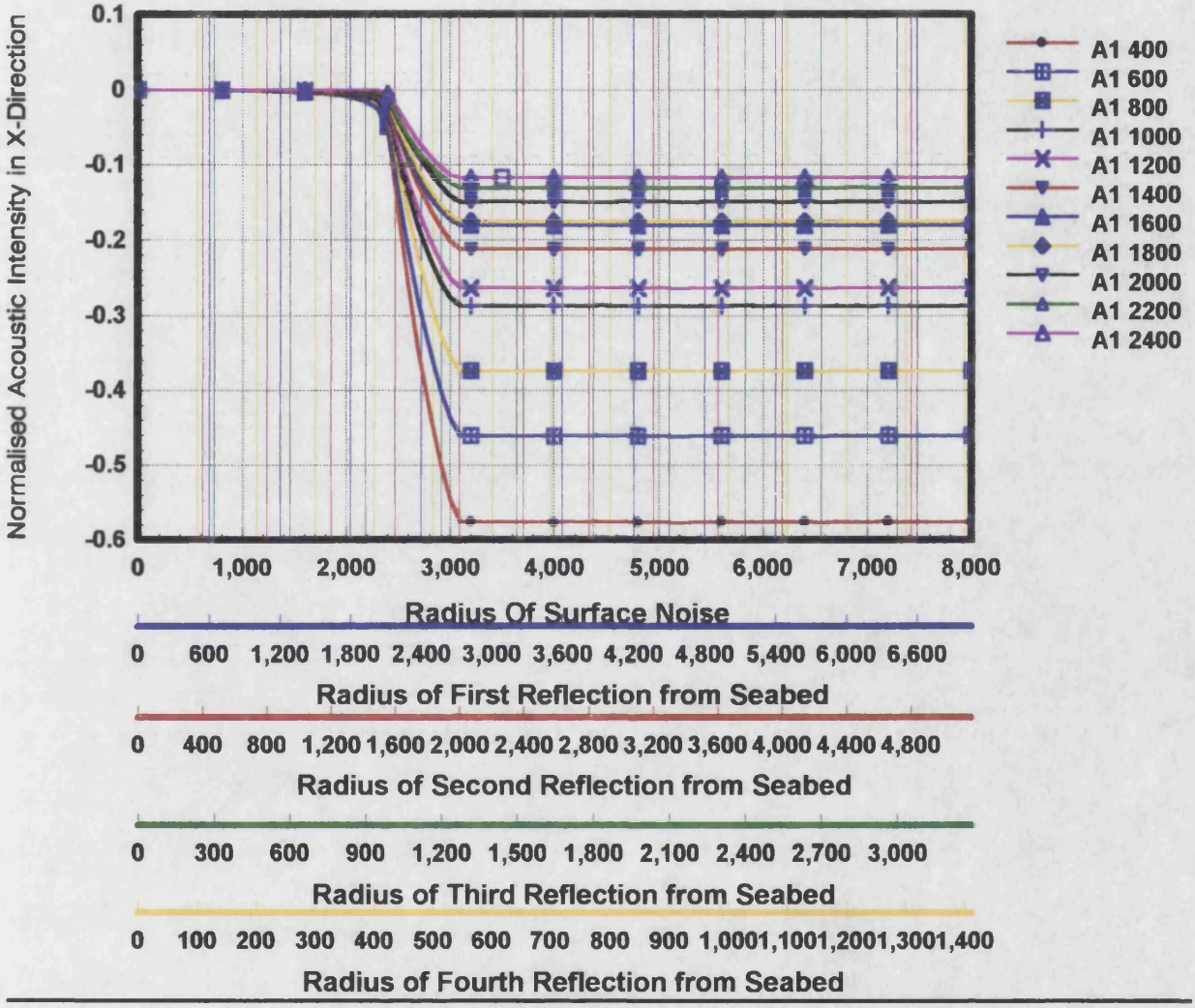

Figure 4.11 shows the normalised acoustic intensity in the x-direction arriving from the sea surface after four reflections with the seabed. The same variables as Figure 4.4 is taken in this figure.

4.3 Normalised Acoustic Intensity in the x-Direction Over a Section of an Annulus

4.3.1 Introduction

It was observed from the above study that the normalised acoustic intensity received due to the small circular patch depends on the horizontal angle φ. This dependence leads to a long computation time. In order to simplify and cut down the computation time, a small patch in the shape of a section of an annulus has been considered in this section. This shape allows the acoustic intensity to be independent of the horizontal angle φ. This independence can be visualised easily by considering Figure 4.12.

The following sub-section will begin with a similar study as presented in the previous section. In addition to changing the shape of the small patch, the scattering effect of the sea surface has also been included. Adding this parameter will force the acoustic intensity from a high number of reflections to decrease rapidly. In reality the problem is not as simple as this, since the scattering from the sea surface depends on many factors (for example the frequency, the sea state and the incident angle). However, detailed analysis of scattering effects is not essential for this project. It is enough to appreciate that the acoustic intensity decreases rapidly with each reflection with the sea surface. Following

this study, the effect of the surface noise on different sizes and types of the small patch will be reviewed.

4.3.2 The Normalised Acoustic Intensity as a Function of the Surface Noise

A model of the surface noise vector in shallow water when the seabed is symmetrical apart from a small patch which is in the shape of a section of an annulus is presented by the following points:-

1. The section of an annulus seabed patch is made of Very Fine Sand and the rest of the seabed is assumed to be made of Coarse Sand.

2. The depth of the hydrophones and the shallow water are 100m and 200m respectively.

3. The scattering effect of each reflection with the sea surface is α=3 dB. This indicates that the wave height of the sea surface is 1 ft, which corresponds to 7 to 10 Knots wind speed (sea state 2) [39].

4. The area of the section of an annulus is given as $A = \varphi\left(A_2^2 - A_1^2\right)$, where A_1 is the distance from the point of origin (the location of the hydrophones) to the leading edge of the small patch. $A_2 = 400 + A_1$ is the distance from the point of origin to the furthest edge of the small patch in meters. $\varphi = 25^o$.

The mathematical expression corresponding to the form of the acoustic intensity resolved in the x-direction from rays received from all horizontal directions can be expressed as the sum of the form of the acoustic intensity from the small patch and the form of the acoustic intensity from the other directions. The received rays from the direction of the small patch is given as follows

$$\vec{I}_x(\theta)=\sum_{q=1}^{q=2}\left(\sum_{L=1}^{L=L_0}\int_{-\varphi}^{\varphi}\int_{0}^{r_0}\left(\frac{\left(R_1^{NR_1}(\theta_{qL})R_2^{NR_2}(\theta_{qL})\right)^2(\alpha)^{NS}\,sin(\theta_{qL})cos\,\varphi}{r_{qL}^2}\right)adad\varphi\right)\hat{x}$$

where q corresponds to whether the acoustic intensity arrives from above or below the horizontal direction, L is the number of reflections with the seabed and NS=L+q-2 represents the number of reflections with the sea surface

The form of the acoustic intensity arriving from the other directions can be expressed as follows:-

$$\vec{I}_x(\theta)=\sum_{q=1}^{q=2}\left(\sum_{L=1}^{L=L_0}\int_{\varphi}^{\varphi_1}\int_{0}^{r_0}\left(\frac{\left(R_1^{2L}(\theta_{qL})\right)(\alpha)^{NS}\,sin(\theta_{qL})cos\,\varphi}{r_{qL}^2}\right)adad\varphi\right)\hat{x}$$

Where $\varphi_1 = 360-\varphi$

In order to study the nature of these equations a computer model has been developed (see Appendix 4B section 4.5). The resulting normalised acoustic intensity produced from this computer model for received rays from below the horizontal for one to four reflections are illustrated in Figure 4.13 to Figure 4.16 (the acoustic intensity is normalised with respect to the first location of the hydrophones after one reflection, see Figure 4.13). These results show that the new shape has the same findings as the previous model (circular shape) where the only difference lies in the change in the size of the small patch and the effect of the new parameter α (a measure of the sea surface scattering).

Figure 4.13 shows the normalised acoustic intensity in the x-direction received from below the horizontal after one reflection with the seabed. The magnitude of the normalised acoustic intensity increases rapidly as the radius of the surface noise increases for hydrophones located near the small patch (A1=0m, where A1 is the distance between the hydrophones and the leading edge of the small patch). This rise is due to the increase in the magnitude of the reflection coefficient which leads to a greater asymmetry in the seabed. However, this rise will be constant after a certain radius due to the critical angle. For hydrophones located at distances equal or greater than A1=200m the normalised acoustic intensity is zero, this is due to the symmetry of the seabed where the hydrophones lie in the region influenced by the critical angle.

Figure 4.14 shows that hydrophones located at distances of 200m and 400m from the leading edge of the small patch, with the rays hitting the seabed twice, the normalised

acoustic intensity is very small. This indicates that the rays miss hitting the small patch due to the small size of the section on an annulus. For hydrophones located at 600m and 800m the rays have a greater chance of hitting the small patch causing an increase in the acoustic intensity. However, this increase is limited by the critical angle.

Figures 4.15 and 4.16 shows the normalised acoustic intensity arriving from below the horizontal for three and four reflections with the seabed respectively. These graphs show similar findings to that mentioned above. The only difference apparent from these graphs is the effect of the scattering at the sea surface, which forces the acoustic intensity to decrease rapidly with an increase in the number of the reflections. This effect can be used as an indication that the sea surface scattering significance of the higher number of reflections. However, as mentioned before, detailed analysis of the scattering effect is not essential for this project, it is enough to appreciate that the acoustic intensity can be decreased rapidly with each reflection with the sea surface.

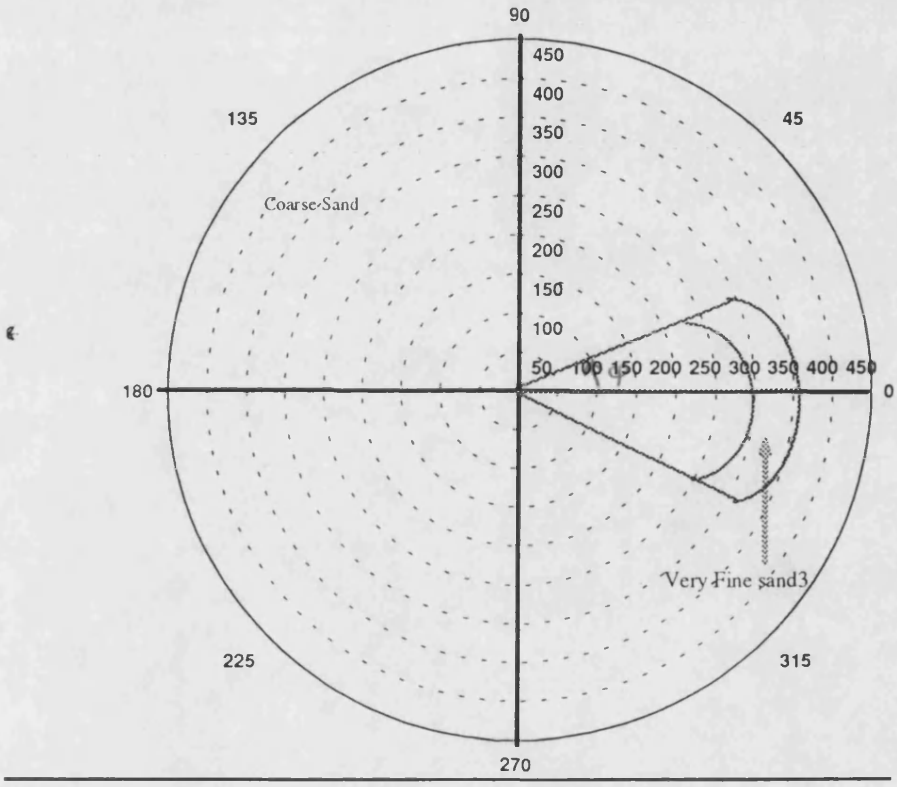

Figure 4.12 is an illustration of the section of an annulus shape in the seabed

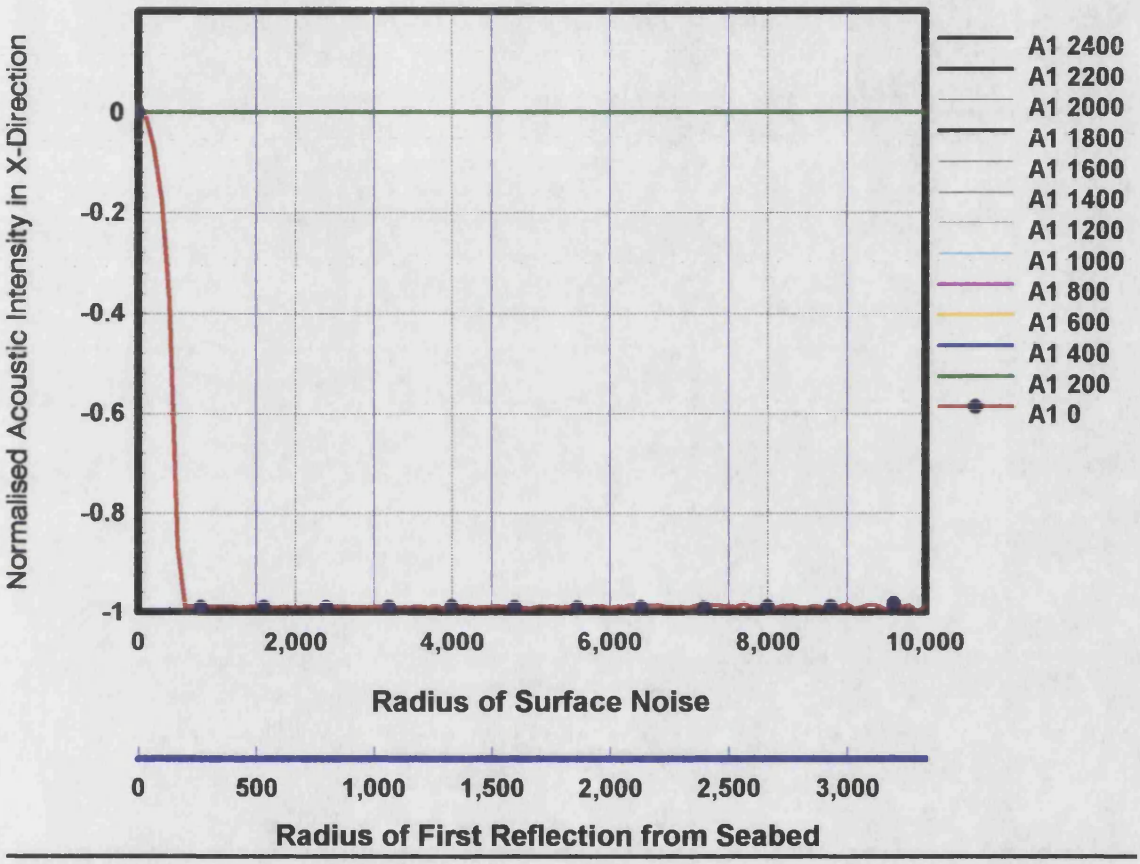

Figure 4.13 represents the normalised acoustic intensity in the x-direction received from the seabed after one reflection. This acoustic intensity plotted against the increases in the radius of the surface noise in meters. A1 corresponds to the locations of the hydrophnes relative to the leading edge of the section of an annulus patch.. The depth of the shallow water and the hydrophones are H=200m and z=100m respectively, the area of the section of an annulus is given as $A = \varphi\left(A_2^2 - A_1^2\right)$ where $A_2 = 400 + A_1$ and φ is the horizontal angle.

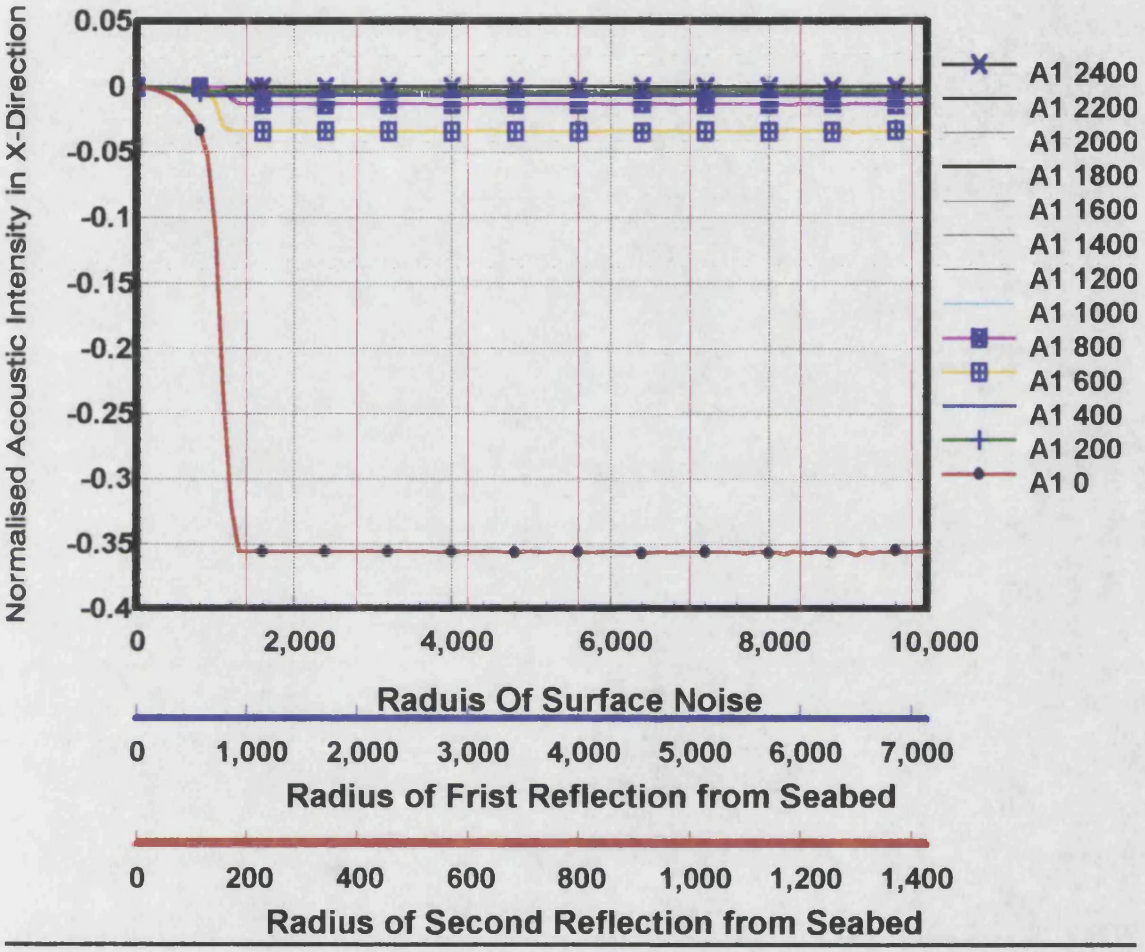

Figure 4.14 shows the normalised acoustic intensity in the x-direction arriving from the sea surface after two reflections with the seabed. The same variables as Figure 4.13 is taken in this figure.

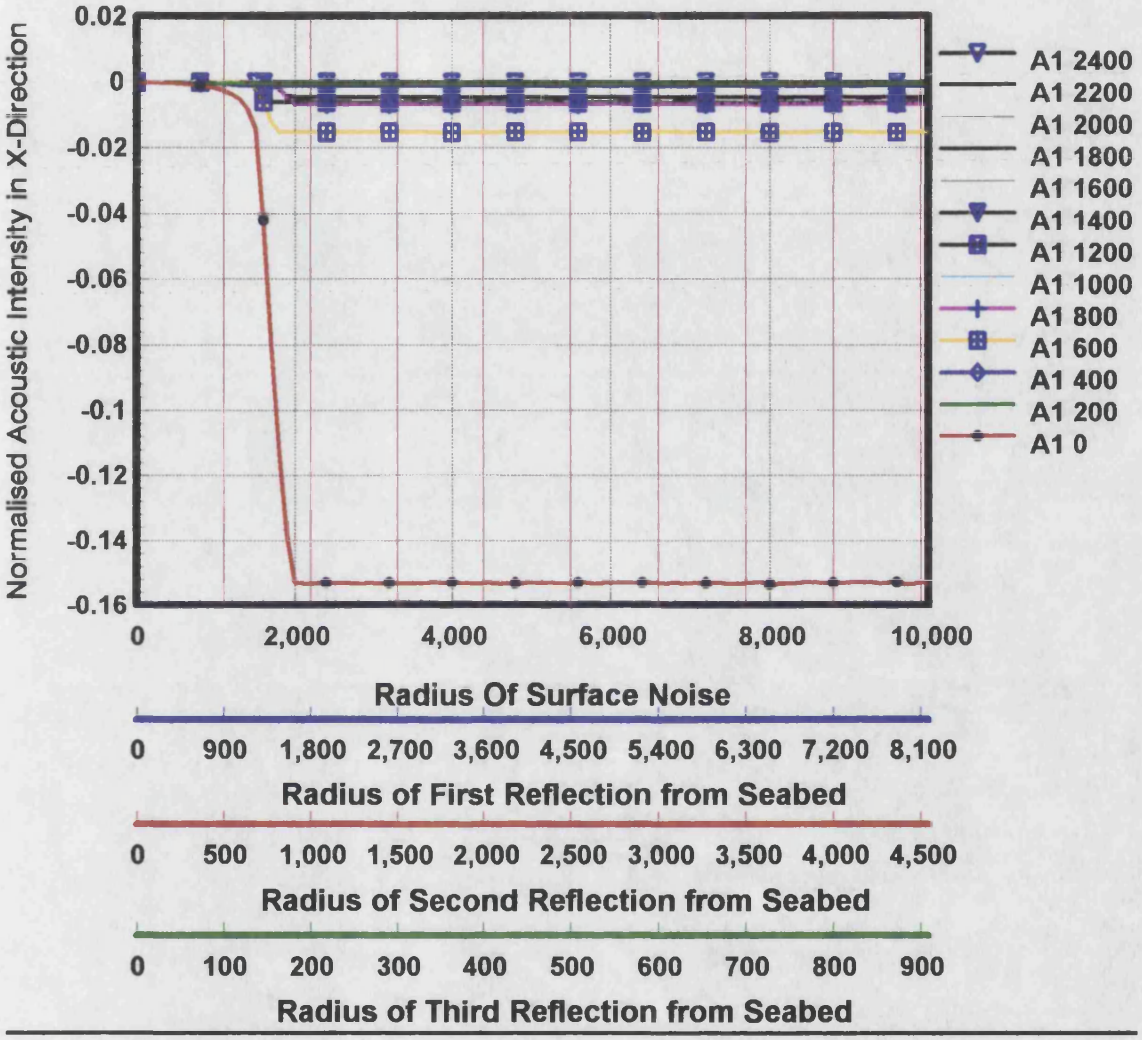

Figure 4.15 shows the normalised acoustic intensity in the x-direction arriving from the seabed after three reflections with the seabed. The same variables as Figure 4.13 is taken in this figure.

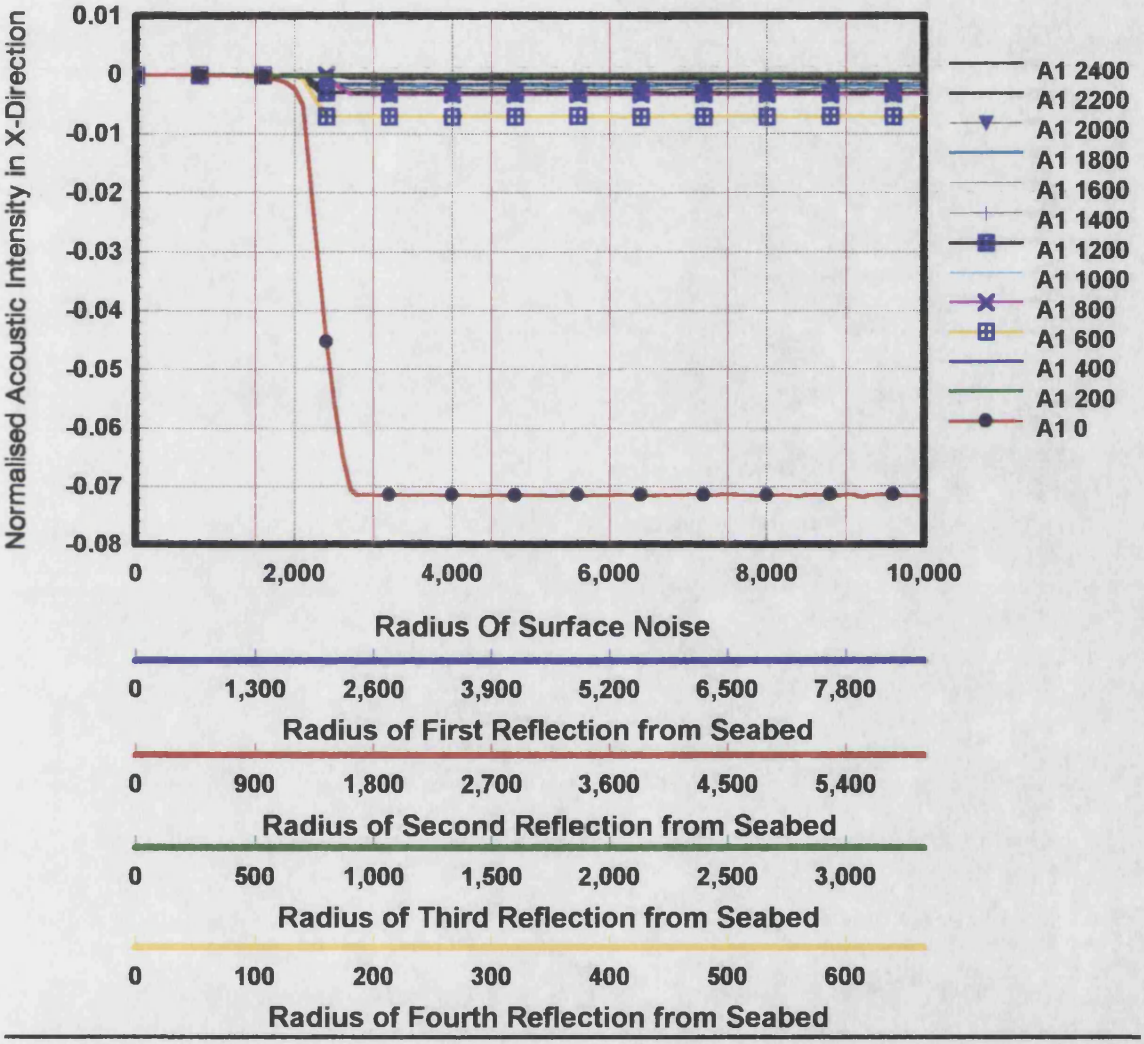

Figure 4.16 shows the normalised acoustic intensity in the x-direction arriving from the sea surface after four reflections with the seabed. The same variables as Figure 4.13 is taken in this figure.

4.3.3 Different Sizes of The Section of an Annulus

The previous computer model has been modified in order to be more capable in evaluating the total normalised acoustic intensity (in terms of the total received rays from above and below the horizontal). This model excludes the scattering effect of the sea surface introduced in the previous model.

Figure 4.17 to Figure 4.20 represents the normalised acoustic intensity versus the location of the small patch (or the hydrophones) for different sizes of the small patch. In this example:

1. The small patch has been assumed to be made of Very Fine Sand, the seabed as a whole assumed to be made of Coarse Sand.

2. The depth of the hydrophones and the shallow water are 100m and 200m respectively.

3. In order to choose the effective radius, different sizes of surface noise radii have been considered (D2=4,000m to 13,000m, in steps of 1,000m).

4. Figure 4.17 and Figure 4.18 shows that there are no significant effects after L=20 reflections with the seabed. However, in this example, L=30 seabed reflections have been considered.

Figure 4.18 shows the normalised acoustic intensity versus the location of the small patch. The area of the small patch is defined as follows:

$$A = \varphi\left(A_2^2 - A_1^2\right)$$

Where:

A_1 is the distance from the point of origin (the location of the hydrophones) to the leading edge of the small patch.

$A_2 = 100 + A_1$, is the distance from the point of origin to the furthest edge of the small patch

$\varphi = 30^o$ is the azimuth angle

The behaviour of the normalised acoustic intensity can be summarised as follows:

1. The total normalised acoustic intensity will increase rapidly as the small patch moves away from the hydrophones. This increase in the intensity occurs due to the increase in the reflection coefficient.

2. If we look at the diagram in Figure 4.3 it will be easier to interpret the drop in the acoustic intensity in Figure 4.18. The drop in the acoustic intensity occurs for two reasons, the first is that the rays arriving from above and below the horizontal have

already reached the critical angle after having hit the seabed once, the second reason is that the rays have missed hitting the small patch.

3. At different positions, the probability of the rays hitting the small patch and the magnitude of the reflection coefficient of the small patch changes. This explains the increases and decreases occurring in the received normalised acoustic intensity. However, the size of these peaks and nulls will get smaller and smaller until the effect of the small patch is insignificant.

However, if the size of the small patch has been changed, see Figure 4.19, such that:

$$A_2 = 400 + A_1 \text{ and } \varphi = 90^o$$

The normalised acoustic intensity in this graph will increase and decrease continuously but will tend to decrease in value overall as the hydrophones move along the x-axis, away from the patch. The normalised acoustic intensity varies with the probability of hitting the small patch. However, since the size of the small patch is bigger than that in the previous example, it is clear that the chances of hitting the small patch increases. As the size of the small patch increases, where

$$A_2 = 800 + A_1 \text{ and } \varphi = 90^o$$

the normalised acoustic intensity will decrease more and more smoothly with range, see Figure 4.20.

4.3.4 Different Types of the Small Patch

This section forms the final part of the theoretical study. The normalised acoustic intensity will be studied for different types of seabed. As was concluded in the previous section, only one radius of the surface noise (effective radius) and a single group of reflections (effective reflection number) with the seabed is significant. Figure 4.21 and Figure 4.22 represent the normalised acoustic intensity for different types and sizes of the small patch, bearing in mind that the rest of the seabed is assumed to be made of Coarse Sand. The conclusion made from Figure 4.21 can be summarised thus:

1. For Fine Sand, Very Fine Sand and Silty Sand the normalised acoustic intensity follows a pattern of peaks and troughs as the hydrophones move away from the small patch. This variation in the intensity is similar to that in the differing sizes of the small patch used (see above). The graphs are similar for all three seabed types, and the variation in the normalised acoustic intensity is only sensitive to the chances of the rays hitting the small patch.

2. The remaining types of seabed (i.e. Silty Clay, Clay, etc.) follow the same pattern. Nevertheless, they do not reach the value zero and they display a smoother variation

before evening out. The reason for the different behaviour is unrelated to the probability of hitting the small patch (since the size of the small patch is unaltered) but is due to the fact of increasingly contrasting types of seabed.

Figure 4.22 displays the same characteristics but are for larger sizes of the small patch, resulting in the increasing possibility of hitting the patch.

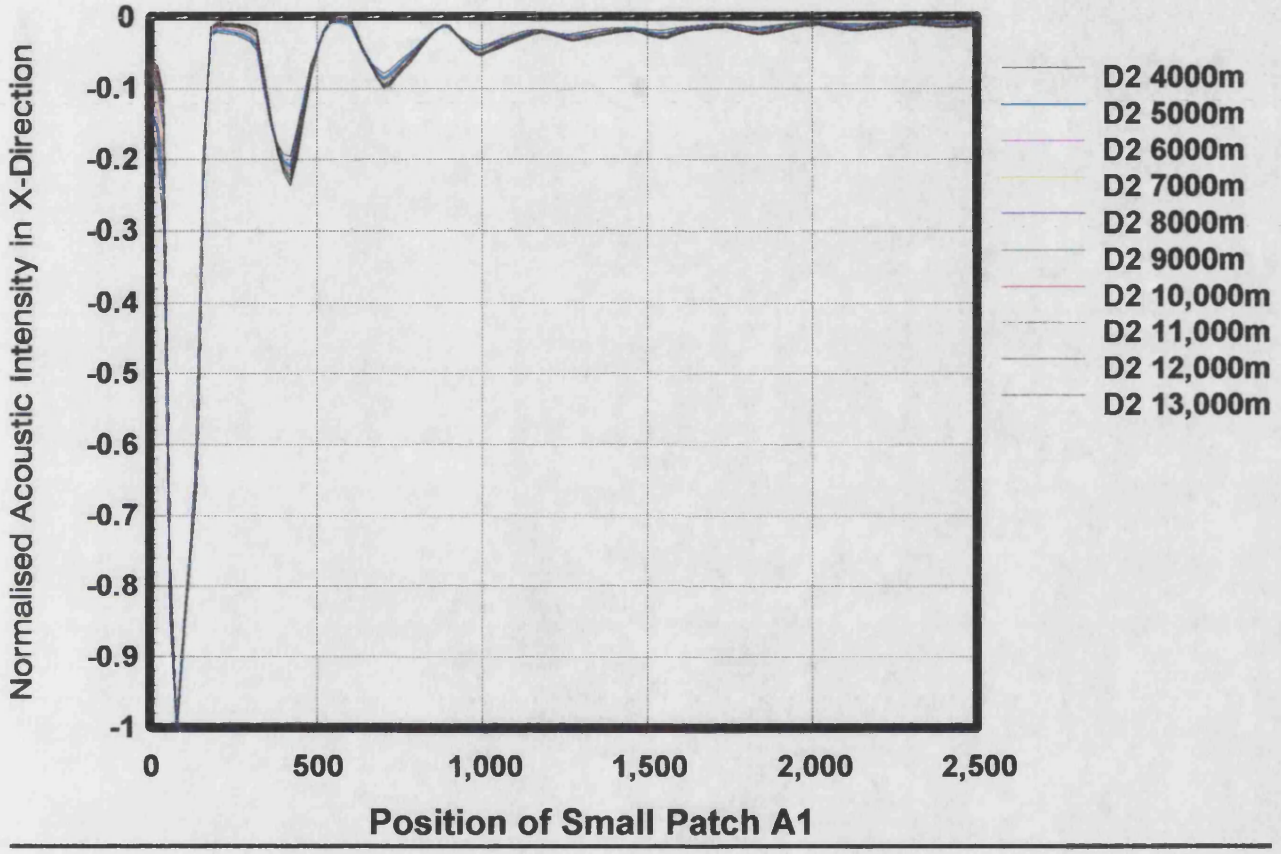

Figure 4.17 represents the normalised acoustic intensity in the x-direction versus the location of the small patch. H=200m, z=100m, after L=20 reflections with the seabed. The radius of the surface noise D2 changes from 4,000m to 13,000m in steps of 1,000m.

The area of the small patch is $A = \varphi\left(A_2^2 - A_1^2\right)$, where $A_2 = 100 + A_1$ $\varphi = 30°$

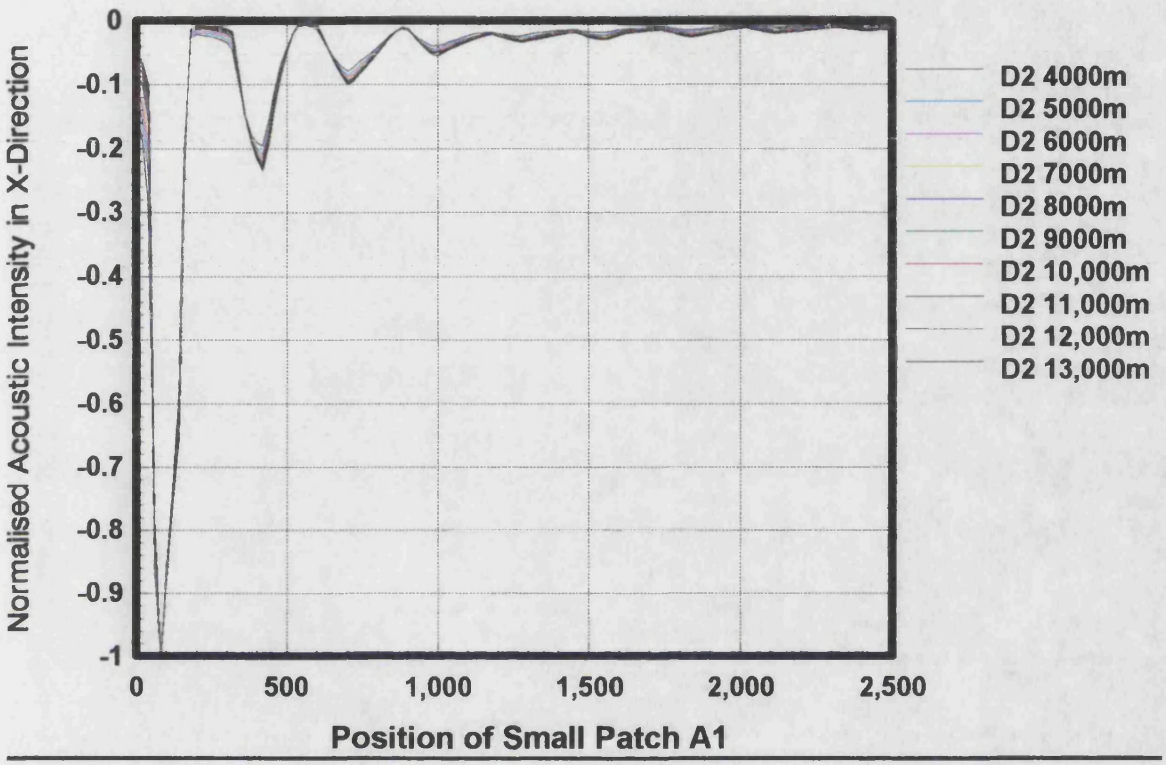

Figure 4.18 represents the normalised acoustic intensity in the x-direction versus the location of the small patch. H=200m, z=100m, after L=30 reflections with the seabed. The radius of the surface noise D2 changes from 4,000m to 13,000m in steps of 1,000m.

The area of the small patch is $A = \varphi\left(A_2^2 - A_1^2\right)$, where $A_2 = 100 + A_1$ $\varphi = 30°$

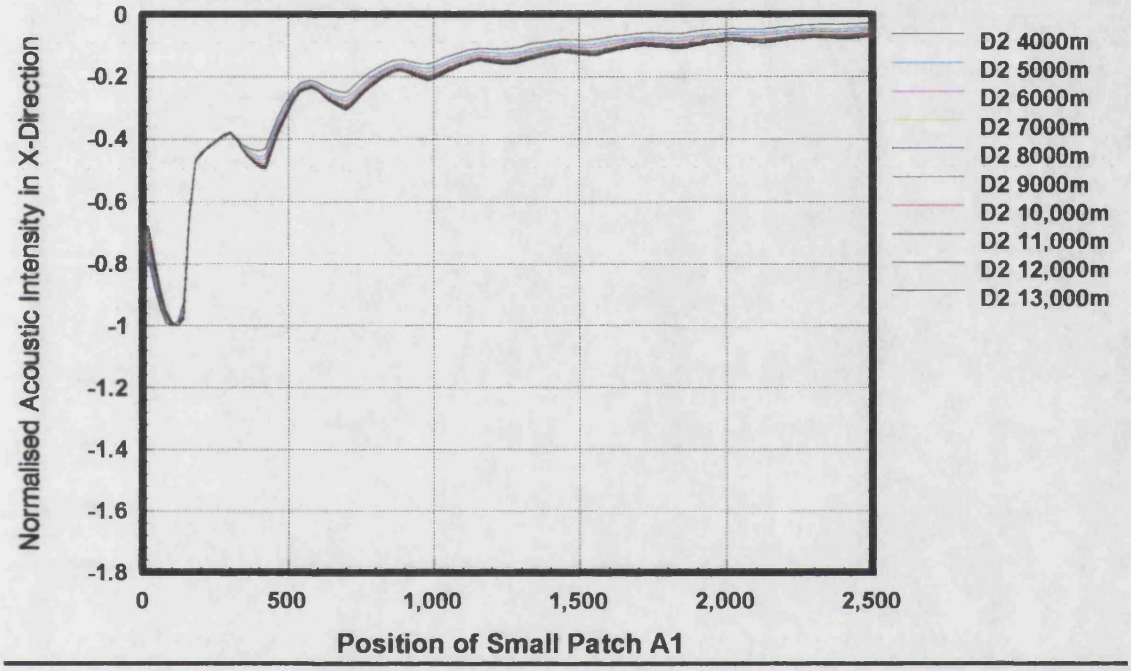

Figure 4.19 represents the normlised acoustic intensity in the x-direction versus the location of the small. H=200m, z=100m, after L=30 reflections with the seabed. The radius of the surface noise changes from 4,000m to 13,000m in steps of 1,000m. The area of the small patch is $A = \varphi\left(A_2^2 - A_1^2\right)$, where $A_2 = 400 + A_1$ $\varphi = 90°$

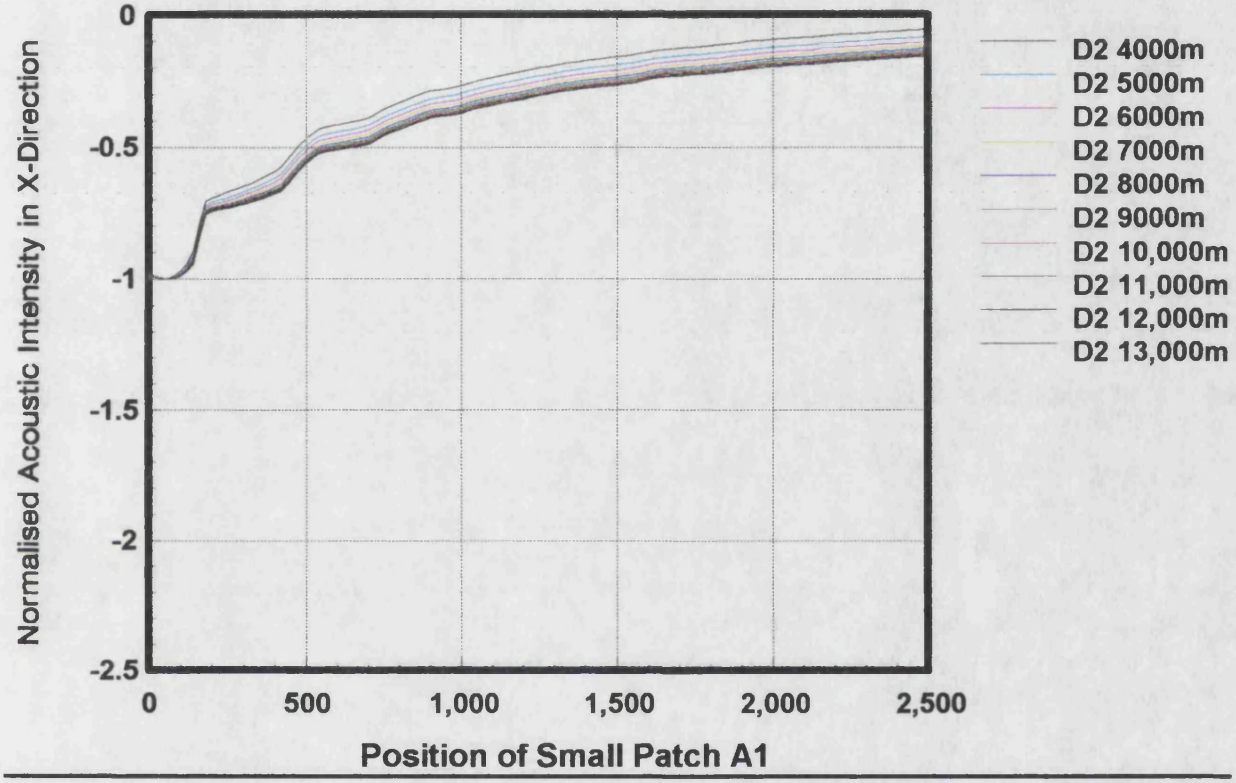

Figure 4.20 represents the normlised acoustic intensity in the x-direction versus the location of the small. H=200m, z=100m, after L=30 reflections with the seabed. The radius of the surface noise changes from 4,000m to 13,000m in steps of 1,000m. The area of the small patch is $A = \varphi\left(A_2^2 - A_1^2\right)$, where $A_2 = 800 + A_1$ $\varphi = 90^\circ$

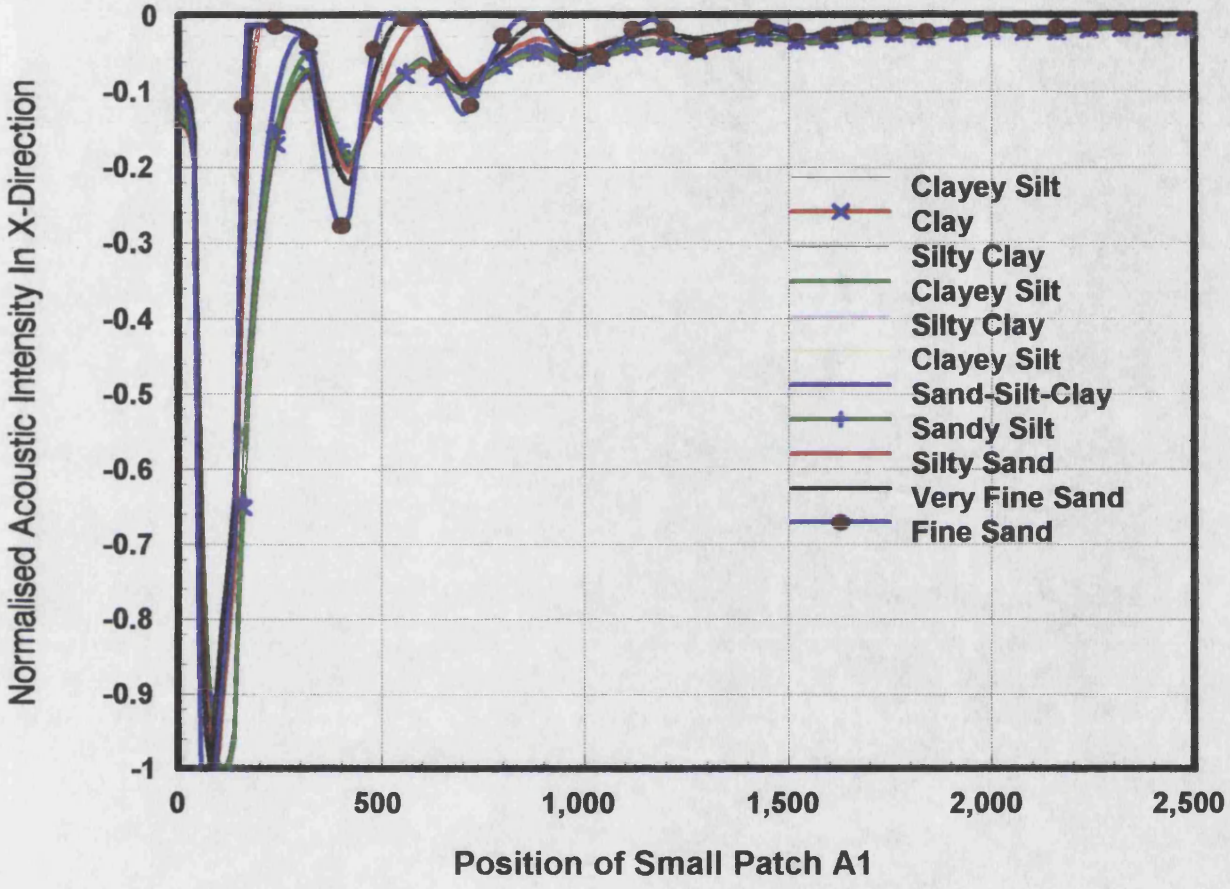

Figure 4.21 represents the normalised acoustic intensity in the x-direction versus the location of the small patch A1 in meters (A1 is the distance from the hydrophones to the leading edge of the small patch) for different types of seabed. H=200, z=100, D2=13,000m, L=30, $A = \varphi\left(A_2^2 - A_1^2\right)$, where $A_2 = 100 + A_1$ $\varphi = 25^o$.

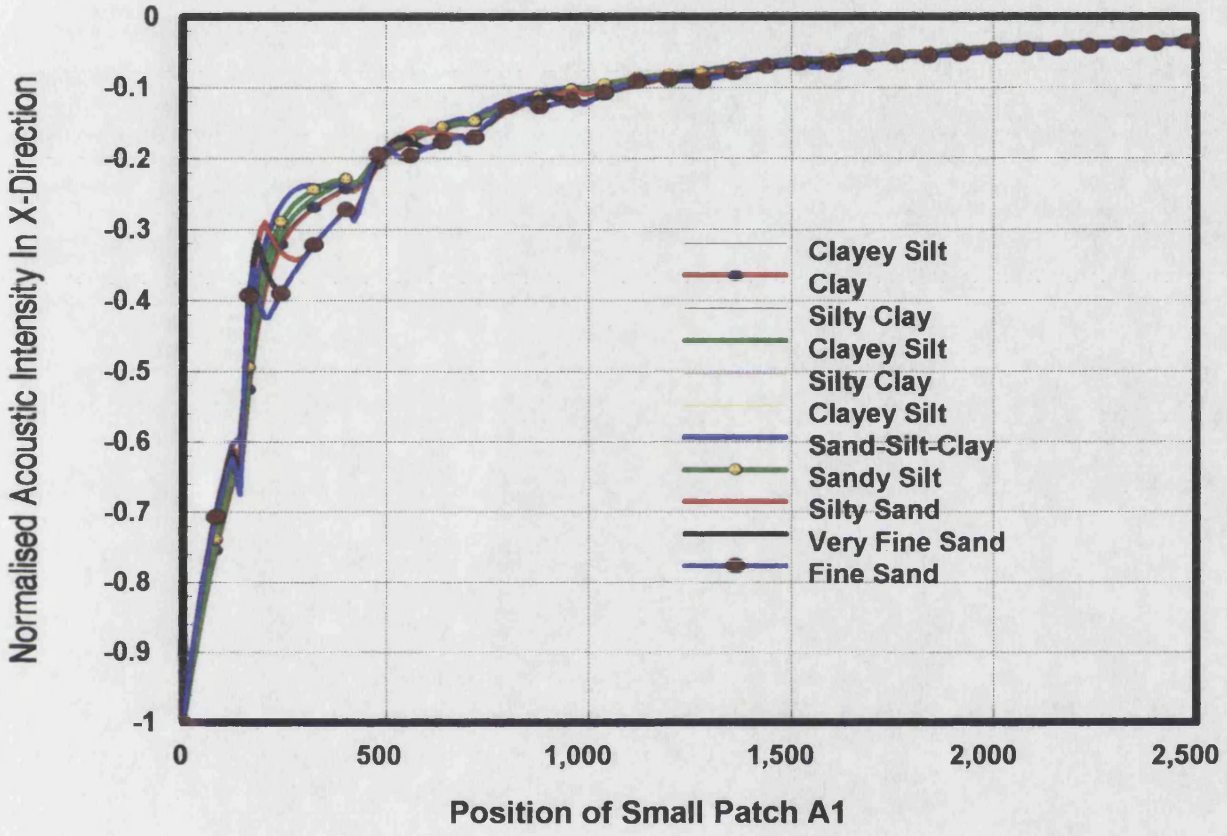

Figure 4.22 represents the normalised acoustic intensity in the x-direction versus the location of the small patch A1 in meters (A1 is the distance from the hydrophones to the leading edge of the small patch) for different types of seabed. H=200, z=100, D2=13,000m, L=30, $A = \varphi\left(A_2^2 - A_1^2\right)$, where $A_2 = 300 + A_1$ $\varphi = 45^o$.

4.4 APPENDIX 4A

This is a FORTRAN program written in order to estimate the acoustic intensity in the x-direction due to the increase in the radius of the surface noise. This program also calculates the acoustic intensity due to the movement of the hydrophones towards the asymmetry in the seabed. In this program the seabed has been divided into two parts: a circular patch which represents the small area and the seabed as a whole. In an effort to obtain the acoustic intensity, the numerical integration over the sea surface and the horizontal angle has been employed.

```
      DOUBLE PRECISION D2,Z,A0,A01,H,M,N,M1,N1,IX1
      DOUBLE PRECISION C,C1,C2,RHO,RHO1,RHO2,PI
      DOUBLE PRECISION RFC,RFC1,D3(2000),TH30
      DOUBLE PRECISION YY,YY0,XX0,XX,Y,X
      DOUBLE PRECISION IXT, IXTT(2000,35), IX11(2),IX2
      DOUBLE PRECISION X1IT1(2000,35),X1IT2(2000,35)
      DOUBLE PRECISION X2IT1(2000,35),X2IT2(2000,35)
      DOUBLE PRECISION X3IT1(2000,35),X3IT2(2000,35)
      DOUBLE PRECISION X4IT1(2000,35),X4IT2(2000,35)
      INTEGER NI,L,LX,KKK,NIN,NX,NP,NP1

C                          INPUT DATA
C                       *****************

      PRINT*,'INPUT SOUND SPEED IN SEA C AND SEABED C1,C2'
      READ(*,*)C,C1,C2

      PRINT*,'INPUT DENSITIES OF SEA RHO AND SEABED RHO1,RHO2'
      READ(*,*)RHO,RHO1,RHO2

      PRINT*,'INPUT VALUE OF RECEIVERS DEPTH Z1'
      READ(*,*)Z1

      PRINT*,'INPUT VALUE OF SHALLOW WATER H'
      READ(*,*)H

      PRINT*,'INPUT STEPS NUMBER OF THE NUMERICAL INTEGRATION'
      READ(*,*)NP,NP1

     PI=ACOS(-1.0D0)
     M=RHO1/RHO
     M1=RHO2/RHO
     N=C/C1
```

```
      N1=C/C2
      NX=0

C     (XX0,YY0) AND (XX,YY) GIVES THE CO-ORDINATES OF THE SMALL
C     CIRCULAR AREA
C     ********************************************************

       YY=0.0D0
       YY0=0.0D0

       DO 1 XX0=2400,400,-200

C      XX REPRESENTS THE HYDROPHONES MOVING TOWARDS
C         THE SMALL CIRCULAR PATCH.
C      ******************************************

          XX=400.0D0+XX0
          NX=NX+1

C          A01 IS THE RADIUS OF THE SMALL PATCH AND
C          A0  IS THE DISTANCE FROM THE ORIGIN TO
C              THE CENTRE OF THE SMALL PATCH
C   ********************************************************

       A01=SQRT((XX-XX0)**2+(YY-YY0)**2)
       A0=SQRT((0.0D0-XX0)**2+(0.0D0-YY0)**2)
       Y=0.0D0
       LX=0

C      D2 IS THE RADIUS OF THE SURFACE NOISE
C      *************************************

       DO 121 X=0,8000.0D0,100
          D2=SQRT((X-0.0D0)**2+(Y-0.0D0)**2)
          LX=1+LX
          D3(LX)=D2

C      L=1 REPRESENTS ACOUSTIC INTENSITY RECEIVED FROM THE SEABED
C      L=2 REPRESENTS ACOUSTIC INTENSITY RECEIVED FROM THE SEA SURFACE
C   ********************************************************************

       DO 3 L=1,2
          IX11(L)=0.0D0

C      NI IS THE NUMBER OF REFLECTIONS WITH THE SEABED
C      ***********************************************

           DO 3 NI=1,4

C      Z IS THE VERTICAL DISTANCE OF EACH IMAGE ABOVE OR BELOW
C        THE HORIZONTAL AFTER SEVERAL REFLECTIONS WITH THE SEABED.
C    ************************************************************

           IF(L.EQ.1)THEN
              Z=2.0D0*H*NI-Z1
            ELSE
```

```
              Z=2.0D0*H*NI+Z1
              END IF

C       SUB-PROGRAMS
C       ************

        IF(D2.LE.(A0-A01))THEN

C        DUE TO THE SYMMETRY IN THE SEABED THE
C        ACOUSTIC INTENSITY IN THE X-DIRECTION IS ZERO.
C      ************************************************

                    IXT=0.0D0
                  ELSE

C       THE FOLLOWING SUBROUTINE SUBW1 ESTIMATES
C       THE ACOUSTIC INTENSITY RECEIVED VIA THE
C       SMALL CIRCULAR PATCH.
C       ********************************************

        CALL SUBW1(NI,L,D2,Z,Z1,H,A0,A01,NP,NP1,M
       *                ,N,M1,N1,IX1,RFC,RFC1)

C       SUBGX  CALCULATES THE ACOUSTIC INTENSITY RECEIVED
C              FROM THE OTHER HORIZONTAL DIRECTIONS.
C     ***********************************************

        CALL SUBGX(NI,D2,Z,A0,A01,NP,M,N,IX2)

C       IXT IS THE TOTAL ACOUSTIC INTENSITY RECEIVED
C           FROM ALL THE HORIZONTAL DIRECTIONS.
C       ******************************************

       IXT=2.0D0*IX1+IX2
       END IF

C      IX11(L) IS THE TOTAL ACOUSTIC INTENSITY RECEIVED FROM
C              ABOVE OR BELOW THE HORIZONTAL IN THE X-DIRECTION
C      ********************************************************

       IX11(L)=IX11(L)+IXT

C      THE ACOUSTIC INTENSITY DUE TO EACH REFLECTION
       NUMBER (NI), EACH VALUE OF THE SURFACE NOISE
C      RADIUS (LX) AND EVERY LOCATION OF THE SMALL PATCH (NX)
C    ************************************************************

          IF(NI.EQ.1)THEN
             IF(L.EQ.1)THEN
               X1IT1(LX,NX)=IXT
               ELSE
                 X1IT2(LX,NX)=IXT
               END IF
               ELSEIF(NI.EQ.2)THEN
                   IF(L.EQ.1)THEN
                     X2IT1(LX,NX)=IXT
```

```
                ELSE
                  X2IT2(LX,NX)=IXT
              END IF
              ELSEIF(NI.EQ.3)THEN
                IF(L.EQ.1)THEN
                  X3IT1(LX,NX)=IXT
                ELSE
                  X3IT2(LX,NX)=IXT
              END IF
              ELSEIF(NI.EQ.4)THEN
                IF(L.EQ.1)THEN
                  X4IT1(LX,NX)=IXT
                ELSE
                  X4IT2(LX,NX)=IXT
            END IF
            END IF

 3        CONTINUE
 121      CONTINUE

          IXTT(LX,NX)=IX11(1)+IX11(2)

 1        CONTINUE
          NI=NI-1

C                          THE OUTPUT DATA
C       ****************************************

      OPEN(3333,FILE='IXTT.DAT')
      DO 671 KKK=1,LX
        WRITE(3333,25)D3(KKK),(IXTT(KKK,NIN),NIN=1,NX)
 671  CONTINUE
      OPEN(1,FILE='X1T1.dat')
      OPEN(2,FILE='X1T2.dat')
      DO 67 KKK=1,LX
         WRITE(1,25)D3(KKK),(X1IT1(KKK,NIN),NIN=1,NX)
         WRITE(2,25)D3(KKK),(X1IT2(KKK,NIN),NIN=1,NX)
 67   CONTINUE
      CLOSE(1)
      CLOSE(2)
      OPEN(11,FILE='X2T1.dat')
      OPEN(41,FILE='Z2T2.dat')
      DO 77 KKK=1,LX
         WRITE(11,25)D3(KKK),(X2IT1(KKK,NIN),NIN=1,NX)
         WRITE(21,25)D3(KKK),(X2IT2(KKK,NIN),NIN=1,NX)
 77   CONTINUE
      CLOSE(41)
      CLOSE(11)
      OPEN(12,FILE='X3T1.dat')
      OPEN(22,FILE='X3T2.dat')
      DO 780 KKK=1,LX
         WRITE(12,25)D3(KKK),(X3IT1(KKK,NIN),NIN=1,NX)
         WRITE(22,25)D3(KKK),(X3IT2(KKK,NIN),NIN=1,NX)
 780  CONTINUE
      CLOSE(12)
      CLOSE(22)
```

```
      OPEN(13,FILE='X4T1.dat')
      OPEN(23,FILE='X4T2.dat')
      DO 790 KKK=1,LX
         WRITE(13,25)D3(KKK),(X4IT1(KKK,NIN),NIN=1,NX)
         WRITE(23,25)D3(KKK),(X4IT2(KKK,NIN),NIN=1,NX)
 790  CONTINUE
      CLOSE(33)
      CLOSE(43)
 25   FORMAT(20(2X,1E10.4))
      END


C     ****************************************************
C     THE MAIN AIM OF THE FOLLOWING SUBROUTINE IS TO CARRY OUT
C     THE NUMERICAL INTEGRATION TO OBTAIN THE ACOUSTIC INTENSITY
C     RECEIVED VIA THE DIRECTION OF THE CIRCULAR PATCH.
C     ****************************************************

      SUBROUTINE SUBW1(NI,L,D2,Z,Z1,H,A0,A01,NP,NP1,M
     +        ,N,M1,N1,IX1,RFC,RFC1)

      DOUBLE PRECISION D2,Z,A0,A01,H1,H2,M,N,M1,N1,IX1
      DOUBLE PRECISION PHI,PHI1,IX,A,A1,A2,FLLL,FLLL1
      DOUBLE PRECISION WX,RFC,RFC1,Z1,H
      INTEGER LLL,LLL1,ODEV,ODEV1,NP,NI,I,L4,NP1,I1,L

C     PHI IS THE HORIZONTAL ANGLE
C     ******************************

      IF(D2.LE.SQRT(A0**2+A01**2))THEN

C     BY USING THE COSINE RULE PHI CAN BE EXPRESSED AS
C     ************************************************

        PHI=ACOS((A0**2+D2**2-A01**2)/(2*A0*D2))
      ELSE
         PHI=ACOS(A0/SQRT(A0*A0+A01*A01))
         END IF

C     THE FOLLOWING PART OF THE PROGRAM USES THE EXTENDED
C     SIMPSONS RULE WHERE H2 AND H1 ARE THE STEP SIZES FOR
C     THE DOUBLE INTEGRATION.
C     ****************************************************

      H2=PHI/NP1
      IX1=0.0D0

C     THE FOLLOWING FIRST TWO DO LOOPS (4) AND (5) REPRESENTS
C     THE NUMERICAL INTEGRATION OVER THE HORIZONTAL ANGLE (PHI).
C     ************************************************************

      DO 4 LLL=1,2

        IF(LLL.EQ.1)THEN
            ODEV=1
            FLLL=4.0D0
```

```
          ELSE
             ODEV=2
             FLLL=2.0D0
             END IF

       DO 5 I1=ODEV,NP1-1,2
             PHI1=REAL(I1)*H2

C       A1 AND A2 ARE THE FIRST AND SECOND BOUNDARIES
C       WHICH SEPARATES THE TWO TYPES OF SEABED.
C       ***********************************************

        A1=A0*COS(PHI1)-SQRT(A0**2*(COS(PHI1))**2-A0**2+A01**2)
        A2=A0*COS(PHI1)+SQRT(A0**2*(COS(PHI1))**2-A0**2+A01**2)

        H1=D2/NP
        IX=0.0D0

C       DO LOOPS 6 AND 7 GIVE THE NUMERICAL INTEGRATION
C          OVER THE RADIUS OF THE SURFACE NOISE (A)
C       ***********************************************

        DO  6 LLL1=1,2

           IF(LLL1.EQ.1.0D0)THEN
               ODEV1=1
               FLLL1=4.0D0
            ELSE
               ODEV1=2
               FLLL1=2.0D0
            END IF

       DO 7 I=ODEV1,NP-1,2

            A=REAL(I)*H1


C      *********************************************************
C      SUBW11 IS A SUBROUTINE WHICH CALCULATES THE ACOUSTIC
C      INTENSITY RECEIVED VIA THE CIRCULAR PATCH. THE VARIABLES
C      OVER WHICH THIS CALCULATION IS CARRIED OUT ARE THE RADIUS
C      OF THE SURFACE NOISE(A) AND THE HORIZONTAL ANGLE(PHI)
C      *********************************************************

       CALL SUBW11(PHI1,A,A1,A2,Z,Z1,H,NI,L,
      *              M,N,M1,N1,WX,RFC,RFC1)

        IX=IX+FLLL1*WX

 7     CONTINUE
 6     CONTINUE

       A=D2
       CALL SUBW11(PHI1,A,A1,A2,Z,Z1,H,NI,L,
      *              M,N,M1,N1,WX,RFC,RFC1)
```

```
      IX=IX+WX
      IX=(IX*H1/3.0D0)
      IX1=IX1+FLLL*IX

5     CONTINUE
4     CONTINUE

      DO 13 L4=1,2

         IF(L4.EQ.1)THEN
            PHI1=0.0
          ELSE
             PHI1=PHI
             END IF

      A1=A0*COS(PHI1)-SQRT(A0**2*(COS(PHI1))**2-A0**2+A01**2)
      A2=A0*COS(PHI1)+SQRT(A0**2*(COS(PHI1))**2-A0**2+A01**2)

      NP=D2/H1
      IX=0.0D0

      DO 10 I=1,NP-1,2
           A=REAL(I)*H1

      CALL SUBW11(PHI1,A,A1,A2,Z,Z1,H,NI,L,
     *                M,N,M1,N1,WX,RFC,RFC1)
      IX=IX+4.0D0*WX

10    CONTINUE

      DO 11 I=2,NP-1,2
         A=REAL(I)*H1

      CALL SUBW11(PHI1,A,A1,A2,Z,Z1,H,NI,L
     *              ,M,N,M1,N1,WX,RFC,RFC1)

            IX=IX+2.0D0*WX

11    CONTINUE

      A=D2
      CALL SUBW11(PHI1,A,A1,A2,Z,Z1,H,NI,L,
     *                M,N,M1,N1,WX,RFC,RFC1)

      IX=IX+WX
      IX=(IX*H1/3.0D0)
      IX1=IX1+IX
13    CONTINUE
      IX1=(IX1*H2/3.0D0)
      END
```

```
C      THE AIM OF THIS SUBROUTINE IS TO CALCULATE THE ACOUSTIC
C      INTENSITY ARRIVING FROM THE SAME DIRECTION AS THE SMALL
C      CIRCULAR PATCH WITH A CERTAIN RADIUS (A) AND HORIZONTAL
C      ANGLE (PHI)
C      ******************************************************

       SUBROUTINE SUBW11(PHI1,A,A1,A2,Z,Z1,
      * H,NI,L,M,N,M1,N1,WX,RFC,RFC1)

       DOUBLE PRECISION  A,Z,R,TH,N1,M1,N,M,A1,A2
       DOUBLE PRECISION  RFC,RFC1,WX,PHI1,WX1,Z1,H
       COMPLEX RF,RF1
       INTEGER NR1,MR1,NI,L

C      ************************************************
C      THE FOLLOWING SUBROUTINE (SUBW111) CALCULATES ALL
C      THE POSSIBILITIES FOR HITTING BOTH SEABED TYPES
C      ************************************************

       CALL SUBW111(A,A1,A2,Z,Z1,H,NI,L,TH,R,NR1,MR1)

C      RF AND RF1 ARE THE REFLECTION COEFFICIENT OF
C      THE TWO TYPES OF SEABED
C      ****************************************

       RF=(M*COS(TH)-SQRT(CMPLX(N**2-(SIN(TH))**2)))
      *   /(M*COS(TH)+SQRT(CMPLX(N**2-(SIN(TH))**2)))

       RF1=(M1*COS(TH)-SQRT(CMPLX(N1**2-(SIN(TH))**2)))
      *    /(M1*COS(TH)+SQRT(CMPLX(N1**2-(SIN(TH))**2)))

       RFC=(SQRT((REAL(RF))**2+(AIMAG(RF))**2))
       RFC1=(SQRT((REAL(RF1))**2+(AIMAG(RF1))**2))

      WX1=(((RFC**NR1)*(RFC1**MR1))**(2)*(COS(TH))**2*(SIN(TH)))

C     WX IS THE ACOUSTIC INTENSITY ARRIVING FROM
C        DIRECTION (PHI) AND RADIUS (A).
C     ****************************************

      WX=(A*WX1*COS(PHI1))/R**2
     END


C     ************************************************
C     THE FOLLOWING SUBROUTINE (SUBW111) CALCULATES ALL
C     THE POSSIBILITIES FOR HITTING BOTH SEABED, WHERE
C     NR1 IS THE NUMBER OF CHANCES OF HITTING THE LARGE PATCH.
C     MR1 IS THE NUMBER OF CHANCES OF HITTING THE SMALL PATCH.
C     ******************************************************

      SUBROUTINE SUBW111(A,A1,A2,Z,Z1,H,NI,L,TH,R,NR1,MR1)

      DOUBLE PRECISION A,A1,A2,Z,Z1,H,TH,R,AD,TH1,PI
      INTEGER NI,L,NR1,MR1,NR,COUNT
```

```
      PI=ACOS(-1.0D0)
      R=SQRT(A**2+Z**2)

C     TH IS THE ANGLE FROM THE NORMAL AND R IS THE DISTANCE
C     FROM A POINT SOURCE TO THE RECEIVER.
C     ******************************************************

      TH=ACOS(Z/R)
      TH1=(90*PI/180.0D0)-TH
      NR1=0
      MR1=0

      COUNT=2*NI
      DO 18 NR=1,COUNT,2

      IF(L.EQ.1)THEN
        AD=(NR*H-Z1)/TAN(TH1)
        ELSE
            AD=(NR*H+Z1)/TAN(TH1)
            END IF

     IF(AD.LE.A1.OR.AD.GT.A2)THEN
         NR1=NR1+1
         ELSEIF(AD.LE.A2)THEN
            MR1=MR1+1
            END IF

  18  CONTINUE
      END


C     ******************************************************
C     THIS SUBROUTINE ESTIMATES THE ACOUSTIC INTENSITY
C     RECEIVED FROM THE OTHER HORIZONTAL DIRECTIONS.
C     ******************************************************

      SUBROUTINE SUBGX(NI,D2,Z,A0,A01,NP,M,N,IX2)
      DOUBLE PRECISION D2,Z,A0,A01,H1,M,N,IX2
      DOUBLE PRECISION PHI,A,IX,GX,GZ,RFC
      INTEGER NP,NI,I

      IF(D2.LE.SQRT(A0**2+A01**2))THEN
        PHI=ACOS((A0**2+D2**2-A01**2)/(2*A0*D2))
        ELSE
           PHI=ACOS(A0/SQRT(A0*A0+A01*A01))
           END IF

      H1=D2/NP
      IX=0.0D0


C     THE FOLLOWING DO LOOPS ARE EMPLOYED TO ESTIMATE THE
C     NUMERICAL INTEGRATION OF THE SURFACE NOISE.
C     ******************************************************

      DO 5 I=1,NP-1,2
```

```
          A=REAL(I)*H1

C    SUBG REPRESENTS THE SUBROUTINE WHICH COMPUTES
C         THE ACOUSTIC INTENSITY DUE TO THE RADIUS (A)
C    ***********************************************

       CALL SUBG(A,Z,NI,M,N,GX,RFC)
       IX=IX+4.0E0*A*GX*(-2*SIN(PHI))
 5     CONTINUE

       DO 6 I=2,NP-1,2
         A=REAL(I)*H1
          CALL SUBG(A,Z,NI,M,N,GX,RFC)
         IX=IX+2.0E0*A*GX*(-2*SIN(PHI))
 6     CONTINUE
         A=D2
           CALL SUBG(A,Z,NI,M,N,GX,RFC)
           IX=IX+A*GX*(-2*SIN(PHI))
           IX2=(IX*H1/3.0E0)
           END


C      *******************************************
C      SUBG REPRESENTS THE SUBROUTINE WHICH COMPUTES
C           THE ACOUSTIC INTENSITY.
C      *******************************************

       SUBROUTINE SUBG(A,Z,NI,M,N,GX,RFC)
       DOUBLE PRECISION A,Z,R,TH,TH1,N,M
       DOUBLE PRECISION RFC,GX
       COMPLEX RF
       INTEGER NI

       R=SQRT(A**2+Z**2)
       TH=ACOS(Z/R)
       TH1=ASIN(A/R)

       RF=(M*COS(TH)-CSQRT(CMPLX(N**2-(SIN(TH1))**2)))
      *  /(M*COS(TH)+CSQRT(CMPLX(N**2-(SIN(TH1))**2)))
       RFC=(SQRT((REAL(RF))**2+(AIMAG(RF))**2))**(2*NI)

       GX=(RFC*(COS(TH))**2*SIN(TH1))/R**2

       END
```

4.5 APPENDIX 4B

The aim of this FORTRAN program is to calculate the acoustic intensity in the x direction due to asymmetry in the seabed structure (the asymmetry is a section of an annulus).

```
      DOUBLE PRECISION D2,Z,A1,A2,H,M,N,M1,N1,IX,A11,A12
      DOUBLE PRECISION C,C1,C2,RHO,RHO1,RHO2,Z1,PI,RFC,RFC1
      DOUBLE PRECISION D3(2000),TH30,PHI,PHI1,PHI2
      DOUBLE PRECISION Y,X,IX11(2),IXTT(2000,20)
      DOUBLE PRECISION X1IT1(2000,35),X1IT2(2000,35)
      DOUBLE PRECISION X2IT1(2000,35),X2IT2(2000,35)
      DOUBLE PRECISION X3IT1(2000,35),X3IT2(2000,35)
      DOUBLE PRECISION X4IT1(2000,35),X4IT2(2000,35)
      INTEGER NI,L,LX,NP,NX,NX1,KKK,NIN

      PRINT*,'INPUT SOUND SPEED IN WATER C AND SEABED C1,C2'
      READ(*,*)C,C1,C2

      PRINT*,'INPUT DENSITIES OF SEA WATER RHO,AND RHO1,RHO2'
      READ(*,*)RHO,RHO1,RHO2

      PRINT*,'INPUT VALUE OF RECEIVERS DEPTH Z'
      READ(*,*)Z1

      PRINT*,'INPUT VALUE OF SHALLOW WATER H'
      READ(*,*)H

      PRINT*,'INPUT STEPS NUMBER FOR THE NUMERICAL INTEGRATION'
      READ(*,*)NP

     PRINT*,'INPUT HORIZONTAL ANGLE PHI1 IN DEGREES WHICH'
     PRINT*,'IDENTIFE INDICATES TO THE AREA OF THE SMALL PATCH.
     READ(*,*)PHI1

      PI=ACOS(-1.0D0)
      M=RHO1/RHO
      M1=RHO2/RHO
      N=C/C1
      N1=C/C2

       PHI2=(PHI1*PI)/180.0D0

C     A11 AND A12 ARE THE FIRST CO-ORDINATES OF
C                 THE SECTION OF AN ANNULUS.
C     ****************************************

        A11=0.0D0
        A12=200.0D0
        NX=0
```

```
C    A1 AND A2  SPECIFIES THE MOVEMENT OF
C               THE HYDROPHONES
C    ************************************

     DO 2 A1=10.0D0,2400.0D0,200.0D0

          A2=200.0D0+A1
          NX=1+NX

         IF(NX.EQ.1)THEN
             PHI=PHI2
             ELSE
             PHI=PHI2*((A12**2-A11**2)/(A2**2-A1**2))
             END IF

        Y=0.0D0
        LX=0

C     THE FOLLOWING DO LOOP REPRESENTS THE INCREASE
C     IN THE RADIUS OF THE SURFACE NOISE
C     *******************************************

      DO 1 X=0,10000.0D0,100

             D2=SQRT((X-0.0D0)**2+(Y-0.0D0)**2)
             LX=1+LX
             D3(LX)=D2

             DO 3 L=1,2
                IX11(L)=0.0D0
                DO 3 NI=1,4
                   IF(L.EQ.1)THEN
                      Z=2.0D0*H*NI-Z1
                   ELSE
                      Z=2.0D0*H*NI+Z1
                   END IF

C    SUBW1 IS A SUBROUTINE USED FOR ESTIMATING THE NUMERICAL
C          INTEGRATION USING THE EXTENDED SIMPSONS RULE.
C    *****************************************************

     CALL SUBW1(PI,PHI,NI,L,D2,Z,Z1,H,A1,A2,NP
    *                  ,M,N,M1,N1,IX,RFC,RFC1)

C    IX11(L) IS THE TOTAL ACOUSTIC INTENSITY RECEIVED FROM
C            ABOVE OR BELOW THE HORIZONTAL IN THE X-DIRECTION
C    ****************************************************

    IX11(L)=IX11(L)+IX

C    THE ACOUSTIC INTENSITY DUE TO EACH REFLECTION
C    NUMBER (NI),FOR EACH OF SURFACE NOISE RADIUS
C    (LX) AND EVERY LOCATION OF THE SMALL PATCH (NX)
C    ***************************************************

     IF(NI.EQ.1)THEN
```

```
        IF(L.EQ.1)THEN
           X1IT1(LX,NX)=IX
           ELSE
              X1IT2(LX,NX)=IX
         END IF
         ELSEIF(NI.EQ.2)THEN
         IF(L.EQ.1)THEN
            X2IT1(LX,NX)=IX
            ELSE
               X2IT2(LX,NX)=IX
         END IF
         ELSEIF(NI.EQ.3)THEN
         IF(L.EQ.1)THEN
            X3IT1(LX,NX)=IX
            ELSE
               X3IT2(LX,NX)=IX
         END IF
         ELSEIF(NI.EQ.4)THEN
         IF(L.EQ.1)THEN
            X4IT1(LX,NX)=IX
            ELSE
               X4IT2(LX,NX)=IX
         END IF
       END IF

 3    CONTINUE

        IXTT(LX,NX)=IX11(1)+IX11(2)
 1      CONTINUE
 2      CONTINUE
             NI=NI-1

C                          THE OUTPUT DATA
C        ****************************************

        OPEN(3333,FILE='IXTT.dat')
        DO 671 KKK=1,LX
             WRITE(3333,25)D3(KKK),(IXTT(KKK,NX1),NX1=1,NX)
 671    CONTINUE
        OPEN(1,FILE='X1T1.dat')
        OPEN(2,FILE='X1T2.dat')
        DO 67 KKK=1,LX
               WRITE(1,25)D3(KKK),(X1IT1(KKK,NIN),NIN=1,NX)
               WRITE(2,25)D3(KKK),(X1IT2(KKK,NIN),NIN=1,NX)
 67     CONTINUE
        CLOSE(1)
        CLOSE(2)
        OPEN(11,FILE='X2T1.dat')
        OPEN(21,FILE='X2T2.dat')
        DO 77 KKK=1,LX
               WRITE(11,25)D3(KKK),(X2IT1(KKK,NIN),NIN=1,NX)
               WRITE(21,25)D3(KKK),(X2IT2(KKK,NIN),NIN=1,NX)
 77     CONTINUE
        CLOSE(11)
        CLOSE(21)
        OPEN(12,FILE='X3T1.dat')
```

```
      OPEN(22,FILE='X3T2.dat')
      DO 780 KKK=1,LX
            WRITE(12,25)D3(KKK),(X3IT1(KKK,NIN),NIN=1,NX)
            WRITE(22,25)D3(KKK),(X3IT2(KKK,NIN),NIN=1,NX)
780   CONTINUE
      CLOSE(12)
      CLOSE(22)
      OPEN(13,FILE='X4T1.dat')
      OPEN(23,FILE='X4T2.dat')
      DO 790 KKK=1,LX
             WRITE(13,25)D3(KKK),(X4IT1(KKK,NIN),NIN=1,NX)
             WRITE(23,25)D3(KKK),(X4IT2(KKK,NIN),NIN=1,NX)
790   CONTINUE
      CLOSE(13)
      CLOSE(23)
25    FORMAT(30(2X,1E10.4))
      END

C     THE AIM OF THIS SUBROUTINE IS TO ESTIMATE
C     THE NUMERICAL INTEGRATION USING THE EXTENDED
C     SIMPSONS RULE FOR THE SEABED DIVIDED INTO TWO TYPES:
C     SECTION OF AN ANNULUS AND THE SEABED AS A WHOLE.
C     ************************************************

      SUBROUTINE SUBW1(PI,PHI,NI,L,D2,Z,Z1,H,A1,A2,NP
     +       ,M,N,M1,N1,IX,RFC,RFC1)
      DOUBLE PRECISION D2,Z,H1,M,N,M1,N1,PI,Z1
      DOUBLE PRECISION PHI,IX,A,A1,A2,H
      DOUBLE PRECISION WX1,WX2,RFC,RFC1
      INTEGER NP,NI,I,L

      H1=D2/NP
      IX=0.0D0
      DO 17 I=1,NP-1,2
            A=REAL(I)*H1

      CALL SUBW11(A,A1,A2,Z,Z1,H,NI,L,M,N,M1,N1
     *            ,WX1,WX2,RFC,RFC1)

        IX=IX+4*(WX1*(2*SIN(PHI))+WX2*(-2*SIN(PHI)))
17    CONTINUE

      DO 7 I=2,NP-1,2

            A=REAL(I)*H1
      CALL SUBW11(A,A1,A2,Z,Z1,H,NI,L,M,N,M1,N1
     *           ,WX1,WX2,RFC,RFC1)

            IX=IX+2*(WX1*(2*SIN(PHI))+WX2*(-2*SIN(PHI)))
7       CONTINUE

        A=D2
        CALL SUBW11(A,A1,A2,Z,Z1,H,NI,L,M,N,M1,N1
     *       ,WX1,WX2,RFC,RFC1)

        IX=IX+(WX1*(2*SIN(PHI))+WX2*(-2*SIN(PHI)))
```

```
          IX=(IX*H1/3.0D0)
          END


C    THE AIM OF THIS SUBROUTINE IS TO CALCULATE THE ACOUSTIC
C    INTENSITY ARRIVING FROM THE SAME DIRECTION AS THE SMALL
C    SECTION OF AN ANNULUS.
C    ******************************************************

       SUBROUTINE SUBW11(A,A1,A2,Z,Z1,H,NI,L,M,N,M1,N1
      *      ,WX1,WX2,RFC,RFC1)

       DOUBLE PRECISION  A,Z,R,TH,N1,M1,N,M,A1,A2,H,Z1
       DOUBLE PRECISION  RFC,RFC1,WX,WX1,WX2
       COMPLEX RF,RF1
       INTEGER NR1,MR1,NI,L,MI

       CALL SUBW111(A,A1,A2,Z,Z1,H,NI,L,TH,R,NR1,MR1)

       RF=(M*COS(TH)-SQRT(CMPLX(N**2-(SIN(TH))**2)))
      *   /(M*COS(TH)+SQRT(CMPLX(N**2-(SIN(TH))**2)))
       RF1=(M1*COS(TH)-SQRT(CMPLX(N1**2-(SIN(TH))**2)))
      *    /(M1*COS(TH)+SQRT(CMPLX(N1**2-(SIN(TH))**2)))
       RFC=(SQRT((REAL(RF))**2+(AIMAG(RF))**2))
       RFC1=(SQRT((REAL(RF1))**2+(AIMAG(RF1))**2))

       IF(L.EQ.1)THEN
           MI=NI-1
          ELSE
               MI=NI
              END IF

  WX=(((RFC**NR1)*(RFC1**MR1))**(2)*(COS(TH))**2*(SIN(TH)))

C    WX1 REPRESENTS THE ACOUSTIC INTENSITY ARRIVING VIA THE
C    CIRCULAR PATCH, THE TERM 0.5 REPRESENTS THE SCATTERING
C    BY THE SEA SURFACE
C    ******************************************************

     WX1=(A*WX*((0.5)**(MI)))/R**2

C    REPRESENTS THE ACOUSTIC INTENSITY ARRIVING FROM THE
C    OTHER DIRECTIONS OF THE SEA.
C    ***************************************************

 WX2=(A*((0.5)**(MI))*(RFC**(2*NI))*((COS(TH))**2)*SIN(TH))/R**2
     END
```

Chapter Five

5. Measuring the Direction of a Point Source

5.1 Introduction

Theoretical studies of the surface noise acoustic intensity vector in shallow water for different seabed structures were presented in the previous chapters. The main conclusion of these theoretical studies was that the normalised surface noise acoustic intensity vector contains information about the seabed. It was shown that the normalised acoustic intensity in the x-y plane is very sensitive to the seabed structure. Resolving this acoustic intensity into its (x,y) components will enable us, in principle, to detect the location of the asymmetry in the seabed.

Practically, in order to measure the direction of the propagating acoustic intensity, at least two closely spaced pressure hydrophones are needed. The pressure at the point

midway between the two hydrophones is related to the mean acoustic pressure, whereas the difference between the pressures corresponds to the pressure gradient, which is proportional to the particle velocity of the acoustic intensity propagating in that direction.

As a first step towards the measurement of the acoustic intensity vector due to the surface generated noise in shallow water, this chapter will introduce some experimental measurements achieved in the laboratory. Detection of the acoustic intensity direction due to a point source is the main target of these measurements. These experimental studies have been put forward in order to check the sensitivity and the accuracy of the hydrophones and the other instruments which will employed in the sea trial (Chapter Six).

This chapter will first measure the direction of the acoustic intensity due to a harmonic point source rotating around the hydrophones. This experiment employed an array of six hydrophones arranged orthogonally to each other, and the role of hydrophone shadowing was shown to have an insignificant effect on the measurements. Good agreement was obtained between the direction of the acoustic intensity measured by using the cross-spectral method, and the direction measured using the known geometry.

Finding the direction of the acoustic intensity due to a noise source rotating around the hydrophones is the second goal of this chapter. Due to the small number of amplifiers available, only two hydrophones could be used at any one time. However, using a pair of hydrophones was sufficient to detect the direction of the noise source.

5.2 Measuring the Direction of a Harmonic Point Source

5.2.1 Introduction

As mentioned in the above introduction, in order to measure the direction of a point source at least two closely spaced pressure hydrophones are needed. Estimating the imaginary part of the cross-spectrum of the two hydrophones will provide the magnitude and the direction of the acoustic intensity propagating in the direction of the hydrophones.

This section discusses the experimental measurements used for detecting the direction of a harmonic point source rotating around the hydrophones. Despite the fact that six hydrophones were used in the experiment, only four of them were processed in order to find the direction of the harmonic point source. The experimental facility and their settings are presented in the following section, followed by the experimental procedure for measuring the direction of the harmonic point source. The last section is devoted to the experimental results.

5.2.2 Experimental Apparatus

The experimental apparatus which were used in the measurement are reviewed as follows:-

5.2.2.1 Hydrophones

Measuring the acoustic intensity in the *r* direction needs at least two closely spaced pressure hydrophones. The pressure at the midway point between the two hydrophones corresponds to the mean acoustic pressure, whereas the difference between the pressures represents the pressure gradient which is related to the particle velocity of the acoustic energy propagating in the *r* direction. In order to measure the acoustic intensity in the three planes (x,y,z), six omnidirectional spherical Bruel and Kjaer (B&K) hydrophones with 21mm diameter are employed in the experiment. The hydrophones are arranged orthogonally to each other. The inner spacing of the hydrophones are shown in Figure 5.1.

As pointed out in the first chapter, some significant errors arise in this method, and these should be carefully dealt with. The first is the finite difference approximation error, which occurs when the spacing of the hydrophones is greater than the wavelength λ of the signal. Figure 5.2 illustrates this error (in dB) versus the increase in the frequency. This error is

about 0.25dB for signals of frequency 8 kHz and a hydrophone spacing of 16.55 mm which can be considered to be irrelevant.

However, the other errors which might occur during the measurement are the instrumentation phase mismatch and the near field effect (see section **1.2.2.2**). The instrumentation phase mismatch occurs at very low frequency, whereas the near field error arises if the acoustic intensity changes within the spacing distance of the hydrophones. Based upon the values chosen for the frequency, the spacing of the hydrophones, and the distance between the source and the receiver, both errors will be ignored in this experiment.

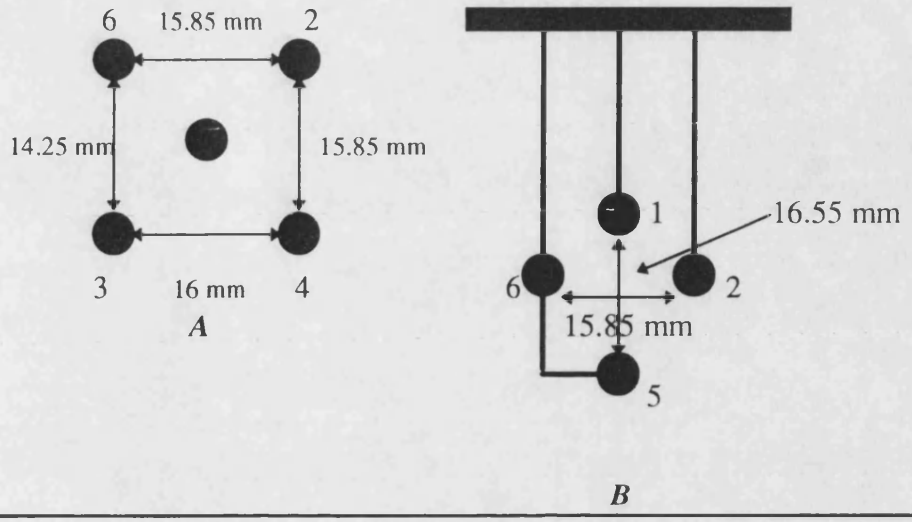

Figure 5.1 shows plan view ***A*** and the cross-section ***B*** of the six Bruel and Kjaer (B&K) hydrophones

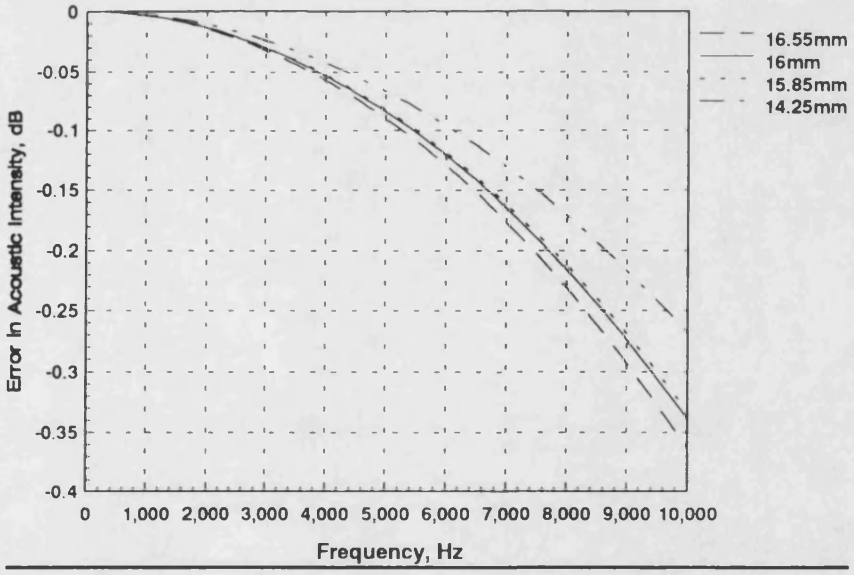

Figure 5.2 shows error in the acoustic intensity due to the finite difference approximation for differently spaced hydrophones

5.2.2.2 The Source and its Location Relative to the Hydrophones

An omnidirectional spherical source with 26.5mm diameter was used as a source for the acoustic signals. This spherical source was placed at a distance far enough from the six B&K hydrophones for the plane wave assumption to be acceptable. The acceptable distance such that a plane wave can be assumed is $\Delta l << \frac{\lambda}{10}$, where λ is the wavelength and Δl is the phase difference due to the spherical shape of the wavefront which can be expressed as $\Delta l = \frac{l^2}{2R}$, where l is the separation distance between each pair of hydrophones and R is the distance between the source and the receiver (see Figure 5.3). Based upon this assumption, for this experiment the separation distance between the source and the hydrophones is $1m$.

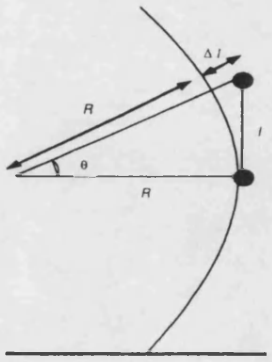

Figure 5.3 illustrates the spherical wave at the hydrophones

5.2.2.3 The Location of the Source and the Hydrophones in the Tank

In order to avoid the interference between the direct and the reflected rays from the tank walls, the following locations of the hydrophones and the source have been chosen (see Figure 5.4):-

1. The hydrophones and the source have been located mid-way between the side walls, (i.e. at a distance of 0.75m from the side walls.).
2. The depth of the hydrophones and the source is 0.8m.
3. The distance between the rear wall and the hydrophones is 1.9m.
4. The distance between the front wall and the source is 2.2m.
5. From the above locations the distance between the hydrophones and the source is 1m.
6. Due to the dimensions of the tank, the hydrophone array will be rotated around itself, which is equivalent to rotating the source around the hydrophones.

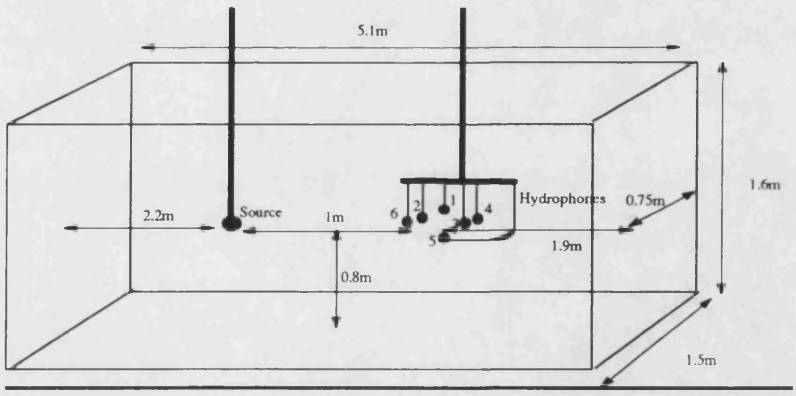

Figure 5.4 illustrates the location of the source and hydrophones in the water tank.

5.2.2.4 Signal Generator

The signals were produced by the spherical source driven by a 20 MHz pulse/function generator (Wavetek model 191). The settings of the function generator are as follows:-

1. The function generator has been adjusted to give signals of frequency 8 kHz.

2. Only two cycles of the signal have been used (pulse width). This is the maximum number of cycles which enables us to separate the first arrival (direct rays) from the second arrival (the reflected rays from the walls).

3. The function generator has been set to send pulses of period 10 ms. This time duration is long enough to avoid the interference between the first and second pulse.

5.2.2.5 Amplifiers

Two Ortec Brookdeal Precision AC amplifiers (model 9452) were connected to two of the B&K hydrophones. The two amplifiers were calibrated to give exactly the same amplification by taking the output signal from the function generator, putting this through the amplifiers and displaying identical signals on a scope (the signal was effectively matched in-phase and amplitude). In this experiment, the amplifiers were adjusted to give a 60dB gain. The upper limit of the filter is 10 kHz, while the lower limit is 1 kHz

5.2.2.6 Data Acquisition

The output signals from the amplifier were sent to a two-channel data acquisition system (A/D Rapid System R2000) which was connected to a computer. The acquisition sampling rate is 200 kHz, which is 5μs per sample.

5.2.2.7 Data processing

Finally, the data was saved by the computer as binary data. A Matlab program (see Appendix 5A section 5.4) was developed in order to process this data. The signals were first multiplied by a hanning window and then processed by using the FFT. After multiplying the fourier transform of the first hydrophone with the complex conjugate of the second hydrophone, the imaginary part gives the imaginary part of the cross spectrum, which is proportional to the acoustic intensity.

5.2.3 The procedure

The following points describe the procedure which was taken in order to measure the acoustic intensity vector due a harmonic point source:-

1. Hydrophone 2 and hydrophone 6 were placed facing the point source (see Figure 5.5). This arrangement gives an angle of 90 degrees between the line connecting hydrophones 2 and 4, and the line connecting hydrophones 2 and 6. This gives the starting position of the rotation, and is given by $\theta = 0^o$.

2. By using a computer, the hydrophones were rotated on-axis in the clockwise direction for 360^o in steps of 2.97^o, giving 121 locations. Due to the complicated design of the hydrophone mounting, there will be a small error for the hydrophones rotating on axis.

3. As a result of the small number of amplifiers available, only the output signal of a pair of hydrophones could be measured simultaneously. However, this problem was overcome by taking measurements four times, with four different pairs of hydrophones. Each time the hydrophones were manually rotated back to their starting position.

4. Due to the arrangement of the experiment, with the hydrophones and receiver being at the same depth, the hydrophones placed in the horizontal (x-y) direction are sufficient to give a complete picture of the harmonic point source direction, even though the hydrophones were designed to give information in the x, y and z directions. The reason for keeping the vertical pair of hydrophones, is to have the same conditions as for the sea trial (Chapter Six), which uses all six hydrophones.

5. The acoustic intensity at the centre of the hydrophone array is given in the x direction as the average of the acoustic intensity measured by the hydrophone pairs 2 and 4, and 6 and 3. Similarly, the acoustic intensity in the y-direction is taken to be the average of the acoustic intensity measured by the hydrophone pairs, 2 and 6, and 4 and 3 (hydrophones position is shown in Figure 5.4).

6. The final practical stage is to digitise the output signals from the amplifiers using the two-channel data acquisition system connected to a computer, where the signals are stored as binary files.

7. In order to process the above data a Matlab program was written, and presented here (Appendix 5A section 5.4). This program firstly converts the binary data into ASCII data. Secondly it evaluates the acoustic intensity in the x-y plane by calculating the imaginary part of the cross-spectrum for each pair of hydrophones.

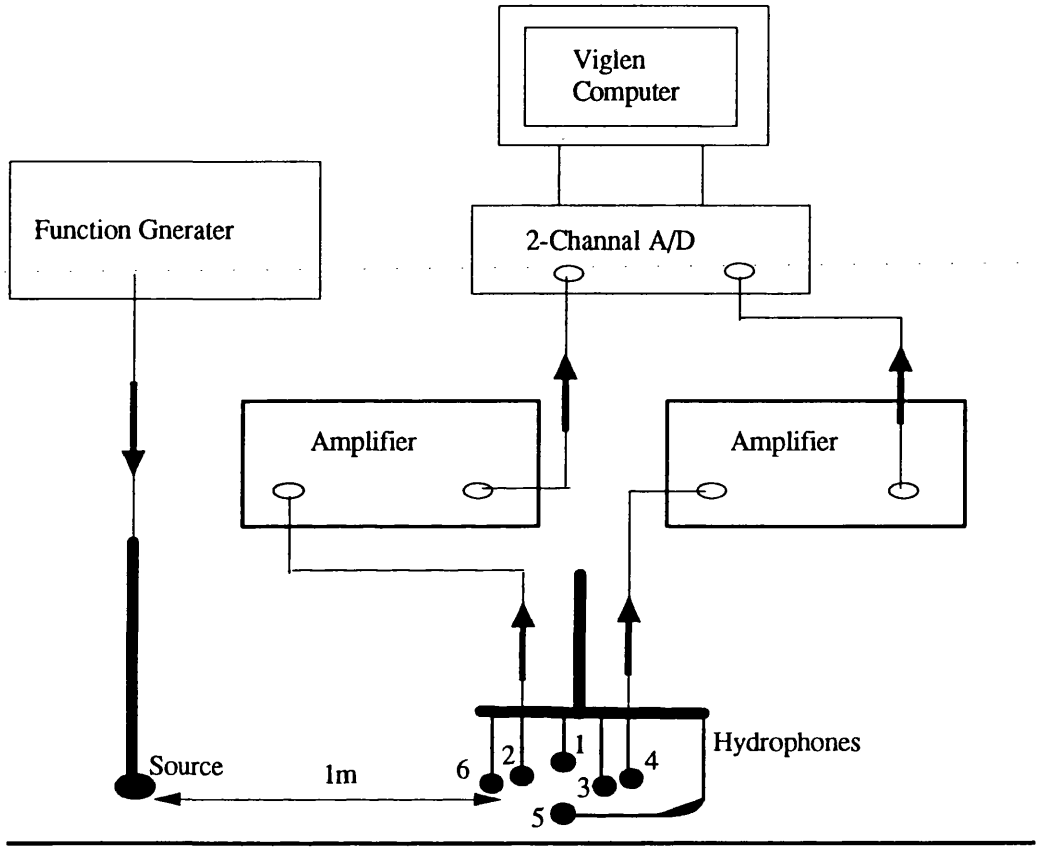

Figure 5.5 Experimental arrangement for measuring the direction of a harmonic point source.

5.2.4 The Results

Figure 5.6a shows the normalised output signals of hydrophone 2 and hydrophone 6 versus the time separation between the source and the hydrophones. Results given are for six different source directions. The data was normalised by dividing the two output signals by the maximum absolute value of the output signal from hydrophone 2. The reason for this normalisation is to show the changes in the relative amplitudes of the two hydrophones. This graph shows the normalised output signals when both hydrophones are facing the source and corresponds to $\theta = 0^o$. In addition to the fact that the two signals are in-phase, further information can be obtained from this graph and is given as follows:-

1. The hydrophones have the same sensitivity, as is clear from the fact that the amplitudes of the two signals are effectively equal.

2. The hydrophones are sufficiently far from the source to make the plane wave approximation acceptable.

Figure 5.6b shows the normalised output signals from the hydrophones for the source rotated by $\theta = 44.55^o$ in the clockwise direction. In addition to the phase shift, the normalised output signal amplitude of hydrophone 2 becomes slightly smaller than that of

hydrophone 6. This decrease in the normalised amplitude is due to the shadowing of hydrophone 6.

Figure 5.6c shows the normalised output signals for a further rotation angle $\theta = 89.1^o$. This graph shows the normalised signals when the phase difference is greatest. The decrease in the normalised amplitude of the signal from hydrophone 2 is more noticeable, as hydrophone 6 almost totally overshadows hydrophone 2.

As the source is rotated further, the phase difference decreases. At $\theta = 133.65^o$, Figure 5.6d, the phase difference decreases from that shown in Figure 5.6c, and at $\theta = 178.2^o$, Figure 5.6e, the phase difference has decreased to zero. These graphs (Figure 5.6d and Figure 5.6e) show that the normalised output signals from the source takes a shorter time to arrive at the hydrophones as the angle θ increases. This can be related to the error in mounting the hydrophones, which results in the hydrophones not rotating around their axis. Due to the complicated design of this mounting it is was very difficult to adjust the hydrophones to be rotated around the axis. However, this error is insignificant as the most important factor in measuring the acoustic intensity direction is the relative phase difference between the hydrophones.

For $\theta = 224.59^o$, Figure 5.6f shows that the normalised signals are again out of phase. However, because hydrophone 2 and hydrophone 6 have swapped positions compared to

Figure 5.6b ($\theta = 44.55^o$) the normalised signal at hydrophone 2 has a shorter time delay than that at hydrophone 6. Also, the shadowing effect is evident from the fact that the normalised signal amplitude at hydrophone 2 has a smaller amplitude than the signals amplitude at hydrophone 6.

Figure 5.7 shows the normalised output signals for a different pair of hydrophones, that is hydrophones 2 and 4. The results presented in this figure show similar findings to those shown in Figure 5.6. The only difference is due to the relative direction of the source and the hydrophones, where for $\theta = 0^o$ the two hydrophones are out of phase by 90 degrees.

In order to be more convinced about the sensitivity of the hydrophones for detection of the point source direction, the direction measured by the gantry is compared to that obtained by using the cross-spectral method. This comparison is displayed in Figure 5.8, and shows a good agreement between the two different methods. The deviation in this graph from a straight line is directly related to the error in mounting the hydrophones.

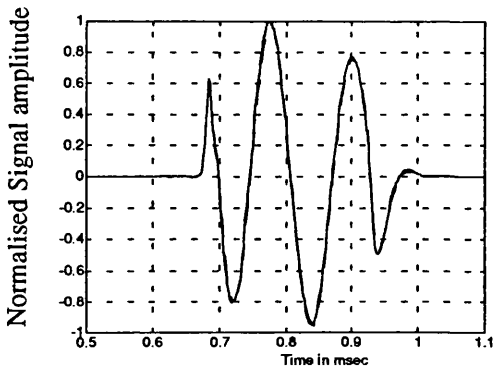

Figure 5.6a $\theta = 0^o$

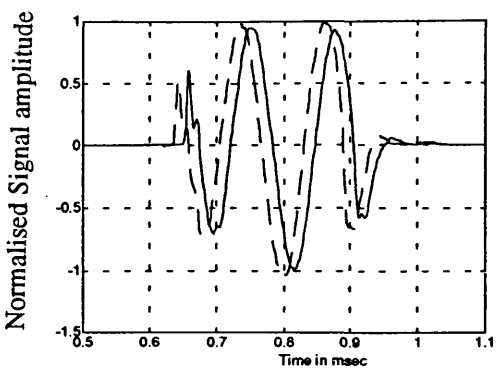

Figure 5.6b $\theta = 44.55^o$

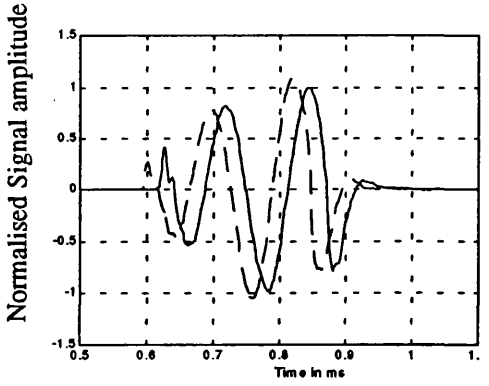

Figure 5.6c $\theta = 89.1^o$

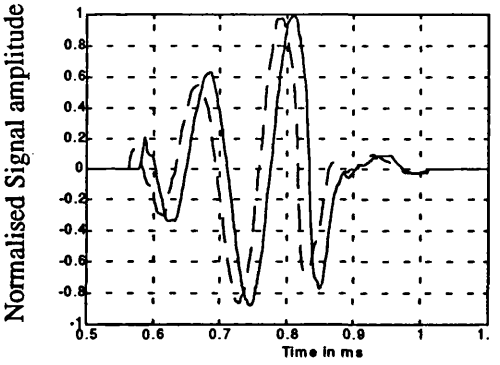

Figure 5.6d $\theta = 133.65^o$

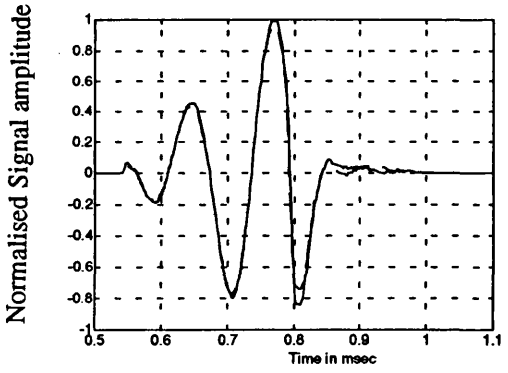

Figure 5.6e $\theta = 178.2^o$

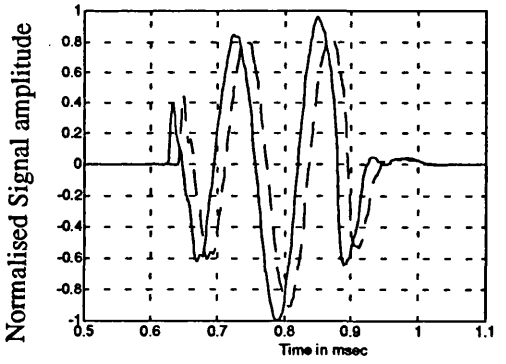

Figure 5.6f $\theta = 224.59^o$

Figure 5.6 shows output signals from hydrophones 2 (solid line) and 6 (dash line) for different source directions.

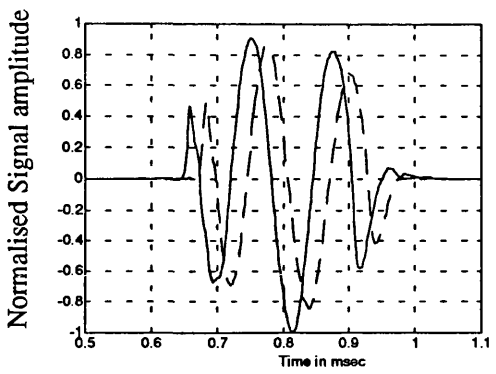

Figure 5.7a $\theta = 0^o$

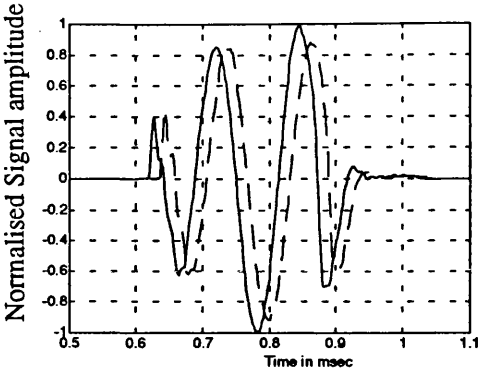

Figure 5.7b $\theta = 44.55^o$

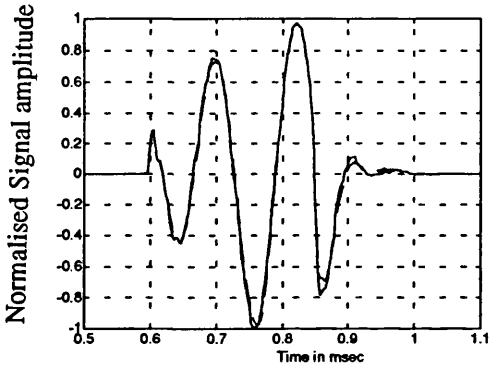

Figure 5.7c $\theta = 89.1^o$

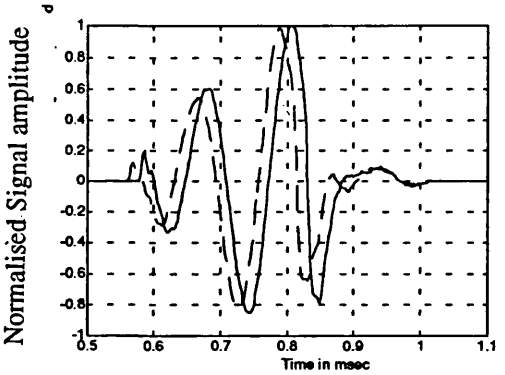

Figure 5.7d $\theta = 133.65^o$

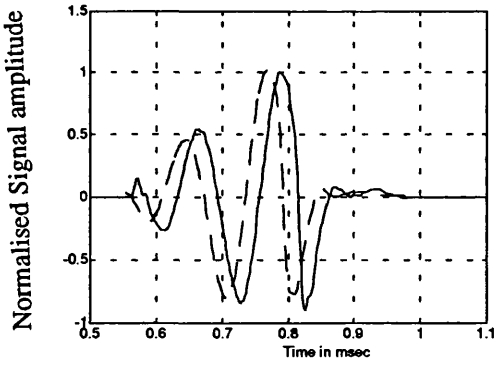

Figure 5.7e $\theta = 178.2^o$

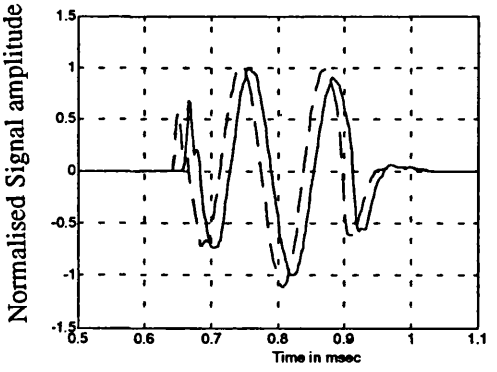

Figure 5.7f $\theta = 224.59^o$

Figure 5.7 shows output signals from hydrophones 2 (solid line) and 4 (dash line) for different source directions.

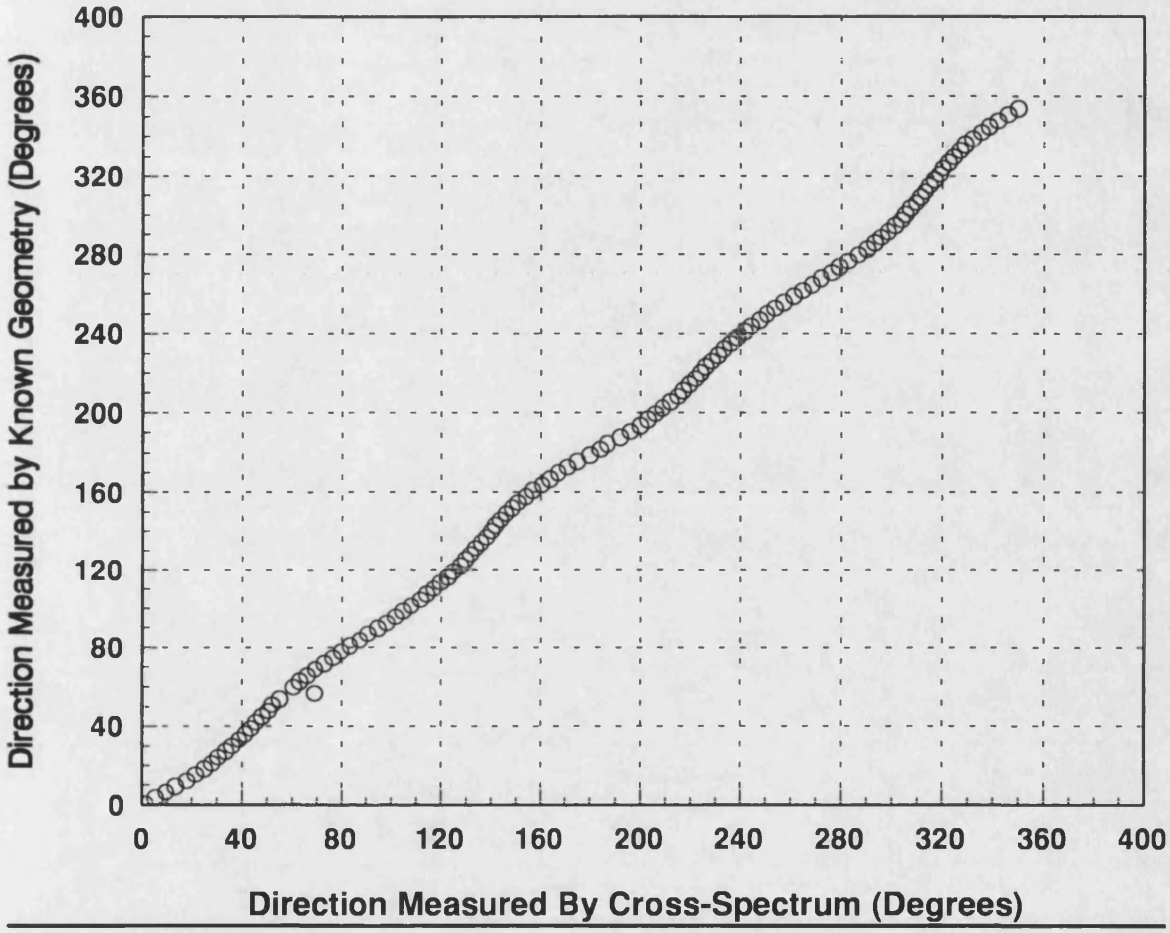

Figure 5.8 shows direction of the harmonic point source measured by the known geometry versus the direction measured by the cross-spectral method.

5.3 Measuring the Direction of a Noise Source

5.3.1 Introduction

In the previous experiment the direction of a harmonic point source was detected successfully using the cross-spectral method. Although only two amplifiers were available, it was possible to present the direction of the harmonic point source using four hydrophones. The technique was to replace the hydrophones in their original position manually after each measurement of a pair of hydrophones.

This section tries to find the direction of a **noise** source using the cross-spectral method. Due to the random behaviour of the noise source, it is no longer possible to use the above technique. Consequently, in order to detect the direction of the noise source, only two hydrophones were used. However, the same hydrophone array presented in the previous example is used here.

The following section gives a description of the experimental apparatus used for generating the noise signal, followed by a section detailing the procedure. The task of the final section will be to present the experimental results.

5.3.2 Experimental Apparatus

This experiment uses the same apparatus and arrangement presented in the above measurement. The only difference is in the apparatus which generates the source signal. Previously a function generator was used, whereas here a noise generator is used as the signal source. The apparatus described below gives the arrangement used for producing the noise signal.:-

5.3.2.1 Noise Generator

A Bruel and Kjaer (B&K) noise generator (type 1405) was employed in these measurements. The noise generator was adjusted to provide a continuous white noise signal up to 20 kHz.

5.3.2.2 Gating System

A gating system (B&K type 4440) was used to separate the direct noise signal and the reflected noise signals which come from the tank walls, tank bottom, and the surface. The pulse width of these noise signals was adjusted to 0.6ms. The pulse delay was controlled by an external gating pulse generator (Lyons Instruments Type PG-71) and was adjusted to 11 ms

5.3.2.3 Power Amplifier

A B&K power amplifier (model 1713) was the final piece of apparatus through which the noise signal was passed before it was sent to the spherical source. Due to the weakness in the noise signal it was given a gain of 20dB.

5.3.2.4 Data Acquisition

The data was collected using a two-channel data acquisition system (A/D Rapid System R2000) connected to the computer. The acquisition sampling rate is 200kHz, which is equivalent to 5μs per sample.

5.3.3 Procedure

As mentioned previously, due to the small number of amplifiers, it was only possible to use two hydrophones simultaneously. Also, due to the random behaviour of the noise source with time, the output signals from each pair of hydrophones cannot be compared with another pair of hydrophones, as was possible when using the harmonic point source in the previous experiment.

The following points present the procedure for measuring the direction of the noise source:-

1. The angle $\theta = 0^o$ represents hydrophones 4 and 2 facing the source (see Figure 5.9).

2. Using the computer the hydrophones array were rotated 90 degrees in steps of 9.96 degrees, giving 10 locations.

3. The signals were collected 500 times per location.

4. The data was collected using the two-channel data acquisition system, where channel *a* corresponds to hydrophone 2 and channel *b* corresponds to hydrophone 4.

5. The data was processed using a Matlab program presented in Appendix 5B section 5.5.

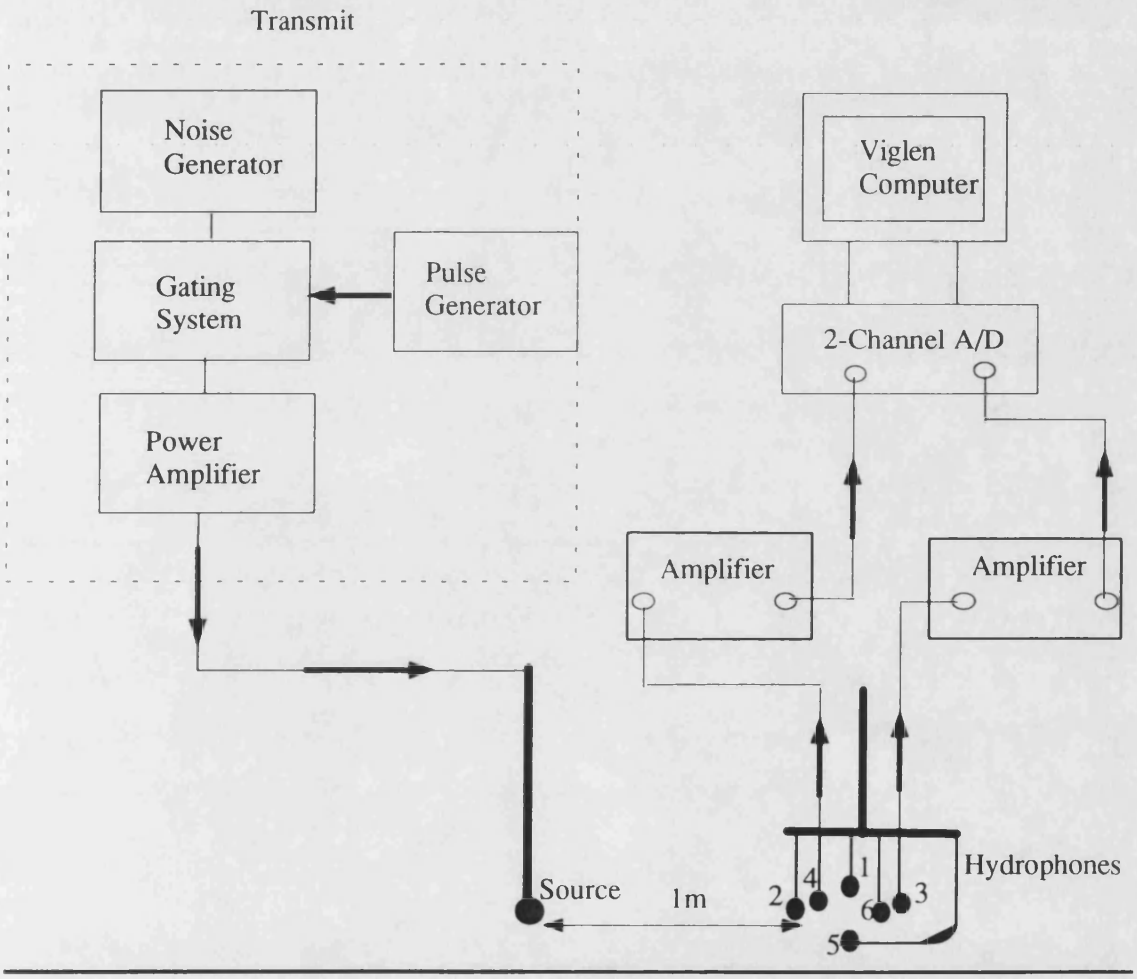

Figure 5.9 Experimental arrangement for measuring the direction of a noise point source

5.3.4 Results

The results obtained with the noise source are shown in Figure 5.10. The normalisation used is the same as that presented in Figure 5.6 (i.e. the output signals from both hydrophones 2 and 6 are divided by the maximum absolute value of the output signal from hydrophone 2). Additionally, these normalised signals were plotted against the relative time separation of the two signals (bearing in mind that these points only corresponds to the equivalent time separation between the two signals).

Figure 5.10a shows the normalised output signals when they are out of phase; this corresponds to the two hydrophones being in line with the noise source. When the normalised output signals are most out of phase, this is related to the maximum energy flow per unit area, and will be shown below. Rotating the hydrophones in the clockwise direction will decrease the phase difference between the two normalised output signals and consequently the direction of the propagating acoustic intensity in this direction will also decrease. Figure 5.10b shows the normalised output signals when the hydrophones are rotated 90 degrees. This graph indicates that there is no sign of the acoustic intensity signals in the direction perpendicular to the direction of the source when the signals are in-phase.

The above conclusion can be easily visualised by considering Figure 5.11. The imaginary part of the cross-spectrum of the two output signals for frequency 9.96 kHz is plotted against the rotation angle θ measured from the gantry for ten different hydrophone directions. The acoustic intensity is shown to vary by only a very small amount if the rotation angle θ is increased up to about 40^o. Above this value the acoustic intensity decreases rapidly. This behaviour can be related to the fall-off seen by the square root function.

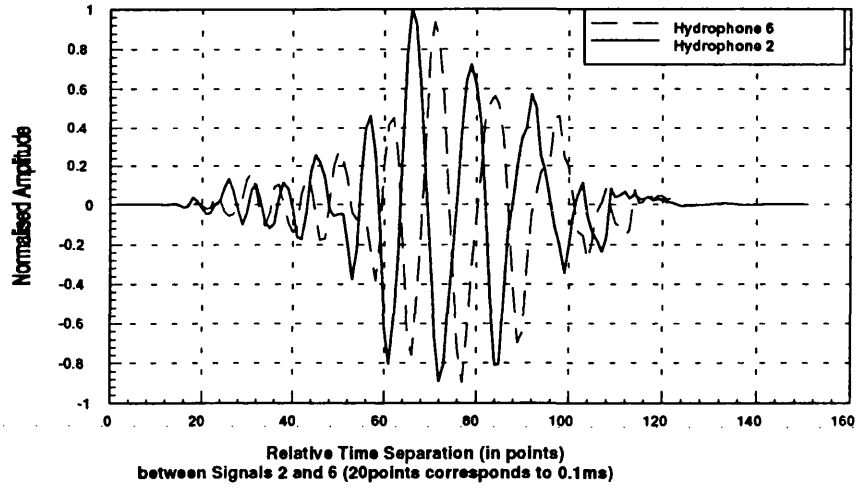

Figure 5.10a $\theta = 0^o$

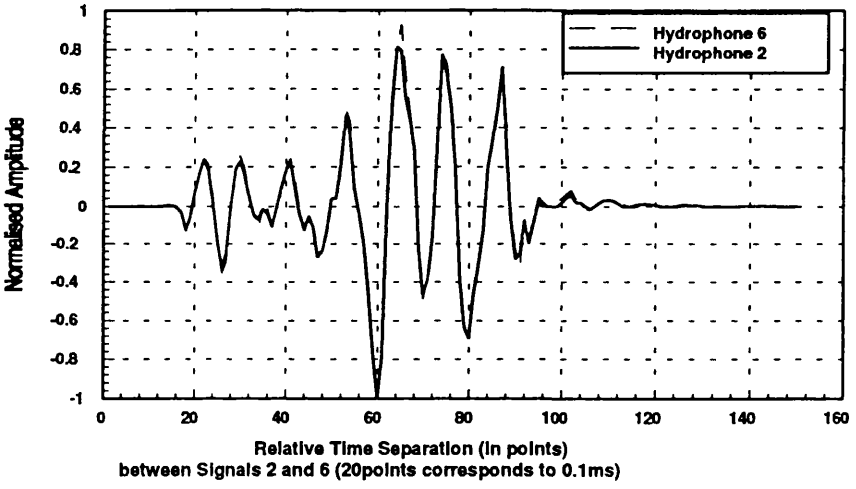

Figure 5.10b $\theta = 90^o$

Figure 5.10 shows the normalised output signals from hydrophones 2 and 6 versus the relative time separation (in points) between the two signals. On the horizontal scale 20 points represents 0.1ms

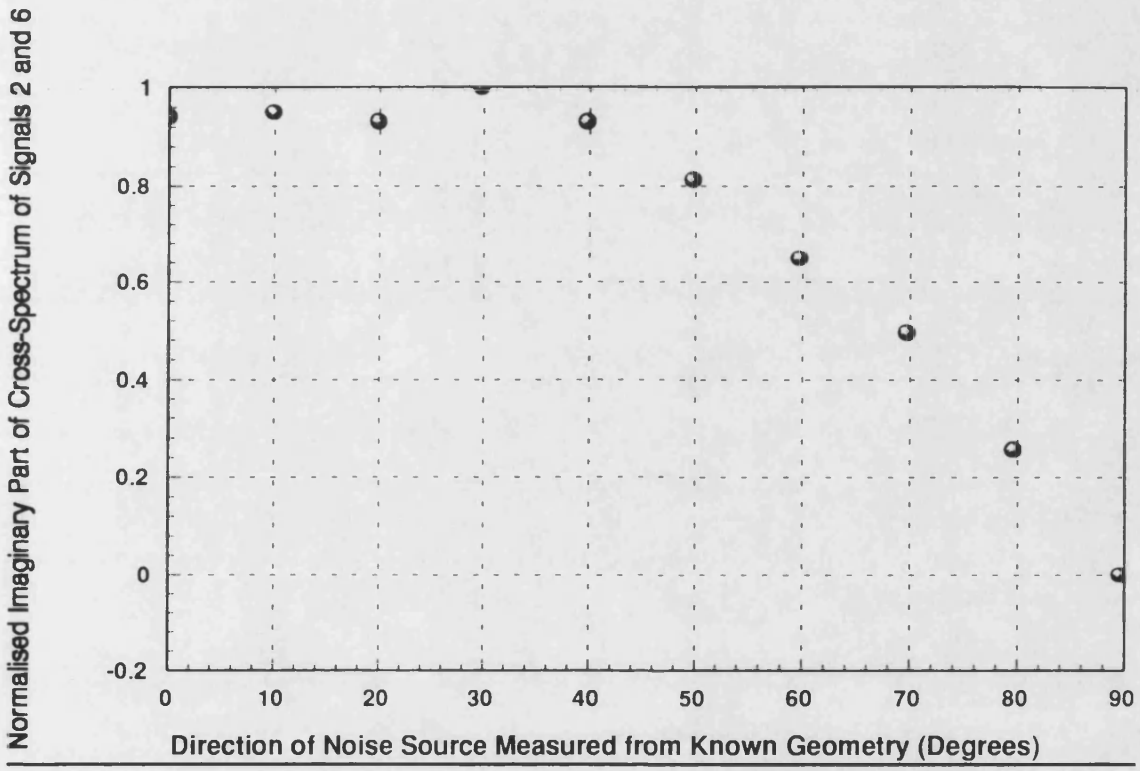

Figure 5.11 shows the changes in the normalised imaginary part of the cross-spectrum of hydrophones 2 and 6 versus the rotation angle measured from the known geometry.

5.4 Appendix 5A

This Matlab program was written in order to calculate the direction of the harmonic point source. The parameters used in this program are based upon the settings presented in the experiment (see section 5.2). This appendix includes only the main program and the subroutine which calculates the acoustic intensity in the 2 and 4 hydrophone directions.

```
% hy24 is a subroutine for calculating the imaginary part
%      of the cross-spectrum of the hydrophones 2 and 4.

  hy24

%   hy26 is a subroutine for calculating the imaginary part
%        of the cross-spectrum of the hydrophones 2 and 6.

  hy26

%   hy43 is a subroutine for calculating the imaginary part
%        of the cross-spectrum of the hydrophone 4 and 3.

  hy43

%   hy63 is a subroutine for calculating the imaginary part
%        of the cross-spectrum of the hydrophone 6 and 3.

      hy63

  iii=0

%   cs42, cs63, cs43, cs62 represents the imaginary part of
%   the cross-spectrum for each pair of hydrophones.

  for i=1:length(cs42);
     m4236(i)=(cs42(i)+cs63(i))/2;
     m3462(i)=(cs43(i)+cs62(i))/2;

%   expt represents the angle in degrees measured from
%        the cross-spectral method.

     if i <= 60
     expt(i)=atan2(m3462(i),m4236(i))*(180/pi);
     else
     expt(i)=360+atan2(m3462(i),m4236(i))*(180/pi);
     end

%   gant represents the angle in degrees measured from
%        the known geometry.
```

```
      gant(i)=iii;
      iii=2.97+iii;
   end

      figure(1)
      plot(expt,gant,'ro')
      set(gca,'XTick',[(0:20:400)]), grid on
      set(gca,'YTick',[(0:20:400)]), grid on
      xlabel(Direction Measured from Cross-Spectral method (Degree)')
      ylabel(Direction Measured from Gantry (Degree)')
      end



%    This is a subroutine for calculating the imaginary part of
%    the cross-specteum of the hydrophones 2 and 4.

     nf=512;

%    s2 and s4 represents the output signals from hydrophones 2 and 4.

     s2=zeros(nf,122);
     s4=zeros(nf,122);

%    The aim of the following is to reorganise the data and to
%    convert from BINARY to ASCII

  for jjj=1:2
       if jjj == 1
        n1=1;
          n2=1;
          n3=60;

%    hr24.a and hr24.b represent the stored data from channel
%    a and b which is the output from hydrophones 2 and 4.

          fid1=fopen('a:\hr24p1.a','r');
          a=fread(fid1)-127;
          status=fclose(fid1);
       else
        n1=n3+1;
        n2=1;
        n3=2*n3;
          fid3=fopen('a:\hr24p2.a','r');
          a=fread(fid3)-127;
          status=fclose(fid3);
       end
for i=n1:n2:n3
     if i==1
        ss=1;
        se=301;
     elseif i == 61
        ss=1;
        se=301;
     else
        ss=se+1;
```

```
        se=ss+300;
     end
    s(:,i)=a(ss:1:se);
end
clear a
end
  clear i ss se
   for iii=1:n3
     s(:,iii)=s(:,iii).*hanning(length(s));
   end
clear iii
      s2(1:1:length(s),1:1:n3)=s(1:1:length(s),1:1:n3);
clear s
for jjjj=1:2
   if jjjj == 1
      n1=1;
      n2=1;
      n3=60;
      fid2=fopen('a:\hr24p1.b','r');
      a=fread(fid2)-127;
      status=fclose(fid2);
   else
      n1=n3+1;
      n2=1;
      n3=2*n3;
      fid4=fopen('a:\hr24p2.b','r');
      a=fread(fid4)-127;
      status=fclose(fid4)
 end
for i=n1:n2:n3
    if i==1
       ss=1;
       se=301;
    elseif i == 61
       ss=1
       se=301;
    else
       ss=se+1;
       se=ss+300;
    end
s(:,i)=a(ss:1:se);
end
clear a
end
  clear i a ss se
   for iii=1:n3
     s(:,iii)=s(:,iii).*hanning(length(s));
   end
clear iii
      s4(1:1:length(s),1:1:n3)=s(1:1:length(s),1:1:n3);
clear s
    for i=1:1:n3

% p42 corresponds to the imaginary part of the cross-spectrum of
% the hydrophones 2 and 4.
```

```
p42(:,i)=(imag(fft(s2(:,i),nf)/(nf/2).*conj(fft(s4(:,i),nf)/(nf/2))));
      for j=1:1:(nf/2);
          if abs(p42(j,i)) == max(abs(p42(:,i)))
             cs42(i)=p42(j,i);
          end,end,end
save c:\thesv3\ch5\result\hrmonic\s24a.dat s24a -ascii
save c:\thesv3\ch5\result\hrmonic\s24b.dat s24b -ascii
clear p42 s4 s2 iii I
```

5.5 Appendix 5B

This Matlab program was written in order to calculate the direction of a noise point source. The parameters used in this program are based upon the settings presented in the experiment (see section 5.3).

```
  n1=1024;
  n2=n1/2;

%   The aim of the following is to reorganise the data and to
%   convert from BINARY to ASCII.

  k1=1;
  k2=1;
  k3=5000

% s26.a and s26.b represents the output signals from hydrophones 2 and 6

  fid=fopen('s26.a');
  a=fread(fid);
  status=fclose(fid);
  a=a-mean(a);
        for i=k1:k2:k3;
       if i == 1
          ss1=1;
          se1=150;
       else
            ss1=se1+1;
            se1=ss1+149;
           end
                  s2(:,i)=a(ss1:1:se1);
        end
        clear a fid i ss1 se1
  save nois_sig26a s2 -ascii
  fid=fopen('s26.b');
  a=fread(fid);
  status=fclose(fid);
  a=a-mean(a);
  for i=k1:k2:k3;
      if i == 1
         ss2=1;
         se2=150;
             else
                 ss2=se2+1;
                 se2=ss2+149;
                 end
       s6(:,i)=a(ss2:1:se2);
       end
```

```
  clear a fid i ss2 se2
  save nois_sig26b s6 -ascii

% f is the freqrncy in Hertz

  f=200000*(0:(n2-1))/n1;
  colm=0;
  ffs=1;
  for ffe=500:500:k3
            colm=colm+1
            for ik=ffs:ffe
                 w2(:,ik)=s2(:,ik).*hanning(150);
                 w6(:,ik)=s6(:,ik).*hanning(150);
                 end
                   fa(:,1:500)=fft(w2(:,ffs:ffe),n1)/n2;
                   fb(:,1:500)=fft(w6(:,ffs:ffe),n1)/n2;

%   pab1 is the imaginary part of the cross-spectrum of
%        hydrophones 2 and 4 (fa and fb), respectively.

                   pab1(:,1:500)=imag(fa(:,1:500).*conj(fb(:,1:500)));
                   cs26(:,colm)=mean(pab1')';
                   clear fa fb pab1
                   ffs=ffe+1;
                   end
                      save image_c26 cs26 -ascii
                      save winhan24b w2 -ascii
                      save winhan26a  w6 -ascii
            clear
            end
```

Chapter Six

6. Sea Trial

6.1 Introduction

The technique for finding the direction of a point source using the cross-spectral method was presented in the previous chapter. Four hydrophones were employed to measure the direction of a harmonic point source. However, due to the small number of amplifiers, only two hydrophones were available for measuring the direction of a random point source. The measured direction of the harmonic point source using the cross-spectral method was shown to be in good agreement with that measured from the gantry. Even though only two hydrophones were used to find the direction of the random point source, the results show the measured direction from the cross-spectral method to be in good agreement with that measured from the known geometry.

These positive results were encouraging in proceeding to the experiment being carried out at sea. The aim of the experiment was to investigate the distribution of the surface noise in the orthogonal (x,y,z) planes in shallow water. This distribution was expected to lead to an alternative method for mapping the seabed as shown in the previous theoretical study. However, for a successful experiment to be carried out, a large financial support was needed. Ideally, measurements should be made far from the coast, as the distribution of the surface noise becomes symmetrical over the effective radius. This would require reliable boats which can go far from the shore. Also, in order to validate the measurements, detailed information about the seabed structure is needed prior to the sea trail. Unfortunately the budget limit of the project was not sufficient to satisfy all the essential needs for taking the measurements. However, this financial problem did not discourage us from going ahead to try and measure the distribution of the surface noise using the available apparatus.

Two sea trials in Weymouth Bay were organised. Even after careful preparation before the first sea trial in trying to avoid the problems which might face the measurements, some unexpected difficulties were encountered. These problems were overcome in the second sea trial. However, more complicated problems were faced during this measurement. These had been foreseen, but could not be solved with the budget available for the project.

This chapter has been divided into two parts. The first introduces the measurements made on **Wednesday 21st June 1994**. The apparatus, geographical location, and the procedure

used in achieving these measurements will be discussed. The second part of this chapter introduces the measurements made on **Thursday 15th July 1994.** The main problem encountered during the first measurements was the mounting of the hydrophones, but this was modified for the second set of measurements. The final part of this chapter lists the ideal apparatus and information needed for a conclusive trial in order that the theoretical study is verified.

6.2 The First Sea Trial

6.2.1 Introduction

These measurements were taken in Weymouth Bay on **Wednesday 21st June 1994.** In order to obtain the necessary measurements, the six-hydrophone array presented in the previous chapter was used. The design for the mounting of the hydrophones resulted in two significant errors which made it difficult to obtain the measurements. The first error arose due to the vibration of the hydrophone mount, caused by the rocking of the boat which led to an overload of the signal. The second error was caused by the rotation of the hydrophone array around its original setting due to the influence of the sea current.

6.2.2 The apparatus

This section introduces the apparatus used in order to measure the surface noise signals.

6.2.2.1 The Hydrophones and its Mounting

The six B&K hydrophones and their orthogonal arrangement presented in the previous chapter were used in these measurements. The errors which might occur using this hydrophone array were discussed in detail in sections (1.2.2.2) and (5.2.2.1).

The hydrophones were mounted with a 4m scaffolding pole via an adapter (see Figure 6.1). The adapter was screwed through the high density machinable plastic attachment holding the hydrophone array. This design was not strong enough to keep the hydrophones in their original position when exposed to the sea current. The other end of the adapter was slid through the pole and fixed by using perpendicular screws. This end of the adapter was rigid enough even in a strong current.

The end of the pole which was connected to the hydrophones was submerged to a depth of about 3.5m in the sea. The other end of the pole was tied to the ladder of the boat which is normally used by divers. Jubilee clips were used in attaching the rod to the ladder, while the cables were tide up using plastic ring electrical cable ties (see Figure 6.2).

This method of fixing the rod to the ladder was strong enough to ensure there was no movement of the mounting. Due to the way the ladder was fixed to the boat, there was movement of the ladder. The movement was due to the diameter of the tube welded to the boat being larger than the diameter of the ladder rung which was inserted in the tube (see Figure 6.3). Due to this difference in diameter the ladder moves with each small movement of the boat, causing the signal to be overloaded.

6.2.2.2 The Boat

The experiment was carried out using a boat which was 10.5m long, 3.3m wide and 0.35m high above the sea surface. The boats navigation and echo sounder equipment, which locate the co-ordinates of the measurements and the depth of the sea (Figure 6.4a), have the advantage of being able to operate while the main engine is off (using a 12 volt battery). The apparatus used for amplifying and recording (see below) the surface noise signals were fitted in the boat cabin (Figure 6.4a).

6.2.2.3 The Amplifiers

As mentioned in the literature survey, the pressure level of the noise signal produced from the sea surface depends on the wind speed. In the case of high wind speed, strong noise signals can be easily detected and recorded, whereas for low wind speeds (for example at

zero sea state) the noise signals needed to be amplified by at least 126 dB in order to be stored on a tape recorder of 1V input sensitivity (see section 6.2.2.4). This gain was calculating using the graph shown in Figure 6.5 (adopted from Burdic [39]) which shows that the noise spectrum decreases from about 42 dB//μPa/Hz at 2 kHz to 28 dB//μPa/Hz at 10 kHz giving a noise signal of $8.11\times10^{-3}Pa$, which corresponds to 0.4547 μV using the B&K hydrophones (the voltage sensitivity of the hydrophones with the cable is 56μV/Pa)

Due to the financial difficulty, only four Ortec Brookdeal Precision AC amplifiers (model 9452) with a 100 dB maximum gain were available for these measurements. Hence in order to obtain the desired noise signal the wind speed should be above 11 knots. The condition of the sea state in this trail is shown in Figure 6.6.

6.2.2.4 The Tape Recorder

Finally, the data from the amplifiers was stored on a RACAL magnetic tape recorder having seven channels. Six of the channels were able to record the signals simultaneously, while the seventh is for voice recording and was used to indicate the beginning and the end of the measurement. FM tape recording was used with a tape speed of 30 in/s, covering a frequency range up to 10 kHz.

6.2.3 The Procedure

In order to avoid the noise produced by the boat, the measurements were taken whilst the engine was turned off. The sea surface noise signals were collected using the hydrophones in the x-y plane with the boat drifting due to the wind. The output signals were first sent to the four amplifiers and then finally stored on tape, using the tape recorder (both were operating from 12 volt battery.)

Before starting the measurements, the hydrophones, the other apparatus, and the connections were all checked just outside harbour at the co-ordinates $50^{o}.36'.53N$ and $002^{o}.24'.80W$ where the depth of the water was H=15.2 m (see Chart 6.1).

The first run of the measurements was started at the point $50^{o}.36'.03N$, $002^{o}.20'.47W$ where the depth of the sea was H=20.5, and ended at $50^{o}.36'.02N$, $002^{o}.20'.54W$ where the depth of the sea was H=20 m (see Chart 6.2). During this run, the output noise signal was overloaded due to the vibration of the ladder which was caused by the rock of the boat. Also, the hydrophones rotated from their original direction due to the strong current in the sea.

In an effort to overcome these problems the measurement was taken again, with modifications. In order to try and stabilise the movement of the ladder, two pieces of rope were tied from each end of the boat to the bottom of the ladder. With this modification

the second run was started at the point $50^o.36'.03N$, $002^o.20'.59W$ where H=21m, and ended at the point $50^o.36'.10N$, $002^o.20'.65W$ which was at the same sea depth (see Chart 6.2). This modification did not totally cancel the vibration problem, and again the rocking of the boat caused the signals to be overloaded.

6.3 The Second Sea Trial

These measurement were taken in Weymouth Bay on **Thursday 15 July 1994**. The apparatus were redesigned to overcome the problems encountered during the first sea trial. As shown in Figure 6.7 the top end of the hydrophone mounting was fixed directly to the boat. The diameter of the attachment at the top end of the rod just fitted the inner diameter of the tube which is fixed to the boat. This allows the hydrophones to be easily lowered into the water when taking the measurement, and raised from the water when the boat is moving. As the hydrophones are lowered into the water to take the measurement, the pole is rigidly fixed to the boat by nuts at each end of the tube, see Figure 6.7. In addition, in order to keep the lower end of the pole from vibrating due to the current in the sea, two eye bolts were welded onto the bottom of the rod, allowing ropes to be tied from each end of the boat to the bottom end of the pole.

Another problem encountered in the first trial was that the hydrophones rotated due to the current. In order to overcome this problem, the high density machinable plastic attachment

holding the hydrophones was fixed to the adapter by adding a screw in the perpendicular direction, see Figure 6.8.

The first run of this sea trial started at the point $50^{o}.37'.38N$, $002^{o}.20'.76W$ where the depth of the sea is H=15.5 m (see Chart 6.2). The new design of the hydrophone mounting proved to be successful in stabilising the movement of the hydrophones, even when the boat was rocking. Also, the hydrophones direction stayed in its original setting position. However, this successful design for the hydrophone mounting was not the end of the story as other problems were faced.

As mentioned previously, in order to measure the sea surface noise signals, either amplifiers with at least 126 dB gain are needed, or the wind speed should be over 11 knots with the amplifiers available.

In addition to the weakness of the acoustic surface noise signals, the signals detected by the hydrophones were dominated by signals sent from the military ships based around the measurement area (Figure 6.9). The frequency of these signals was well above the 8 kHz design optimum for the six B&K hydrophones intensity array, so even a study of the direction of these signals as a secondary exercise was not possible.

6.4 Suggestions For a Successful Measurement

The two attempts to measure the vector noise intensity at sea have shown that such experiments require far more resources than were available. Of particular importance are the requirements listed below:-

1. Six amplifiers with exactly the same sensitivity are needed. In order to measure the distribution of the surface noise for any sea state, the amplifiers should have at least 126 dB gain with the tape recorder used.

2. In order to make the hydrophones more stable in the vertical direction (caused by the rocking of the boat), more advanced mountings are needed.

3. The measurement is recommended to be made far from the coast, as the distribution of the surface noise becomes symmetrical over the effective radius. This needs reliable boats which can go far from the shore.

4. In an effort to be more convinced about the validity of the measurements, detailed information about the seabed structure is needed prior to the sea trial.

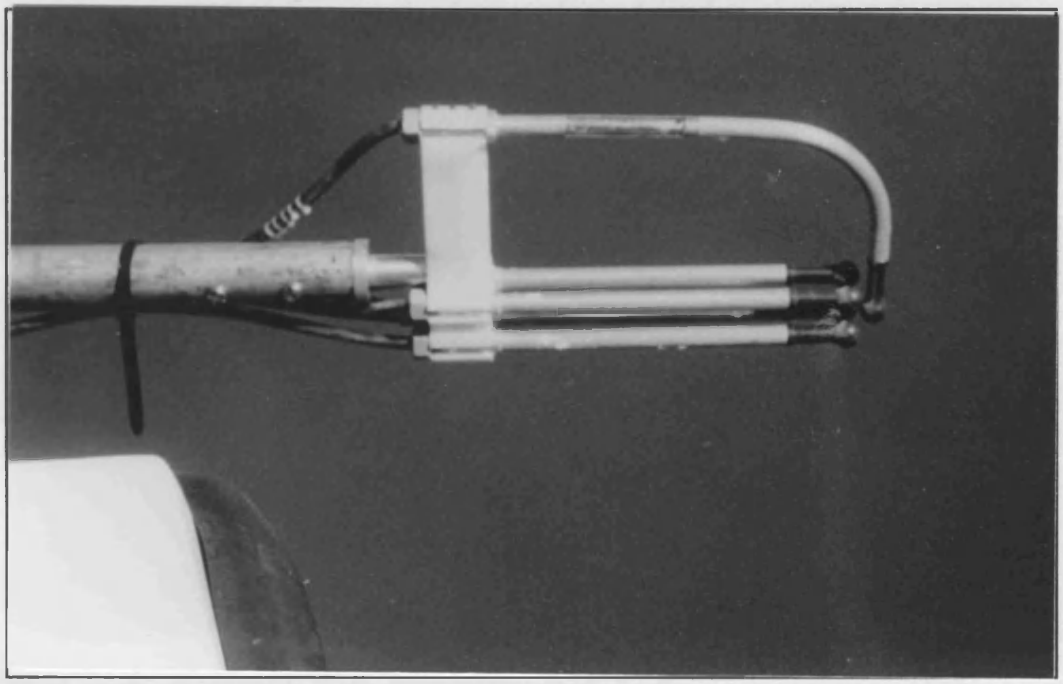

Figure 6.1 Shows the bottom end of the pole where the hydrophones are attached.

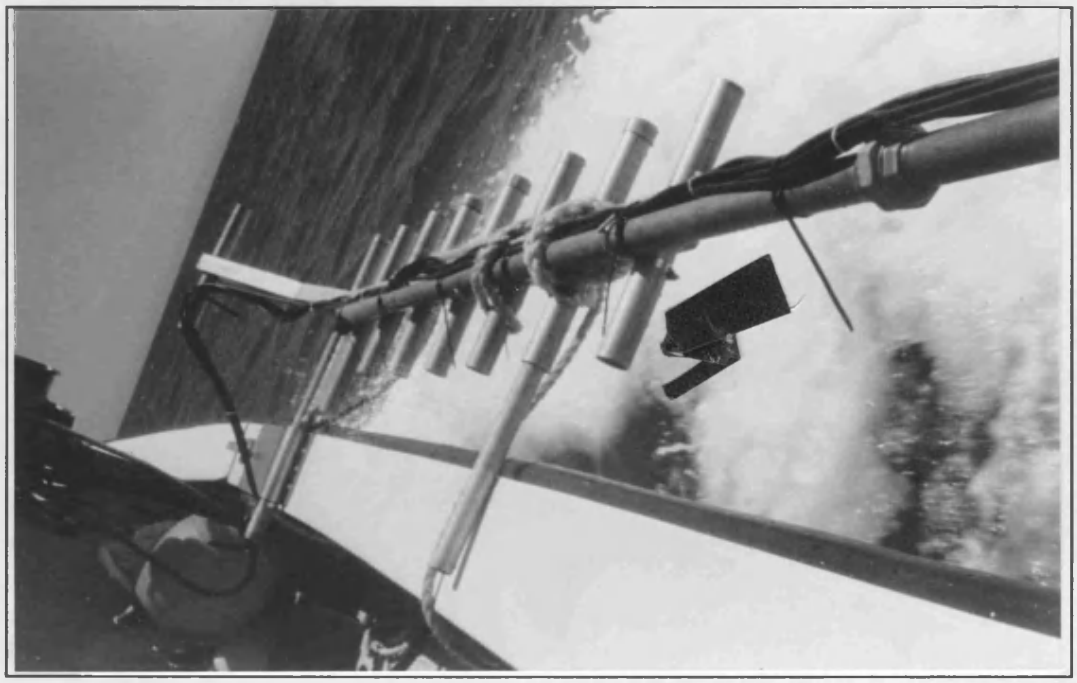

Figure 6.2 Shows the design for fixing the ladder and the pole.

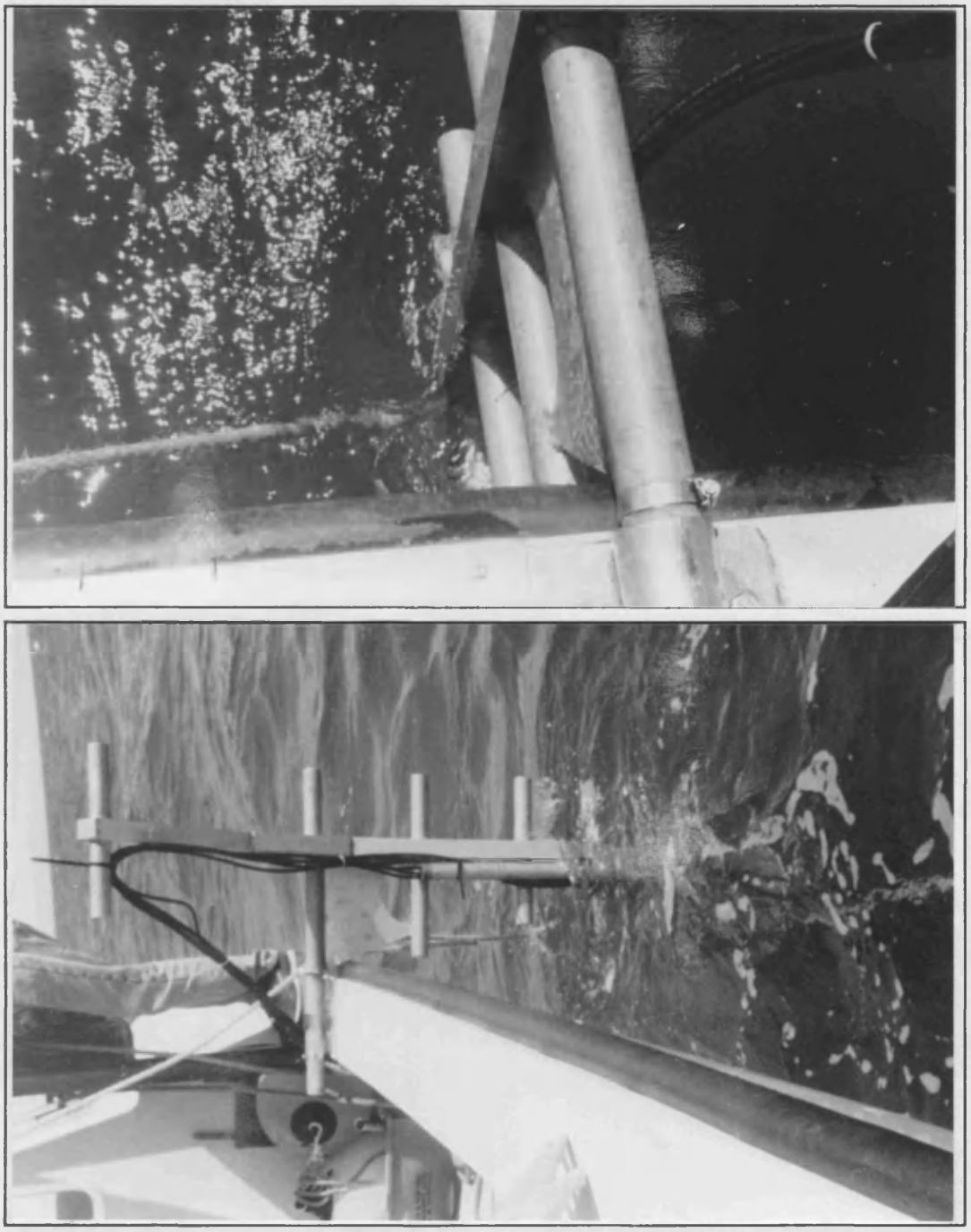

Figure 6.3 Shows how the ladder is connected to the boat (from different angles).

Figure 6.4a

Figure 6.4b

Figure 6.4 Shows the equipment which provides the information about the co-ordinates of the boat, the depth of the sea (6.4a), and the apparatus used for processing the surface noise signals (6.4b)

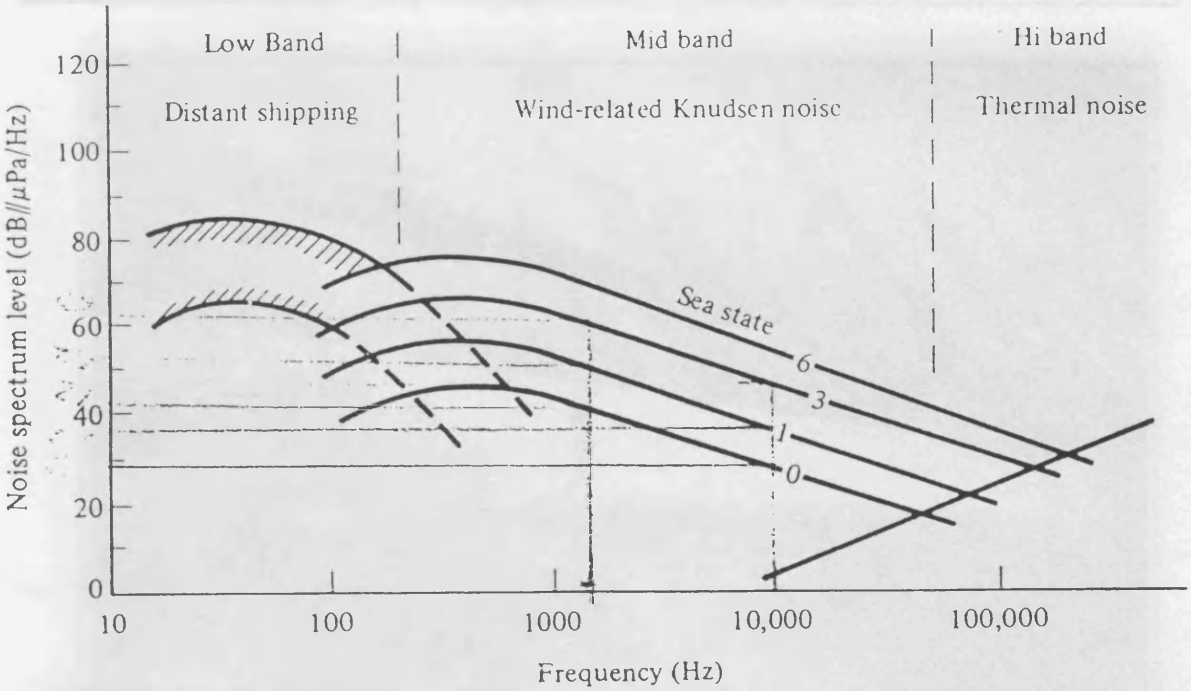

Figure 6.5 Illustrate the ambient noise spectra as measured with an omnidirectional hydrophone.

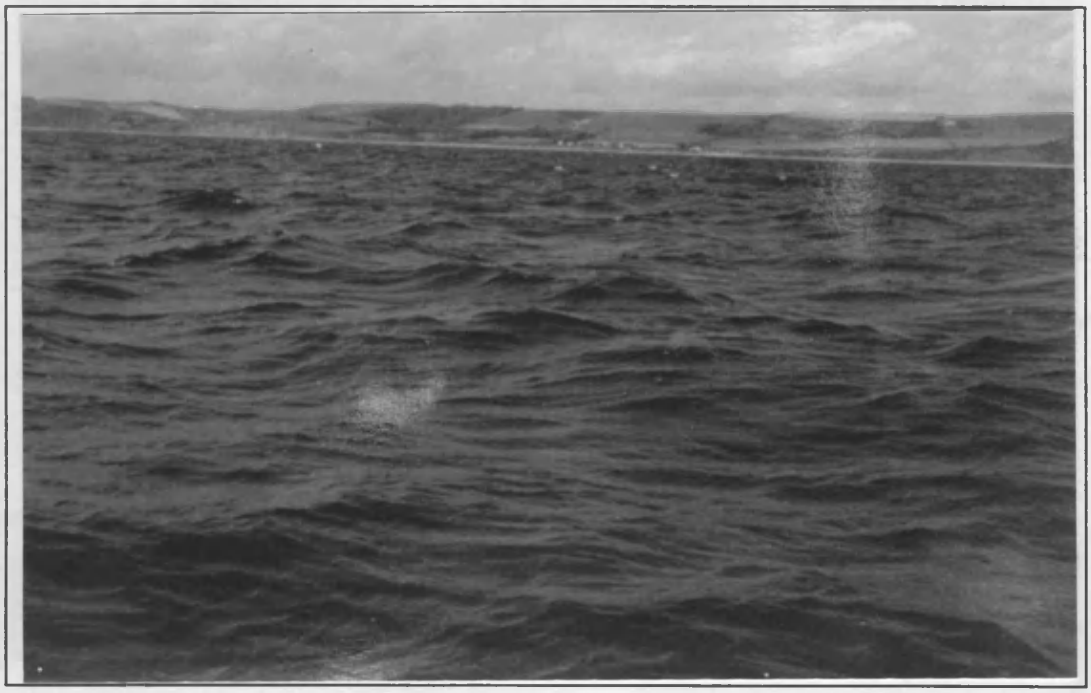

Figure 6.6 Shows the condition of the sea state in the first trial.

Figure 6.7 Shows the hydrophones mounting design for the second trial.

Figure 6.8 Shows eye bolts at the bottom end of the rod used in the second sea trial.

Figure 6.9 Shows the sea conditions and the military ships based around the measurement area.

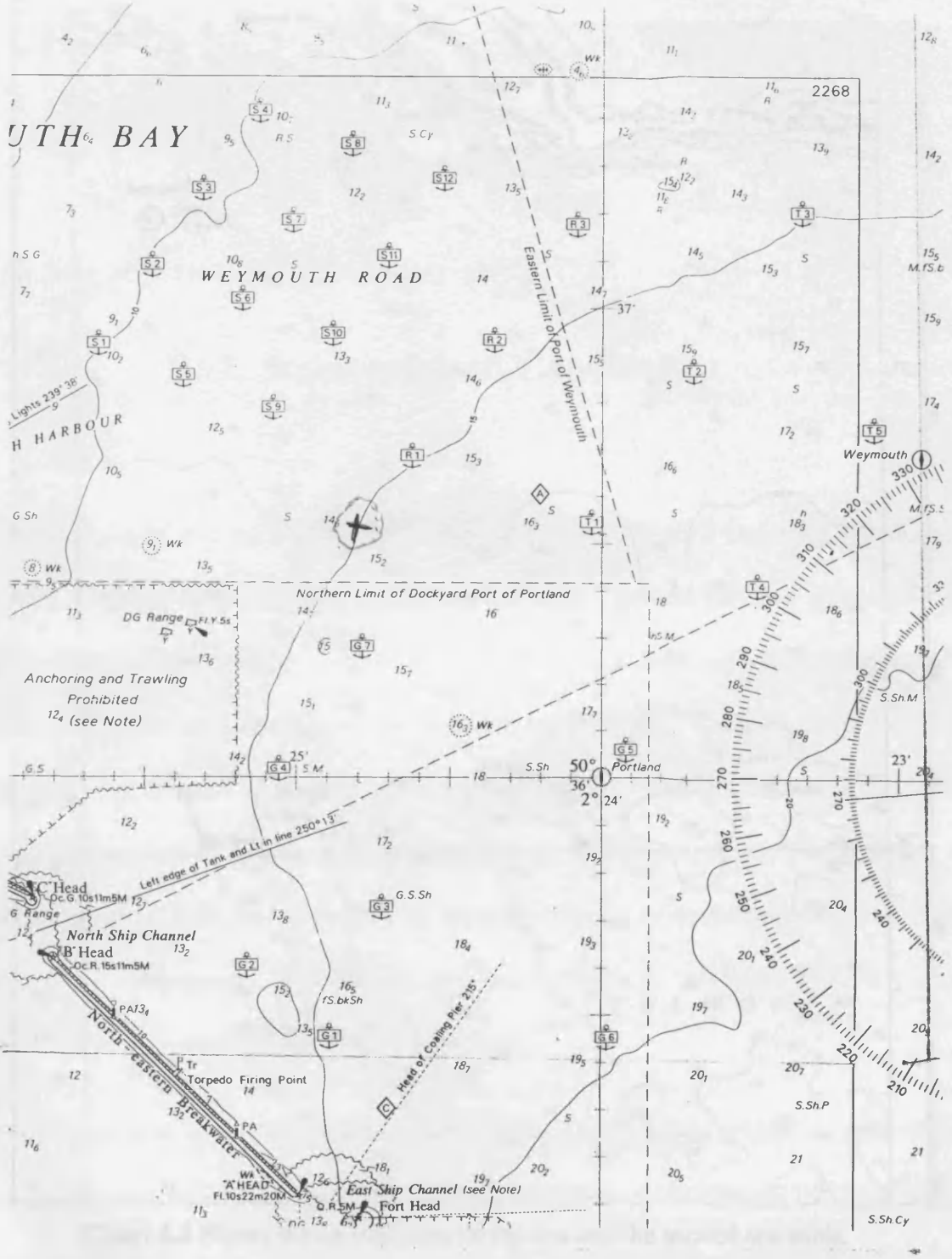

Chart 6.1 Shows the co-ordinates where the experimental apparatus were checked.

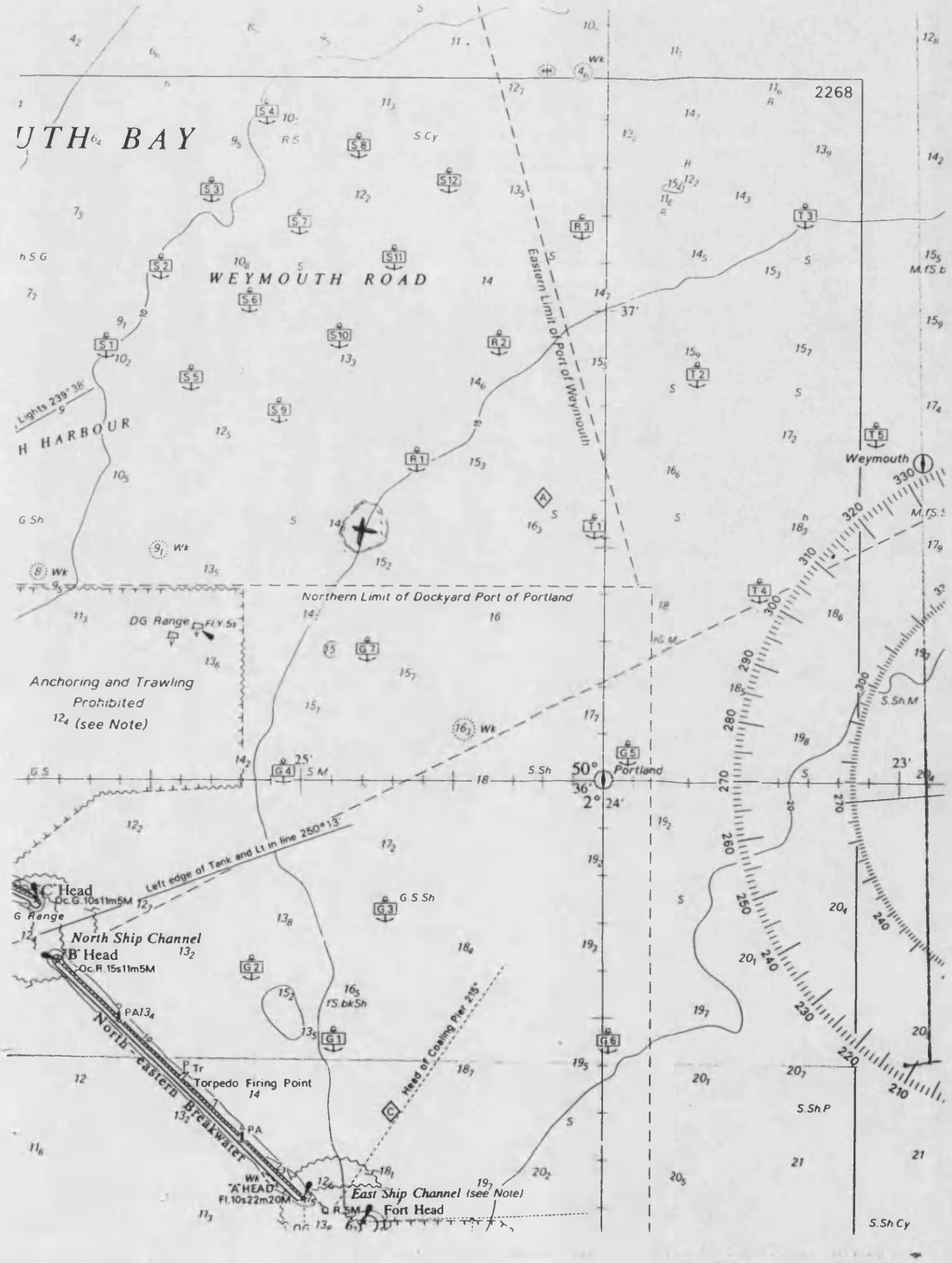

Chart 6.1 Shows the co-ordinates where the experimental apparatus were checked.

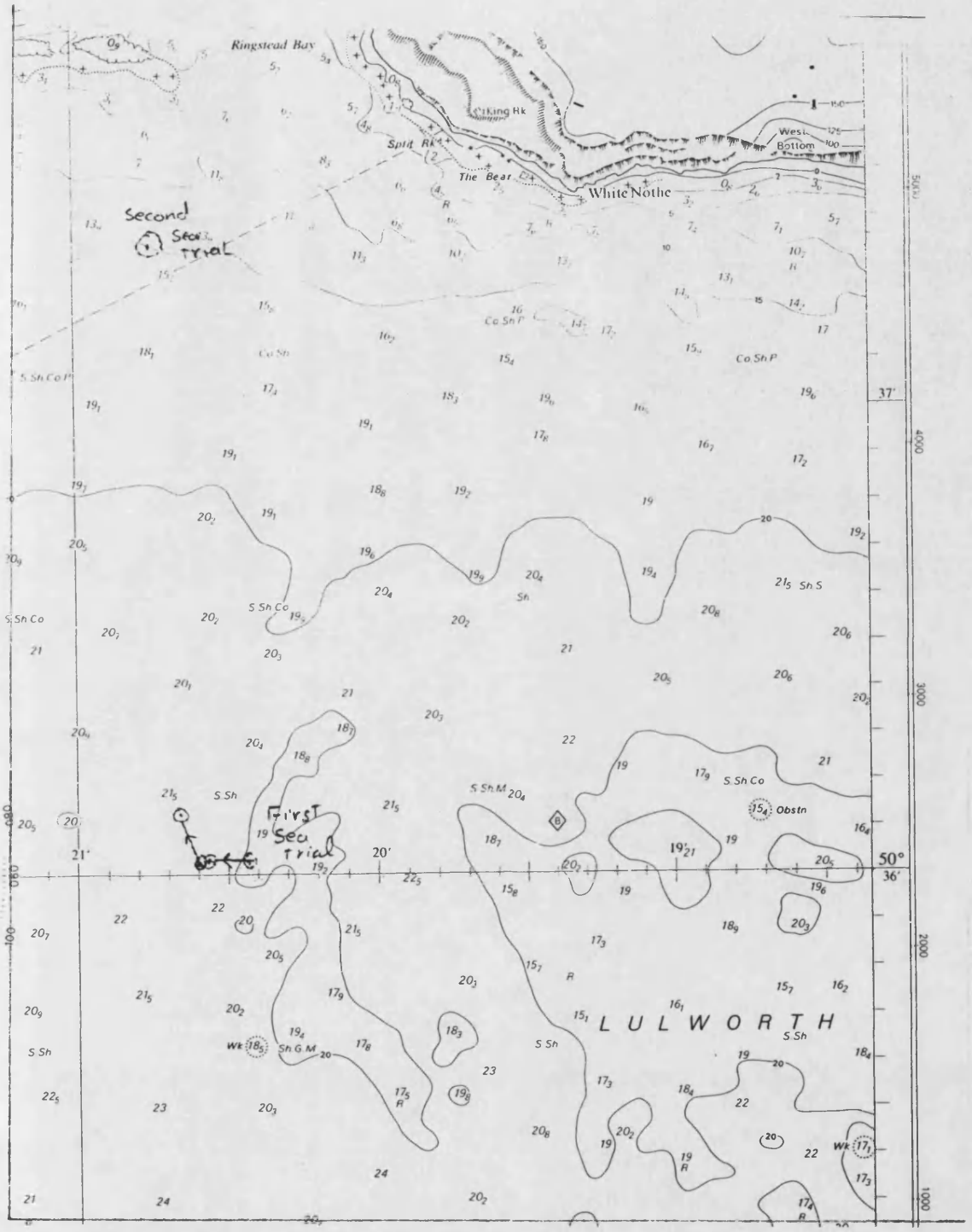

Chart 6.2 Shows the co-ordinates of the first and the second sea trials.

Chapter Seven

7. Summary and Conclusions

The main aim of this project was to investigate the possibility of obtaining information about the seabed structure using the sea surface noise. Several previous methods have been used to study the structure of the seabed by looking at the distribution of the surface noise around the horizontal plane relative to the hydrophones. These methods involved measuring the pressure squared, which is a scalar quantity. This project has developed a new approach where the sea surface noise acoustic intensity has been considered as a vector quantity. This concept allows the acoustic intensity to be resolved into its (x,y,z) orthogonal components. The acoustic intensity in the (x,y) horizontal plane has been shown to be very sensitive to the seabed structure.

In the theoretical part of this thesis three different models of the seabed structure have been presented. In the first model the seabed was taken to be divided into four equal regions of a circle whose radius increase as the radius of the surface noise increases. The other two models assumed the seabed to be uniform over a circle, except in a small

area. The second model takes the small area to be a small circle, whereas the third model takes the small area to be a section of an annulus.

The main aim of the first theoretical model was to illustrate the behaviour of the acoustic noise intensity in the orthogonal directions as a function of the surface noise radius. The results from this model indicate that for a small surface noise radius, the acoustic noise intensity in the z-direction is dominated by the direct acoustic intensity rays (*i.e.* the rays that have no chance of hitting the seabed). The effect of the seabed in the z-direction becomes noticeable by increasing the surface noise radius, which corresponds to an increase in the reflection coefficient, and bigger areas of different seabed types. However, once a limiting surface noise radius has been reached the direct rays again dominate. This occurs due to the cancellation between the rays received from above and below the horizontal on reaching the critical angle where the only difference is in the extra path length, which becomes small for sources located at a distance.

The acoustic intensity in the horizontal plane has been shown to be totally dependent on the seabed structure, as this plane is free from the contribution of the direct rays. The model showed that the acoustic intensity in the x-direction increases rapidly as the radius of the surface noise increases. This increase is directly related to the increase in the difference of the seabed types, as well as the magnitude of the reflection coefficient. The model also shows that for rays with a small number of reflections between the seabed and

the sea surface, the effective radius (*i.e.* the radius beyond which no major changes in the acoustic intensity occur) can be easily estimated. This is due to the symmetrical shape of the seabed which leads to the cancellation of received rays once the critical angle has been reached.

In order to gain a deeper understanding into the significant effect of the seabed on the distribution of the acoustic intensity in the (x,y) horizontal plane, more realistic seabed structures were presented. In these models the shape of the seabed was assumed to be uniform over a circle except in a small patch. The small patch was first taken to be a small circular shape. This model studied the surface noise acoustic intensity in the x-direction as a function of the sea surface noise radius while the hydrophones moved away from the circular patch. Due to the long computation time for this model, the shape of the small patch has been modified in order to cut down on the computation time. The modified shape has been chosen to be a section of an annulus. However, this modified shape leads to the same conclusion as for the case of taking the small patch to be a circle.

The results obtained from the circular shape model indicate that for a small number of reflections between the seabed and the sea surface, the range of the hydrophones is relatively small in order to detect the small patch. This range is directly related to the critical angle of the seabed. Increasing the number of reflections of rays between the seabed and the sea surface leads to an increases in the range of the critical angle which

gives the hydrophones a larger range for detecting the asymmetry in the seabed. However, the increase in the range is limited by the high number of reflections since the spherical spreading effect becomes significant.

In addition to the parameters presented in the above model which causes a limitation on the effective radius, the model containing the section of an annulus as the small patch shows that the range of effective radius can be even smaller if the scattering effect of the sea surface is included in the model (This effect was included only to show that the range of the surface noise can be reduced to the local area only).

The final stage of the theoretical studies used the section of annulus to represent the small patch, and showed that the sensitivity in detecting the asymmetry of the seabed in the (x,y) plane depends mainly on three parameters. The three parameters being; the type, the size of the small patch relative to the seabed as a whole, and the location of the hydrophones relative to the asymmetry. In the case when the small patch and the main seabed are roughly the same type, the acoustic intensity is shown to have peaks and nulls as the hydrophones move away from the asymmetry in the seabed (small patch). The peaks and nulls correspond to the critical angle and the increase and decrease in the probability of the acoustic rays hitting the small patch. Consequently, increasing the size of the small patch leads to an increase in the probability of the rays hitting the asymmetry in the seabed, which gives a smooth decrease in the acoustic intensity as the hydrophones move away

from the asymmetry. This behaviour of the acoustic intensity can be used in order to estimate the size of the asymmetry in the seabed.

As the estimated acoustic intensity is dependent on the difference of the two seabeds (either in size or in characteristic) further information about the difference in the seabed types can be obtained from the behaviour of the acoustic intensity in the horizontal plane. In the case of taking a relatively small patch, the minimum in the acoustic intensity approaches zero magnitude due to the similarity in the two types of seabed, whereas the minimum is further away from the zero for larger differences in the seabed types.

The characteristic changes in the acoustic intensity for different sizes of the small patch is different to the characteristic changes in the acoustic intensity for different types of seabed. This makes it possible to distinguish between changes in size and type of the seabed.

The conclusions drawn from the theoretical models discussed above can be summarised in the following points:-

1. The acoustic intensity in the horizontal plane is strongly dependent on the structure of the seabed, since this acoustic intensity is free from the contribution of the direct rays.

2. At a certain number of reflections between the seabed and the sea surface, and at certain surface noise radius, the characteristic of the acoustic noise intensity does not change, which leads to a limitation on the scanning area.

3. The direction, the size, and the difference in the types of the seabed can be obtained for hydrophones located relatively near the asymmetrical area. However, the ability of the hydrophones in detecting the asymmetry of the seabed is dependent on various parameters. The parameters are the difference between the type and size of the small patch and the main area, and the location of the hydrophones relative to the small asymmetry.

The above theoretical results encouraged the project to proceed to practical measurements to find the distribution of sea surface noise in shallow water. As a first step towards this measurement, and to gain experience in measuring acoustic vector intensity, experimental studies for the use of the acoustic intensity vector for identifying the direction of a point source were carried out in the laboratory. This experiment showed the ability of the acoustic intensity vector for detecting the direction of a harmonic point source, and noise point source, successfully. The acoustic intensity direction was estimated by the cross-spectral method. In order to measure the direction of the harmonic point source four hydrophones were used, whereas for the random noise point source only two hydrophones were employed. These results further encouraged the project to proceed to taking

measurements at sea despite the knowledge of a lack of available apparatus. It was anticipated that the lack of available apparatus would affect the success of the measurements. Two sea trial were carried out in Weymouth. In the first sea trial an unexpected problem was faced while taking the measurements but this was overcome in the second sea trial. These measurements were taken while the boat drifted with the current (the engine of the boat was turned off). The results from the trials indicates that in order to make a successful measurement reliable apparatus are needed; for example, at low wind speed (low noise) six amplifiers with high gain are needed.

The main aim of this project was to study the surface noise acoustic intensity vector since it contains information about the seabed. A detailed theoretical study of the surface noise acoustic intensity vector has been presented. Modelling has shown that the acoustic intensity in the horizontal plane is sensitive to the seabed structure. In principle the sea surface noise vector can be used as a tool for mapping the seabed. In addition to the ability of detecting the location of the asymmetry in the seabed, the size of the small patch and the difference in the two types of seabed can be estimated. For completeness a practical study of the surface noise acoustic intensity vector has also been presented. This thesis has recognised that problems will be encountered in measuring the surface noise acoustic intensity in a practical situation, and the consequent difficulty in measuring this quantity in the real survey application.

References

1. G. M. Wenz, "Acoustic Ambient Noise in the Ocean: Spectra and Sources" J. Acoust. Soc. Am., **34,** pp. 1936-1956, 1962
2. R. J. Urick, " Ambient Noise in the Sea", Undersea Warfare Technology Office,Washington D.C., 1984.
3. B. F. Cron and C. H. Sherman, " Spatial Correlation Functions for Various Noise Models" J. Acoust. Soc. Am., **34,** pp. 1732-1736, 1962
4. W. S. Liggett and M. J. Jacobson "Covariance of Surface-Generated Noise in a Deep Ocean" J. Acoust. Soc. Am., **38,** pp. 303-312, 1965.
5. H. Cox " Spatial Correlation in Arbitrary noise fields with application to ambient sea noise" J. Acoust. Soc. Am., **54,** pp. 1289-1300, 1973.
6. V. C. Anderson "Arrays for the Investigation of Ambient Noise in the Ocean" J. Acoust. Soc. Am., **30**, pp. 470-477, 1958.
7. G. R. Fox "Ambient-Noise Directivity Measurements" J. Acoust. Soc. Am., **36,** pp. 1537-1540, 1964.
8. M. J. Buckingham " A theoretical Model of Ambient Noise in a low-loss, shallow water channel," J. Acoust. Soc. Am., **67,** pp. 1186-1192, 1980.
9. W. A. Kuperman and F. Ingenito, " Spatial Correlation of Surface Generated Noise in a Stratified Ocean," J. Acoust. Soc. Am., **67,** pp. 1988-1996, 1980.

10. M. J. Buckingham, " Spatial Coherence of Wind-Generated Noise in a Shallow Ocean Channel." J. Acoust. Soc. Am. **70,** pp. 1412-1420, 1981.

11. M. J. Buckingham and S. A. Jones " A New Shallow-Ocean technique for determining the critical angle of the seabed from the vertical directionality of the ambient Noise in the water column." J. Acoust. Soc. Am., **81,** pp. 938-945, 1987.

12. D. L. Evans, D. R. Watts, D. Halpern and S. Bourassa " Oceanic Winds Measured From the Seafloor." Journal of Geophysical Research **89**, pp. 3457-3461, 1984.

13. D. D. Lemon, D. M Farmer and D. R. Watts " Acoustic Measurements of Wind Speed and Precipitation Over a Continental Shelf." Journal of Geophysical Research **89,** pp. 3462-3472, 1984.

14. D. M. F. Chapman " Surface-Generated Noise in Shallow water: a model." Proc. I. O. A., **9,** Part 4, pp. 1-11, 1987.

15. H. Dupuis and A. Weill " Modelling of Omnidirectional response of an hydrophone in shallow water reflecting seabed" Proc. I. O. A., **13,** Part 3, pp. 174-182, 1991.

16. F. N. Spiess, J. Northrop and E. W. Werner, " Location and Enumeration of Underwater Explosions in the North Pacific", J. Acoust. Soc. Am., **43,** pp. 640-641, 1968.

17. J. H. Shooter, T. E. DeMary and R. A. Koch, "Ambient Noise in the Western Gulf of Mexico" Applied Res. Lab., University of Texas, **ARL-TR-82-15,** 1982.

18. M. Strasberg "Nonacoustic noise interferece in measurements of infrasonic ambient noise" J. Acoust. Soc. Am., **66,**1487-1493, 1979.

19. V. O. Knudsen, R. S. Alford and J. W. Emling "Survey of Underwater Sound Report No. 3: Ambient Noise" Office of Scientific Research and Development National Defense Research Committee Division 6 - Section 6.1

20. A. J. Perrone "Deep-Ocean Ambient-Noise Spectra in the Northwest Atlantic" J. Acoust. Soc. Am. **46,** pp. 762-770, 1969.

21. A. J. Perrone "Infrasonic and Low-Frequency Ambient Noise Measurements on the Grand Banks" J. Acoust. Soc. Am., **55,** pp. 754-758, 1974.

22. B. Hughes, "Estimates of Underwater Sound (and Infrasound) Produced by Nonlinearly Interacting Ocean Waves" J. Acoust. Soc. Am. **60,** pp. 1032-1039, 1976.

23. J. H. Wilson "Very Low Frequncy (VLF) Wind-Generated Noise Produced by Turbulent Pressure Fluctuations in the Atmosphere Near the Ocean Surface," J. Acoust. Soc. Am., **66,** pp. 1499-1507, 1979.

24. J. H. Wilson "Low-Frequency Wind-Genereted Noise Produced by the Impact of Spray with the Ocean's Surface," J. Acoust. Soc. Am., **68,** pp. 952-956, 1980.

25. R. H. Mellen "Thermal-Noise Limit in the Detection of Underwater Acoustic Signals" J. Acoust. Soc. Am., **24,** pp. 478, 1952.

26. M. S. Longuet-Higgins "A Theory of the Origin of Microseisms," Trans. Roy. Soc. (London), **A243,** pp. 1, 1950.

27. H. W. Marsh "Origin of the Knudsen Spectra" J. Acoust. Soc. Am., **35,** pp. 409-410, 1963.

28. M. A. Isakovich and B. F. Kur'yanov "Theory of Low-Frequency noise in the Ocean" Sov. Phys. Acoust., **16,** pp. 49-58, 1970.

29. V. V. Goncharov "Sound Generation in the Ocean by the interaction of surface waves and turbulence" Atmospheric and Oceanic Physics, **6,** pp. 710-714, 1970.

30. P. A. Crowther "Bubble Noise Creation Mechanisms" in Sea Surface Sound: Natural Mechanisms of Surface Generated Noise in the Ocean, R. Kerman(ed.), Kluwer Academic Publishers, pp. 131-150, 1988.

31. J. Tichy "Use of the Complex Intensity for Sound radiation and Sound field studies" 2nd International Congress on Acoustic Intensity (CETIM), Senlis(France), pp. 113-120, 1985.

32. J. C. Pascal "Structure and Patterns of Acoustic Intensity Fields" 2nd International Congress on Acoustic Intensity (CETIM), Senlis(France), pp. 97-104, 1985.

33. T. J. Schultz "Acoustic Wattmeter" J. Acoust. Soc. Am., **28,** pp. 693-699, 1956.

34. F. J. Fahy ''Measurement of Acoustic Intensity Using the Cross-Spectral Density of two Microphone Signals" J. Acoust. Soc. Am, **62,** pp. 1057-1059, 1977.

35. J. K. Thompson and D. R. Tree "Finite Difference Approximation Errors in Acoustic Intensity Measurements" Journal of Sound and Vibration., **75,** pp. 229-238, 1981.

36. S. Gade " Sound Intensity (Theory)", Technical Review, **No.3**, Bruel & Kjaer Instruments, Inc., 1982.

37. E. L. Hamilton "Elastic Properties of Marine Sediments" Journal of Geophysical Research, **76,** pp 579-603, 1971.

38. NAG Fortran Library Routine Document-D01AJF, Mark 15, **1**, D01-Quadrature, pp.1-6.

39. W. S. Burdic "Underwater Acoustic System Analysis", Prentice Hall, 1984.